



Multilayer coating of gold nanoparticles (AuNP) with drug-polymer complex: Development and characterization

Dissertation

zur Erlangung des Grades
des Doktors der Naturwissenschaften

„doctor rerum naturalium“

(Dr. rer. nat.)

in der Wissenschaftsdisziplin Pharmazeutische Technologie

eingereicht an der

Naturwissenschaftlichen-Technischen Fakultät III
Chemie, Pharmazie, Bio- und Werkstoffwissenschaften
der Universität des Saarlandes

von

Nico Reum

geboren am 28.08.1977 in Suhl

Saarbrücken, Januar 2011

**Die vorliegende Arbeit wurde in der Zeit von März 2007 bis Januar 2011 an
der Universität des Saarlandes in Saarbrücken angefertigt.**

Tag des Kolloquiums: 01.07.2011
Dekan: Univ.-Prof. Dr. Wilhelm F. Maier
Berichterstatter: Prof. Dr. Claus-Michael Lehr
Jun. Prof. Dr. Marc Schneider
Vorsitz: Prof. Dr. Rolf Hempelmann
Akad. Mitarbeiter: Dr. Michael Schmitt

Die vorliegende Dissertation entstand unter der Betreuung von

Prof. Dr. Claus-Michael Lehr
Jun. Prof. Dr. Marc Schneider

In der Fachrichtung Biopharmazie und Pharmazeutische Technologie der Universität
des Saarlandes

*Bei Herr Prof. Lehr und Herr Jun. Prof. Schneider möchte ich mich für die
Überlassung des Themas und die wertvollen Anregungen und Diskussionen herzlich
bedanken.*

Table of Contents

1	<i>Summary</i>	3
2	<i>Zusammenfassung</i>	4
3	<i>Chapter 1: General Introduction</i>	5
3.1	<i>Photodynamic therapy</i>	6
3.2	<i>Photosensitizers</i>	8
3.3	<i>Polyelectrolytes</i>	11
3.4	<i>Layer-by-Layer technique (LbL)</i>	13
3.5	<i>Nanoparticles in medicine</i>	17
3.6	<i>Gold nanoparticles (AuNP) in medicine</i>	18
3.7	<i>Aim of this thesis:</i>	21
4	<i>Chapter 2: Polymer-drug complex</i>	33
4.1	<i>Introduction</i>	35
4.2	<i>Materials and methods</i>	36
4.2.1	<i>Materials</i>	36
4.2.2	<i>Methods</i>	37
4.3	<i>Results and Discussion</i>	40
4.3.1	<i>PSS/mTHPP complexation efficiency</i>	40
4.3.2	<i>Preparation and characterization of PSS/mTHPC complex</i>	43
4.3.3	<i>Singlet oxygen measurements</i>	47
4.3.4	<i>Photodynamic activity and cytotoxicity</i>	47
4.4	<i>Conclusion</i>	49
4.5	<i>Supporting information</i>	49
5	<i>Chapter 3: Drug-multilayer coating of AuNP</i>	55
5.1	<i>Introduction</i>	57
5.2	<i>Materials and methods</i>	59
5.2.1	<i>Materials</i>	59
5.2.2	<i>Methods</i>	60
5.3	<i>Results and discussion</i>	64
5.3.1	<i>Preparation of PSS/mTHPP complex</i>	64
5.3.2	Synthesis of gold nanoparticles (AuNP)	68
5.3.3	<i>Preparation of PAH and PSS/mTHPP coated AuNP</i>	70
5.4	<i>Conclusion</i>	76
5.5	<i>Supporting information</i>	78
6	<i>Chapter 4: Drug-loaded AuNP for PDT</i>	87
6.1	<i>Introduction</i>	89
6.2	<i>Materials and methods</i>	91
6.2.1	<i>Materials</i>	91
6.2.2	<i>Methods</i>	91
6.3	<i>Results and Discussion</i>	97
6.3.1	<i>Synthesis of Gold nanoparticles (AuNP)</i>	97
6.3.2	<i>Characterization of mAuNP (AuNP(PAH/PSS))</i>	98
6.3.3	<i>Characterization of mAuNP_{drug} (AuNP(PAH/PSS+mTHPC/PAH/PSS))</i>	98
6.3.4	<i>Determination of cytotoxicity after long time incubation with mAuNP</i>	102
6.3.5	<i>Determination of after-effects following unloaded mAuNP incubation</i>	104

6.3.6	Cellular accumulation of unloaded mAuNP	106
6.3.7	Cellular uptake and intracellular distribution of mAuNP	107
6.3.8	Determination of phototoxicity of free and mAuNP-bound mTHPC	110
6.4	<i>Conclusion</i>	111
6.5	<i>Supporting information</i>	112
7	<i>Overall Conclusion and Outlook</i>	87
8	<i>List of Abbreviations</i>	119
9	<i>Curriculum Vitae</i>	120
10	<i>Publication List</i>	122
11	<i>Danksagungen/Acknowledgements</i>	124

1 Summary

Photosensitizers (PS) in combination with visible light are approved in photodynamic therapy for treatment of several types of cancer. Recent strategies for higher bioavailability and the reduction of side effects include PS loaded nanoparticle formulations. The subject of the present thesis is the development and characterization of gold based and surface modified nanoparticulate drug delivery systems for the PS 5,10,15,20-tetrakis(3-hydroxyphenyl)chlorin (mTHPC) for intravenous administration.

Gold nanoparticles (AuNP) with a diameter of 15 nm were prepared and used as template for the Layer-by-Layer (LbL) approach. The PS and the negatively charged polyelectrolyte (PE) poly(styrene sulfonate) sodium salt (PSS) were complexed with a new developed method using freeze-drying resulting in a dramatically increased water solubility of the PS. The phototoxicity of the PSS/mTHPC complex in water was increased compared to the free mTHPC in ethanol. A drug-multilayer system based on the LbL technique utilized the water-soluble complex as anionic layer material and poly(allylamine hydrochloride) (PAH) as cationic layer. For the first time, a nanoparticulate system with three adsorbed drug layers was prepared.

The mTHPC-loaded modified AuNP were taken up by cells and the dark toxicity was strongly decreased. The mTHPC was released and effective as anticancer drug after illumination. In conclusion, the modified AuNP can be considered as promising carrier for such types of PS.

2 Zusammenfassung

Photosensibilisatoren (PS) in Kombination mit sichtbarem Licht sind in der Photodynamischen Therapie zur Behandlung von Krebs zugelassen. Mit PS beladene Nanopartikel (NP) sind eine neue Strategie, um die Bioverfügbarkeit von PS zu erhöhen und Nebenwirkungen zu reduzieren. Das Thema dieser Doktorarbeit ist die Entwicklung und Charakterisierung von auf Gold (Au) basierten und oberflächenmodifizierten nanopartikulären Trägersystemen zur intravenösen Verabreichung des PS 5,10,15,20-Tetrakis(3-hydroxyphenyl)chlorin (mTHPC).

Es wurden AuNP ($d = 15 \text{ nm}$) hergestellt, die als Vorlage für die Layer-by-Layer (LbL) Technik dienten. Der PS und das negativ geladene Poly(styrol sulfonat) Natriumsalz (PSS) wurden mit einer neuen Methode komplexiert, die eine starke Erhöhung der Wasserlöslichkeit von mTHPC zur Folge hatte. Die Phototoxizität vom PSS/mTHPC Komplex verglichen mit dem freien mTHPC war erhöht. Der Komplex wurde als negativ geladenes Schichtmaterial verwendet und Polyallylamin-hydrochlorid (PAH) als positives Schichtmaterial, um ein mehrschichtiges Wirkstoffsystem basierend auf der LbL Technik aufzubauen. Damit konnte erstmalig die Herstellung eines nanopartikulären Systems mit drei Wirkstoffschichten gezeigt werden.

Die mit mTHPC beladenen und modifizierten AuNP wurden von Zellen aufgenommen und die Dunkeltoxizität wurde stark gesenkt. Das mTHPC wurde freigesetzt und war nach Bestrahlung wirksam gegen die Krebszellen. Zusammenfassend gesagt, sind die modifizierten AuNP ein vielversprechendes Transportsystem für diese Arten von PS.

3 Chapter 1: General Introduction

The background and the motivation of this thesis was the application improvement of the active pharmaceutical ingredient (API) Temoporfin or meta-5,10,15,20-tetrakis-hydroxyphenyl-chlorin (mTHPC). It is the API of the pharmaceutical product *Foscan*[®] which is applied intravenously as anticancer drug in photodynamic therapy (PDT). But, the bioavailability of mTHPC is very low caused by its water insolubility. A lot of the drug is precipitating immediately at the puncture of the injection needle because *Foscan*[®] is a liquid consisting of mTHPC dissolved in a mixture of ethanol and ethylene glycol. The unspecific tissue accumulation of mTHPC is a further challenge. Desirable would be the specific accumulation of mTHPC into the cancer cells without any accumulation in the healthy tissue. To solve the problems and thereby reduce the adverse effects, the usage of nanoparticles is a promising approach. As proof of concept, nanoparticles which can be simply identified in water as well as inside of cancer cells could be an advantageous choice. Gold nanoparticles (AuNP) have those characteristics and even more because AuNP aggregation or AuNP surface modification can be easily detected by UV/Vis spectroscopy. In this context, the Layer-by-Layer technology is a very comfortable instrument for changing the nanoparticle surface, for example for the API loading to the nanoparticle surface or an antibody linkage for the specific drug transport to the cancer cells. The following thesis will give you a short introduction about those working fields and definitions and demonstrate as well as discuss the obtained results.

3.1 Photodynamic therapy

Photodynamic therapy (PDT) has now become an established treatment modality for several medical indications [1]. Notably, in the cases of skin actinic keratosis [2-4], several forms of cancer [5-8], and blindness due to age-related macular degeneration [9-11] PDT has been successful. Furthermore, PDT is a photochemical process that requires multiple steps to achieve tissue destruction [12]. First, a compound with photosensitizing properties which is called photosensitizer (PS) is required. The second need is visible light to activate the PS, preferentially in the red region of the visible spectrum ($\lambda \leq 600$ nm) to obtain an improved tissue penetration by light. The third and last requirement is the presence of oxygen. $^1\text{O}_2$, a short-lived product of the reaction between an excited PS molecule and oxygen, plays a key role. The reactive oxygen species (ROS) that are generated by PDT can kill tumor cells directly by apoptosis and/or necrosis. PDT also damages the tumor-associated vasculature, leading to tissue deprivation of oxygen and nutrients and consequent tumor infarction

[13]. Finally, PDT can activate an immune response against tumor cells [14]. These three mechanisms can also influence each other. In contrast to radiation therapy and chemotherapy, PDT has a low mutagenic potential and, except for skin phototoxicity, few adverse effects [15].

The first step in the photosensitizing process is the absorption of a photon by the photosensitizer in the ground state and its promotion to the short-lived excited singlet state (P_1) (Figure 1). The singlet state can relax back into the ground state, resulting in the emission of light in the form of fluorescence. Alternatively, it can convert by intersystem crossing to the more stable triplet excited state (P_3), accompanied by a spin conversion. The triplet state is sufficiently long-lived to take part in chemical reactions and therefore, the photodynamic action takes place for the most part when in the triplet state.

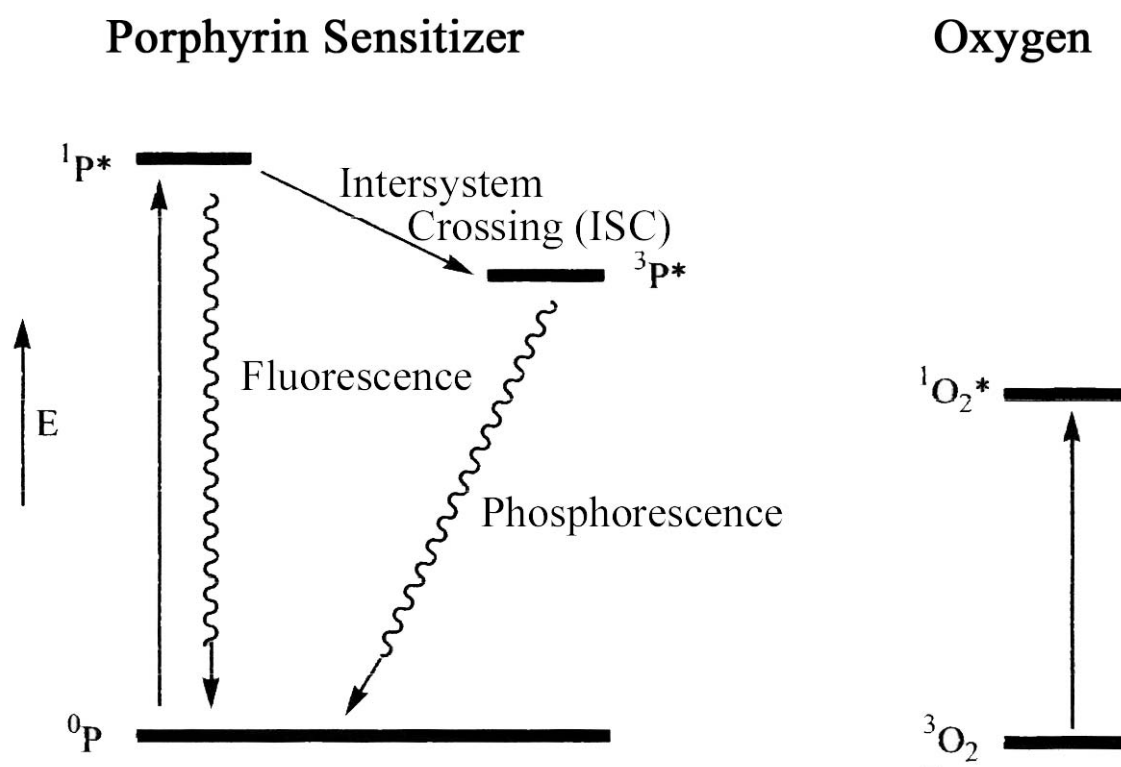


Figure 1: Simplified Jablonski diagram showing porphyrin and oxygen singlet and triplet state. P=Porphyrin; * = electronically excited state; 0 = ground state; 1 = singlet excited state; 3 = triplet excited state [16].

There are two types of photodynamic reactions: type I photoprocesses are electron- or hydrogen-transfer reactions between the triplet photosensitizer and other molecules. These processes produce reactive intermediates that are harmful to cells, such as superoxides, hydroperoxyls and hydroxyl radicals, as well as hydrogen

peroxide; thereby the photosensitizer usually returns to the ground state (P_0). The type II photoprocess is an electron spin exchange between the photosensitizer in the triplet state and ground-state triplet dioxygen (3O_2). This produces a cytotoxic excited singlet state of oxygen (1O_2) [17], while the photosensitizer returns to its ground state. Both, type I and type II reactions cause oxidation of electron-rich biomolecules such as unsaturated lipids and amino acids in the cells but 1O_2 is regarded as the main mediator of phototoxicity in PDT [18].

Recent studies have shown that the intracellular lifetime of singlet oxygen is $\sim 3 \mu\text{s}$ in a viable, metabolically active cell [19]. The resulting intracellular diffusion coefficient of singlet oxygen has been estimated to be $2 - 4 \times 10^{-6} \text{ cm}^2 \text{ s}^{-1}$ means that the spatial domain of intracellular singlet oxygen activity will likely have a spherical radius of approximately 100 nm [20]. This short singlet oxygen lifetime and resulting diffusion distance makes PDT a highly selective form of cancer treatment due to the localized effect it produces.

The mechanism of action of PDT is dependent on various factors including cell genotype [21, 22], PDT dose [22], intracellular adenosine triphosphate levels [23], and photosensitizer localization. Most PDT sensitizers tend not to accumulate in nuclei; therefore, PDT is unlikely to induce DNA damage, mutations and carcinogenesis [24]. Mitochondrial-localizing photosensitizers are likely to induce apoptosis, while plasma membrane-localizing sensitizers are more likely to cause necrosis when exposed to light [25]. In general, the mode of cell death switches from apoptotic to necrotic cell death when the intensity of the insult is excessive, producing rapid cell lysis rather than an organized programmed cell death effect [26].

3.2 Photosensitizers

Photosensitizing drugs have been known and applied in medicine for several thousand years. However, the scientific basis for such use was vague or non-existent before about 1900 [15]. Photosensitizers are generally classified as porphyrins and nonporphyrins. An overview of photosensitizing drugs can be seen in Figure 2. Porphyrin-derived photosensitizers are further classified as first, second, or third generation photosensitizers. First generation photosensitizers include hematoporphyrin derivatives and Photofrin. A number of second generation photosensitizers have been developed to alleviate certain problems associated with first generation molecules such as prolonged skin photosensitization and suboptimal tissue penetration [27]. These second generation photosensitizers absorb light at a

longer wavelengths and cause significantly less skin photosensitization post-treatment compared with first generation compounds. In addition, second generation compounds must be at least as efficient in eradicating tumors as Photofrin, the current gold standard for PDT [28]. Second generation photosensitizers bound to carriers such as antibodies, liposomes, and nanoparticles for selective accumulation in tumor tissue are referred to as third generation photosensitizers and currently represent an active research area in the field [29].

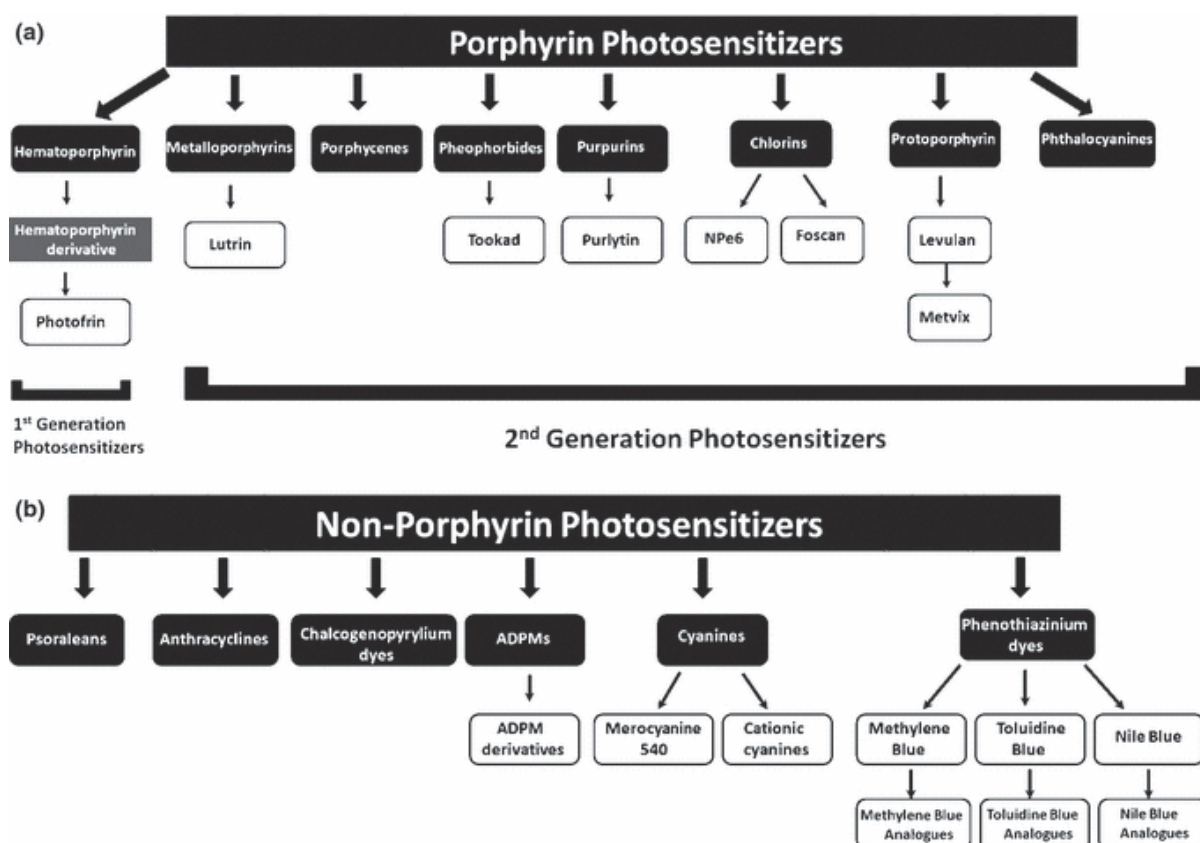


Figure 2: Classification of photosensitizers as (a) porphyrin-based or (b) nonporphyrin-based molecules.

[17] A. E. O'Connor, W. M. Gallagher, A. T. Byrne. Porphyrin and nonporphyrin photosensitizers in oncology: Preclinical and clinical advances in photodynamic therapy. *Photochemistry and Photobiology*. **2009**; 85 (5), 1053-1074. Copyright Wiley-VCH Verlag GmbH & Co. KGaA. Reproduced with permission.

PDT with porphyrin derivatives as photosensitizing drugs was developed from about 1960 [30]. The basic structural formulas of some porphyrins are presented in Figure 3. Porphyrins are a class of tetrapyrroles, which comprise a major component of hemoglobin and myoglobin, two O₂-binding proteins found in human blood. Porphyrins are essential for the biological activity of a living organism. These

molecules possess a highly conjugated, heterocyclic macrocycle and may also contain a central metallic atom such as iron (heme as part of hemoglobin) or magnesium (chlorophyll). The presence of a 22 π electron system gives rise to their long wavelength absorption. As a result, porphyrins have attracted the attention of researchers globally for application as photosensitizing agents in medicine [31].

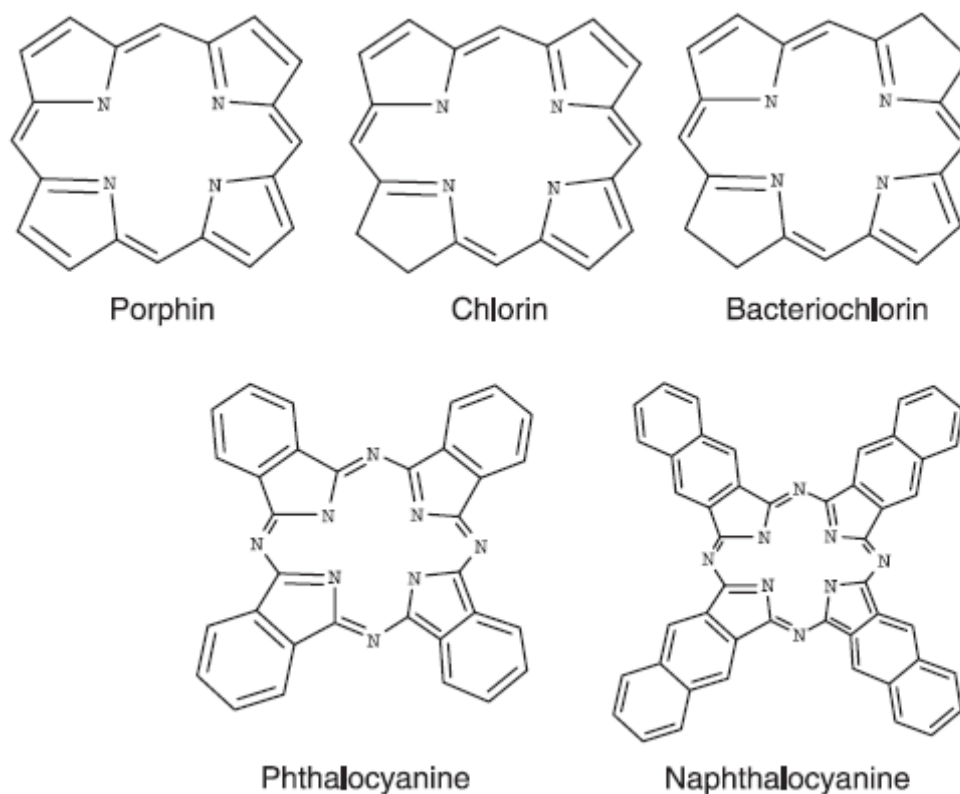


Figure 3: Basic structure of some photosensitizers.

[32] K. Berg, P. K. Selbo, A. Weyergang, A. Dietze, L. Prasmickaite, A. Bonsted, B. O. Engesaeter, E. Angell-Petersen, T. Warloe, N. Frandsen, A. Hogset. Porphyrin-related photosensitizers for cancer imaging and therapeutic applications. *Journal of Microscopy*. **2005**; 218 (2), 133-147. Copyright Wiley-VCH Verlag GmbH & Co. KGaA. Reproduced with permission.

In this study, Temoporfin was used. This drug, which is also known as *Foscan*[®], *meso*-tetra-hydroxyphenyl-chlorin, or meta-5,10,15,20-tetrakis-hydroxyphenyl-chlorin is a member of the chlorin family. It is a commercial available and widely utilized photosensitizer for PDT [33]. Temoporfin is among the most potent PS's as it yields an extraordinary amount of singlet oxygen at 652 nm and has a molar extinction coefficient of $3 \times 10^4 \text{ M}^{-1} \text{ cm}^{-1}$ [17, 34]. It is a hydrophobic second generation photosensitizer and has been shown to have a plasma half-life time in humans of ~45-65 h [33]. *Foscan*[®] was approved in Europe for the palliative treatment of neck

and head cancers in 2001 [17]. In general dosing is between 0.1 and 0.2 mg/kg and illumination requires only 20 J cm^{-2} . Moreover, drug doses and light intensity required to obtain a similar response to Photofrin are up to 100 times lower due to the superior photophysical properties and higher singlet oxygen yield of *Foscan*[®] [34]. The mechanism of action of Temoporfin is via direct tumor cell toxicity as well as vascular damage. In addition, the drug has been shown to preferentially accumulate in the tumor cells of orthotopic brain tumor implants, with a tumor to normal brain tissue ratio of 100:1, thus making Temoporfin-mediated PDT a highly selective form of cancer therapy [35-37]. Treatment time is only a few minutes. However, significant pain can occur during this time. Further, clinically, it takes about 4 days to achieve accumulation in the tumor and clearance from normal tissue for treatment to begin. For the first day post infusion even very dim light can lead to severe skin photosensitivity. Illumination itself must be precise with significant effort to block light from reaching normal tissues as even reflected light is potent enough to generate a photodynamic reaction in unwarranted regions. A major drawback of the drug is prolonged skin photosensitivity, which can last up to 6 weeks, but usually about 2-4 weeks following treatment. A significant body of clinical literature shows *Foscan*[®] can work well under a number of different treatment protocols. Excellent response for head and neck cancer patients has been reported, including tumors of the lip and oral cavity [38-42].

3.3 Polyelectrolytes

The term polyelectrolyte describes a polymer system that is composed of a macromolecule consisting of largely charged monomer units, and low-molecular counterions ensuring electroneutrality. Well-known examples are DNA, RNA, polysaccharides, and proteins. Depending on the charge, one can distinguish between polycations and polyanions. A special case of polyelectrolytes are the polyampholytes, which contain positively as well as negatively charged functional groups in the polymer chain. Polyelectrolytes dissolve in aqueous media under dissociation in a charged polymer chain and counterions, even if the polymer backbone is hydrophobic. The respective degree of dissociation and thus the charge density depends on the strength of the polyacid or polybase. According to their acid/base strength polyions can be classified into: (1) strong polyelectrolytes that are almost completely dissociated over a broad pH range as their charge density is

nearly independent of the solution pH and (2) weak polyelectrolytes whose degree of dissociation α strongly varies with the pH value [43].

As polyelectrolytes combine the properties of polymers and electrolytes, the theoretical description of their structure in aqueous media is rather complex. Long flexible chains can acquire a number of different conformations, therefore their shape and size can be treated only statistically. But it is known that if the polymer is strongly charged, the polyion chain is characterized by a high expansion or stretching compared to neutral polymers due to the strong electrostatic repulsion of the charged segments [43].

The mixing of a solution containing a polyanion $(\text{P}^-\text{c}^+)_n$ with a solution of a polycation $(\text{P}^+\text{a}^-)_m$ leads to the formation of polyelectrolyte complexes $(\text{P}^-\text{C}^+)_x$, [44], and can be described by the following chemical equation:



The driving force of this process is the gain in entropy due to the release of counterions, c^+ and a^- , which are initially located in the vicinity of the polyion chains. Besides electrostatic interactions between the charged species, also other factors such as hydrophobic interactions or hydrogen bonding may contribute to the complex formation. Usually complex formation between polyelectrolytes of similar chain length yields highly aggregated particles, which consist of a neutralized hydrophobic core and a shell of the excess component, which stabilizes particles against further coagulation. Macroscopic flocculation of the system occurs at 1:1 charge stoichiometry. Figure 4 depicts the two borderline cases for the structure of the polyelectrolyte complex precipitates: the ladder structure with fixed ionic cross-links between two oppositely charged chains and the “scrambled egg” structure with statistical charge compensation. The real structure is somewhere between, but mostly nearer to the “scrambled egg” structure.



Figure 4: Limiting structures of polyelectrolyte complex precipitates. Left: Ladder model. Right: “Scrambled egg” model.

[45] H. Dautzenberg, W. Jaeger, J. Kötzt, B. Philipp, C. Seidel, D. Stscherbina. *Polyelectrolytes: Formation, Characterization and Application*. Munich: Hanser Publishers **1994**. Copyright Carl Hanser Verlag GmbH & Co. KG. Reproduced with permission.

The complex formation proceeds very fast with polymer diffusion being the rate-limiting step. After collision the formed polyanion-polycation complexes are “frozen” in a non-equilibrium state at very low salt concentrations. In contrast, in the presence of external salt the back reaction of complex formation (see above) becomes more favored, so that intramolecular and intermolecular rearrangements to an equilibrium structure can occur on a reasonable timescale. Even polyion exchange reactions have been observed at increased ionic strength [46].

3.4 Layer-by-Layer technique (LbL)

In the early 1990s Decher et al. developed a method that applies the electrostatic complex formation between polyanionic and polycationic compounds to build up organized multilayered thin films [47]. During this Layer-by-Layer (LbL) template assisted assembly [44, 48-51], which was already proposed by Iler in 1966 [52], a charged solid substrate is alternately immersed in aqueous solutions of positively and negatively charged polyelectrolytes (Figure 5). The polyelectrolyte molecules adsorb to the oppositely charged surface until the deposition is limited by electrostatic repulsions. Before the adsorption of next layer, the substrate is washed to remove excess polyelectrolyte. These steps can be repeated limitlessly and films with up to 1000 layers have been successfully built [53]. The thickness of one layer varies between several angstroms and a few nanometers depending on the deposition conditions [43].

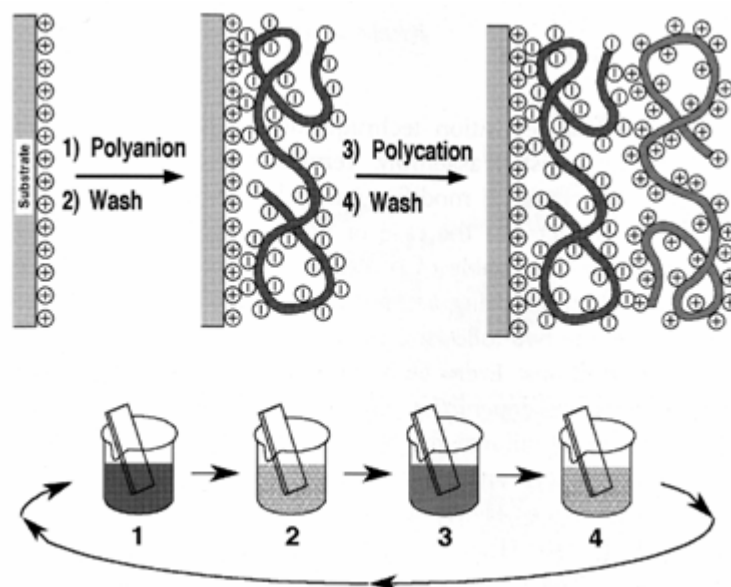


Figure 5: Simplified principle of LbL technique.

[44] G. Decher, J. B. Schlenoff "Multilayer thin films: Sequential assembly of nanocomposite materials." G. Decher, 1 ed. Weinheim: Wiley-VCH, p. 4, **2003**. Copyright Wiley-VCH Verlag GmbH & Co. KGaA. Reproduced with permission.

The main advantage of this technique is its wide versatility relating to the used layer material. Possible polyelectrolytes are synthetic polyelectrolytes [54], polysaccharides [55], polypeptides [56], proteins [57], enzymes [54, 58, 59] and nucleic acids [59, 60]. This large choice of layer material allows surface coatings with interesting chemical, biological, optical, electronic, magnetic, adhesive or anti-bacterial properties giving rise to a variety of possible applications in different fields [44]. Besides of electrostatic interactions also other possibilities are available to built up multilayer systems such as hydrogen bonding or covalent interactions [61].

According to the zone model of Ladam et al. [62] multilayers can be subdivided into three domains (Figure 6):

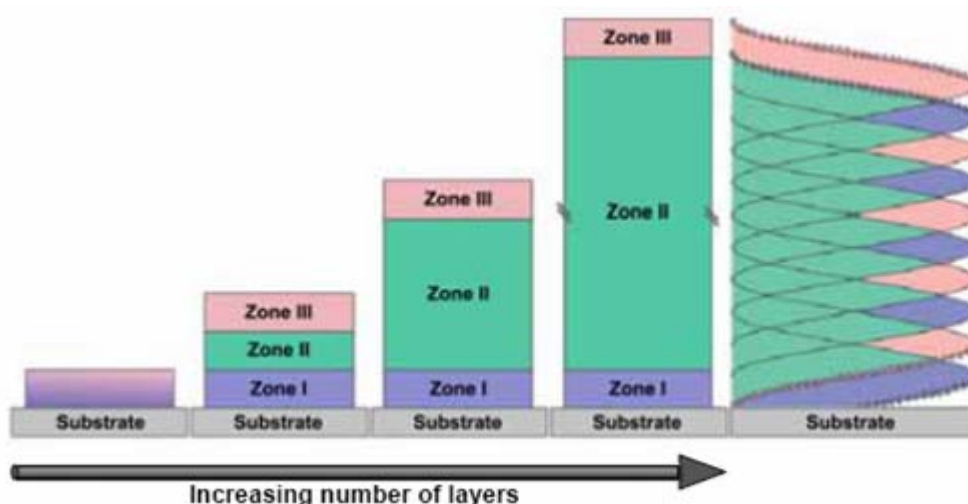


Figure 6: The zone model for the growth of polyelectrolyte multilayers. The first layer pair is shown on the left and a film consisting of several layers is shown on the right. Only zone II grows with increasing numbers of layers. On the very right is depicted how the three zones can be correlated with a model consisting of individual but strongly overlapping layers.

[44] G. Decher, J. B. Schlenoff "Multilayer thin films: Sequential assembly of nanocomposite materials." G. Decher, 1 ed. Weinheim: Wiley-VCH, p. 19, **2003**. Copyright Wiley-VCH Verlag GmbH & Co. KGaA. Reproduced with permission.

Zone I, II, and III would normally differ in both chemical composition and in structure. Simplified, zone II is neutral and the zones I and III are charged. Depending on the charge density of the substrate and on the substrate roughness, varying amounts of small counterions may be present in zone I. Counterions are ubiquitous in zone III because the adsorption of every layer leads to an overcompensation of the original surface charge and the newly created excess charge of the last deposited layer with polymer chains dangling into the solution must be accompanied by the presence of small counterions [44].

Note that the borders between the zones I and II and between zones II and III are not sharp but gradual. At present it is not known how many layers actually contribute to zone I and III, but this should be a function of the substrate, of the chemical structure of the respective polyion pair used for the deposition and of the deposition conditions [44].

When the multilayer is fabricated, at first, only zone I and III exist. Initially, there will probably a situation in which zones I and III will not have reached their final thickness

and the transition between them may occur directly without forming a zone II. As more layers are added they will reach their final thickness and composition while zone II starts to grow [44].

Without zone II the growth characteristic of such a layer system is exponentially. During this growth phase the thickness of zone III steadily increases leading to an increased penetration depth of the diffusing polyion (first stage in Figure 6), and thus a higher amount of polymer being deposited per adsorption step. When the film reaches a critical thickness the diffusing polyelectrolyte cannot penetrate the whole film depth anymore (from second stage in Figure 6 onwards) and zone II develops. As the penetration depth (zone III) stays constant from there on, an equal amount of polyelectrolyte is adsorbed per bilayer leading to a transition from the exponential to the linear growth regime [44].

For some polyelectrolyte pairs, such as the most frequently studied poly(allylamine hydrochloride) (PAH) and poly(styrene sulfonate) (PSS) at low ionic strength and temperature, zone III extends only over one or two polyelectrolyte layers, leading to a linear layer growth right after the initial build-up zone [43]. On the contrary, other polyion combinations can diffuse deeply into the film [63], so that the exponential growth passes into a linear growth only after 25 or more layers (e.g. poly(L-lysine)/hyaluronic acid) [43, 64, 65].

In zone II, most of the charged polymer segments are intrinsically compensated by oppositely charged polyion segments [66, 67]. Any rearrangement of the chains is kinetically hindered as they are highly interconnected with each other by multiple ionic bonds. In contrast, due to the charge overcompensation the less densely packed zone III contains a substantial amount of counterions showing a gradient of increasing concentration towards the water interface. Although being quite hydrophobic in the interior polyelectrolyte multilayers include typically 40 - 60% water [68, 69]. Even in the dried state the films are strongly hydrated: Water contents of 10 - 20% have been found [70, 71]. Multilayers are permeable for small molecules [72, 73]. Depending on the layer thickness, the polyelectrolytes used for preparation and the environmental conditions, their cut-off size can be precisely tuned. Furthermore due to their bipolar structure multilayer membranes exhibit a high selectivity for differently charged ions or even polar vs. non-polar compounds making them attractive as separation membranes for ions, gases, and solutes [44, 74-78].

In addition to the type of polyions, multilayer growth was found to be affected by a range of other parameters such as the ionic strength [68, 70, 79, 80], and the type of salt of the deposition solution [79, 81], the polymer charge density varied either by charge dilution in copolymers [80, 82, 83], or by changing the pH of weak polyion solutions [84, 85], the type of solvent [79, 86], temperature [64, 87-89], adsorption time [79, 90], polymer concentration [79], and the molecular weight of the polyions [91, 92]. Both an increase of ionic strength and an increase of temperature were shown to increase the thickness of the deposited layers, at the same time extending the exponential growth regime [64]. At higher ionic strength polyions in solution adopt a more coiled conformation with a lower radius of gyration due to screening of the charges. Upon adsorption they retain their solution conformation and therefore occupy a lower surface area per chain and in parallel lead to thicker layers with an increased internal and external roughness [43, 70].

Not only the growth of polyelectrolyte multilayers can be influenced by a number of different parameters, also after preparation the films are sensitive to a change of the external conditions such as humidity [93, 94], solvent [95], pH [96, 97], ionic strength [98, 99], or temperature [100, 101]. In the fabrication of multilayers adsorbed to nanoparticles, additional aspects have to be considered such as nanoparticle concentration to polyelectrolyte concentration to avoid coagulation of partly covered particles [102]. Additionally, the corresponding timescales of adsorption and coagulation are crucial for successful multilayer formation on single colloids [43, 50].

3.5 Nanoparticles in medicine

The regulation of engineered nanoparticles requires a widely agreed definition of such particles. Several definitions for nanoparticles were provided by researchers, institutes, and governments. For example, the Joint Research Centre of the European Commission defines nanoparticles as particles in a size range between 1 and 100 nm. The National Nanotechnology Initiative (NNI), on the other hand, defines nanotechnology as the understanding and control of matter at dimensions of roughly 1 to 100 nanometers, where unique phenomena enable novel applications. Furthermore, they emphasize that at the nanoscale the physical, chemical, and biological properties of materials differ in fundamental and valuable ways from the properties of individual atoms and molecules or bulk matter [103]. The National Cancer Institute gives the following nanoparticle definition: A particle of that is smaller than 100 nanometers. In medicine, nanoparticles can be used to carry antibodies,

drugs, imaging agents, or other substances to certain parts of the body. Nanoparticles are being studied in the detection, diagnosis, and treatment of cancer [104]. In general, nanoparticles can be defined as particles with sizes between about 1 and 100 nm that show properties that are not found in bulk samples of the same material [105].

Nanoscale drug delivery systems are emerging technologies for the rational delivery of chemotherapeutic drugs in the treatment of cancer. Their use offers improved pharmacokinetic properties, controlled and sustained release of drugs, and more importantly, lower systemic toxicity [106]. A wide variety of nanoparticles e.g., inorganic nanoparticles [107-109], polymeric nanoparticles [110-112], solid lipid nanoparticles [113-115], liposomes [116-120], nanocrystals or quantum dots [121, 122], nanotubes [123, 124], and dendrimers [125, 126] exist already, and diverse methods of synthesis have been developed. Nevertheless, only a few numbers of commercial available nanoparticle formulations are on the open market today. One of five formulations is the liposomal formulation Doxil[®] with doxorubicin as active pharmaceutical ingredient and another one is the albumin-nanoparticle-based Abraxane[®] with paclitaxel as active pharmaceutical ingredient [127].

Mainly two advantages are responsibly for the increased interest of nanoparticles in research. First, the larger size of nanoparticles relative to small molecule drugs, can avoid first-pass clearance from the bloodstream if intravenously administrated [127]. Second, nanoparticles can selectively accumulate in tumor tissue via the enhanced permeability and retention effect, also known as passive targeting [128]. Furthermore, an active targeting of nanoparticles is possible, which is characterized by attachment of specific ligands such as peptides, antibodies, aptamers, or small molecules to the nanoparticle surface [129, 130].

3.6 Gold nanoparticles (AuNP) in medicine

AuNP are characterized by their excellent optical and photoelectrical properties. Furthermore, studies have confirmed that AuNP are non-toxic [131] but nevertheless this is a size-dependent parameter [132]. Additional advantages of AuNP are their simple preparation, long stability, and possibility of surface modification by place-exchange reactions [133] or LbL technology [134].

The control of AuNP size, shape, and surface modification is desirably because these properties influence the pharmacokinetic parameters of AuNP [127, 135]. To synthesize monodisperse distributed and spherical AuNP, one method is the two-

phase Brust-Schiffrin method [136], in which aqueous sodium borohydride is used to reduce AuCl_4^- in toluene in the presence of stabilizing thiols. Another reliable method is the older Turkevich synthesis [137], where gold salt is boiled together with citrate to get 10 - 100 nm water-soluble particles (Figure 7 a). The preparation of rod-shaped AuNP in different aspect-ratios can also be carried out (Figure 7 c and d).

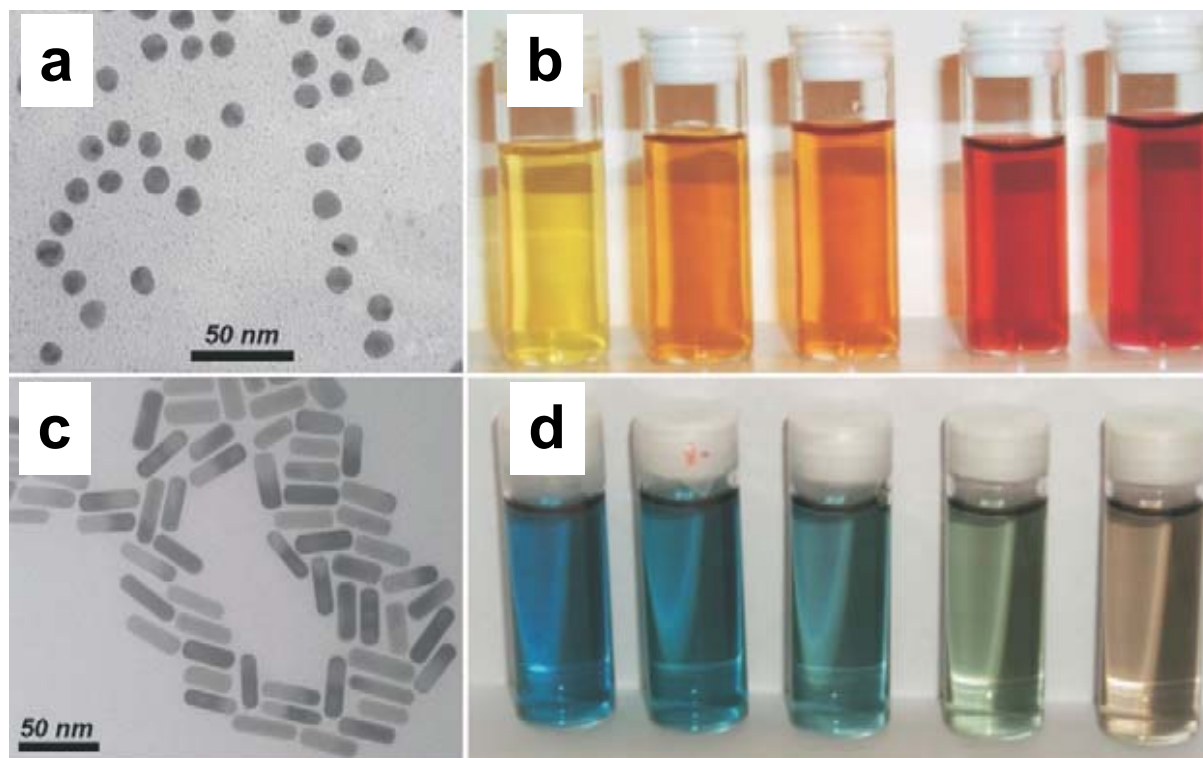


Figure 7: (a) Transmission electron micrographs of Au nanospheres, (b) Photographs of colloidal dispersions of AuAg alloy nanoparticles with increasing Au concentration, (c) Transmission electron micrographs of nanorods, (d) Photographs of colloidal dispersions of Au nanorods of increasing aspect ratio.

[138] L. M. Liz-Marzan. Nanometals: Formation and color. *Materials Today*. **2004**; 7 (2), 26-31. Copyright Elsevier B.V. Reproduced with permission.

In medicine, AuNP can be used as drug delivery system [139], in diagnostic [140], and for detection of proteins and nucleic acids [141, 142]. The focus of this study will be on drug delivery systems, which provide positive attributes to a free drug by improving solubility, *in vivo* stability, and biodistribution.

Following, two commercial examples for the application of AuNP in medicine are named. Aurimune, a pegylated AuNP formulation with surface attached tumor necrosis factor of the company CytImmune Science against solid tumors for intravenous application is the first AuNP formulation in Phase I/II of clinical trials

[127]. Moreover, a lot of patents exist in the field of AuNP in connection with drug carriers. One commercial home pregnancy test even uses AuNP to form the pink line, which is actually made of 40 nm AuNP functionalized with a human antibody [143, 144].

A further promising application of AuNP is the photothermal cancer therapy caused by the ability of AuNP to convert absorbed light ($\lambda \sim 520$ nm) efficiently into localized heat [140]. Several articles were already published about AuNP as drug delivery system for small drug molecules and biomolecules such as nucleic acids and proteins [134, 139, 145]. Schneider et al. developed a multifunctional, AuNP based, and multilayered drug delivery system as a kind of template for different diseases (Figure 8) [146]. As a proof of concept, they prepared AuNP with a diameter of around 13 nm, attached three layers of PAH and two of PSS, and covalent attached a terpolymers on the PAH surface to allow the covalent bond of the drug doxorubicin on the nanoparticle surface. This promising and multifunctional model raises hope for more efficient tumor therapy with reduced side effects in the future.

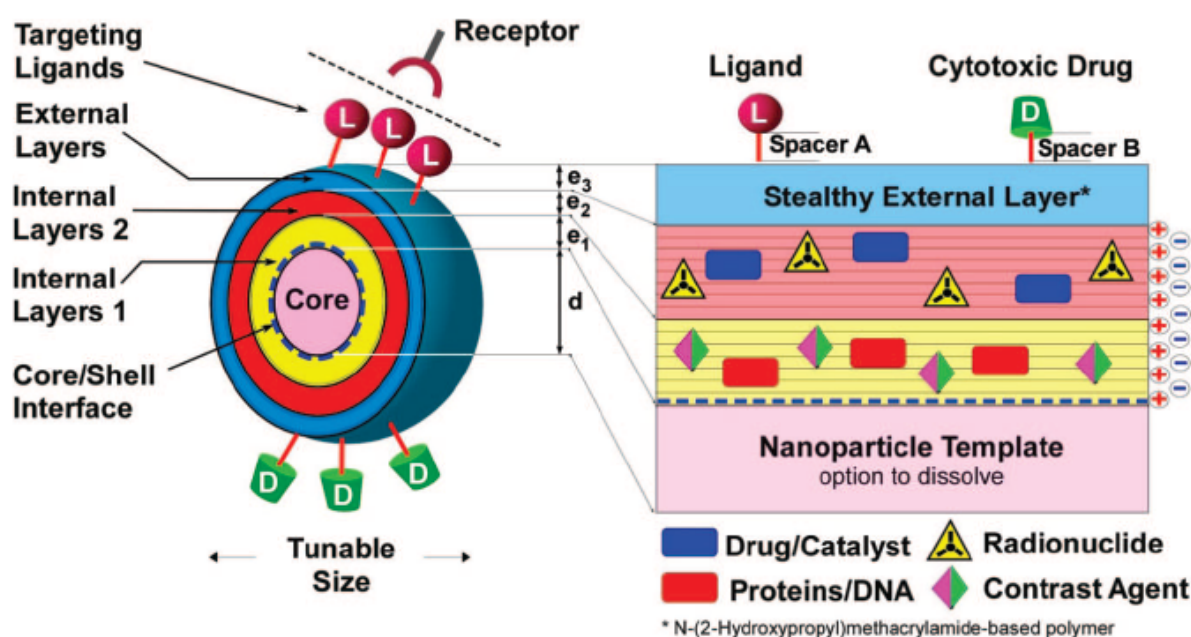


Figure 8: Schematic representation of a multiple coated and AuNP-based complex drug delivery system.

[146] G. F. Schneider, V. Subr, K. Ulbrich, G. Decher. Multifunctional cytotoxic stealth nanoparticles. A model approach with potential for cancer therapy. *Nano Letters*. **2009**; 9 (2), 636-642.

Copyright Wiley-VCH Verlag GmbH & Co. KGaA. Reproduced with permission.

3.7 Aim of this thesis:

In this thesis, the main goal was to develop a nanoparticulate and Layer-by-Layer (LbL) surface modified carrier system for the intravenous delivery of the water insoluble photosensitizer (PS), 5,10,15,20-tetrakis(3-hydroxyphenyl)chlorin (mTHPC), for the treatment of head and neck cancer by photodynamic therapy (PDT). The LbL technique was carried out with the positively charged polyelectrolyte (PE) poly(allylamine hydrochloride) (PAH) and the negatively charged PE poly(styrene sulfonate) sodium salt (PSS)

The major aims of this thesis were:

- 1.) Preparation and characterization of mTHPC loaded AuNP and their stability in biological environment like different cell culture media.
- 2.) Application of the LbL technology to incorporate the drug mTHPC into the polyelectrolyte layer system around the AuNP cores.
- 3.) Adjustment of the mTHPC concentration in relation to one carrier by preparation of drug-multilayers attached to the AuNP templates.

References:

- [1] A. Juarranz, P. Jaèn, F. Sanz-Rodríguez, J. Cuevas, S. González. Photodynamic therapy of cancer. Basic principles and applications. *Clinical and Translational Oncology*. **2008**; 10 (3), 148-154.
- [2] B. Berman, S. Amini, W. Valins, S. Block. Pharmacotherapy of actinic keratosis. *Expert Opinion on Pharmacotherapy*. **2009**; 10 (18), 3015-3031.
- [3] S. Choudhary, K. Nouri, M. L. Elsaie. Photodynamic therapy in dermatology: A review. *Lasers in Medical Science*. **2009**; 24 (6), 971-980.
- [4] T. Smits, A. C. E. Moor. New aspects in photodynamic therapy of actinic keratoses. *Journal of Photochemistry and Photobiology B: Biology*. **2009**; 96 (3), 159-169.
- [5] M. G. Bredell, E. Besic, C. Maake, H. Walt. The application and challenges of clinical PD-PDT in the head and neck region: A short review. *Journal of Photochemistry and Photobiology B: Biology*. **2010**; 101 (3), 185-190.
- [6] V. G. Schweitzer, M. L. Somers. PHOTOFRIN-mediated photodynamic therapy for treatment of early stage laryngeal malignancies. *Oncology Reviews*. **2010**; 4 (4), 203-209.
- [7] R. J. M. Lammers, J. A. Witjes. Developments in intravesical therapy for non-muscle-invasive bladder cancer. *Expert Review of Anticancer Therapy*. **2010**; 10 (12), 1903-1916.
- [8] A. Sanchez, M. Reza, J. A. Blasco, D. Callejo. Effectiveness, safety, and cost-effectiveness of photodynamic therapy in Barrett's esophagus: A systematic review. *Diseases of the Esophagus*. **2010**; 23 (8), 633-640.
- [9] A. J. Augustin, S. Scholl, J. Kirchhof. Treatment of neovascular age-related macular degeneration: Current therapies. *Clinical Ophthalmology*. **2009**; 3 (1), 175-182.
- [10] J. P. Hubschman, S. Reddy, S. D. Schwartz. Age-related macular degeneration: Current treatments. *Clinical Ophthalmology*. **2009**; 3 (1), 155-166.
- [11] A. F. Cruess, G. Zlateva, A. M. Pleil, B. Wirostko. Photodynamic therapy with verteporfin in age-related macular degeneration: A systematic review of efficacy, safety, treatment modifications and pharmacoeconomic properties. *Acta Ophthalmologica*. **2009**; 87 (2), 118-132.
- [12] M. L. Davila. Photodynamic Therapy. *Gastrointestinal Endoscopy Clinics of North America*. **2011**; 21 (1), 67-79.
- [13] A. P. Castano, T. N. Demidova, M. R. Hamblin. Mechanisms in photodynamic therapy: Part three - Photosensitizer pharmacokinetics, biodistribution, tumor localization and modes of tumor destruction. *Photodiagnosis and Photodynamic Therapy*. **2005**; 2 (2), 91-106.

- [14] K. Plaetzer, T. Kiesslich, T. Verwanger, B. Krammer. The modes of cell death induced by PDT: An overview. *Medical Laser Application*. **2003**; 18 (1), 7-19.
- [15] J. Moan, Q. Peng. An Outline of the Hundred-Year History of PDT. *Anticancer Research*. **2003**; 23 (5 A), 3591-3600.
- [16] J. A. Hargus. Naturally-derived porphyrin and chlorin photosensitizers for photodynamic therapy. Baton Rouge: Louisiana State University; 2005.
- [17] A. E. O'Connor, W. M. Gallagher, A. T. Byrne. Porphyrin and nonporphyrin photosensitizers in oncology: Preclinical and clinical advances in photodynamic therapy. *Photochemistry and Photobiology*. **2009**; 85 (5), 1053-1074.
- [18] E. S. Nyman, P. H. Hynninen. Research advances in the use of tetrapyrrolic photosensitizers for photodynamic therapy. *Journal of Photochemistry and Photobiology B: Biology*. **2004**; 73 (1-2), 1-28.
- [19] S. Hatz, J. D. C. Lambert, P. R. Ogilby. Measuring the lifetime of singlet oxygen in a single cell: Addressing the issue of cell viability. *Photochemical and Photobiological Sciences*. **2007**; 6 (10), 1106-1116.
- [20] S. Hatz, L. Poulsen, P. R. Ogilby. Time-resolved singlet oxygen phosphorescence measurements from photosensitized experiments in single cells: Effects of oxygen diffusion and oxygen concentration. *Photochemistry and Photobiology*. **2008**; 84 (5), 1284-1290.
- [21] R. D. Almeida, B. J. Manadas, A. P. Carvalho, C. B. Duarte. Intracellular signaling mechanisms in photodynamic therapy. *Biochimica et Biophysica Acta - Reviews on Cancer*. **2004**; 1704 (2), 59-86.
- [22] L. Wyld, M. W. R. Reed, N. J. Brown. Differential cell death response to photodynamic therapy is dependent on dose and cell type. *British Journal of Cancer*. **2001**; 84 (10), 1384-1386.
- [23] K. Plaetzer, T. Kiesslich, B. Krammer, P. Hammerl. Characterization of the cell death modes and the associated changes in cellular energy supply in response to AIPcS₄-PDT. *Photochemical and Photobiological Sciences*. **2002**; 1 (3), 172-177.
- [24] R. W. Boyle, D. Dolphin. Structure and biodistribution relationships of photodynamic sensitizers. *Photochemistry and Photobiology*. **1996**; 64 (3), 469-485.
- [25] T. J. Dougherty, C. J. Gomer, B. W. Henderson, G. Jori, D. Kessel, M. Korblick, J. Moan, Q. Peng. Photodynamic therapy. *Journal of the National Cancer Institute*. **1998**; 90 (12), 889-905.
- [26] M. Leist, P. Nicotera. The shape of cell death. *Biochemical and Biophysical Research Communications*. **1997**; 236 (1), 1-9.

- [27] C. S. Nayak. Photodynamic therapy in dermatology. *Indian Journal of Dermatology, Venereology and Leprology*. **2005**; 71 (3), 155-160.
- [28] J. J. Schuitemaker, P. Baas, H. L. L. M. Van Leengoed, F. W. Van Der Meulen, W. M. Star, N. Van Zandwijk. Photodynamic therapy: A promising new modality for the treatment of cancer. *Journal of Photochemistry and Photobiology B: Biology*. **1996**; 34 (1), 3-12.
- [29] A. Juzeniene, Q. Peng, J. Moan. Milestones in the development of photodynamic therapy and fluorescence diagnosis. *Photochemical and Photobiological Sciences*. **2007**; 6 (12), 1234-1245.
- [30] R. R. Allison, C. H. Sibata. Oncologic photodynamic therapy photosensitizers: A clinical review. *Photodiagnosis and Photodynamic Therapy*. **2010**; 7 (2), 61-75.
- [31] S. K. Pushpan, S. Venkatraman, V. G. Anand, J. Sankar, D. Parmeswaran, S. Ganesan, T. K. Chandrashekar. Porphyrins in photodynamic therapy - A search for ideal photosensitizers. *Current Medicinal Chemistry - Anti-Cancer Agents*. **2002**; 2 (2), 187-207.
- [32] K. Berg, P. K. Selbo, A. Weyergang, A. Dietze, L. Prasmickaite, A. Bonsted, B. O. Engesaeter, E. Angell-Petersen, T. Warloe, N. Frandsen, A. Hogset. Porphyrin-related photosensitizers for cancer imaging and therapeutic applications. *Journal of Microscopy*. **2005**; 218 (2), 133-147.
- [33] A. M. Ronn, M. Nouri, L. A. Lofgren, B. M. Steinberg, A. Westerborn, T. Windahl, M. J. Shikowitz, A. L. Abramson. Human tissue levels and plasma pharmacokinetics of Temoporfin (Foscan®[®], mTHPC). *Lasers in Medical Science*. **1996**; 11 (4), 267-272.
- [34] S. Mitra, T. H. Foster. Photophysical parameters, photosensitizer retention and tissue optical properties completely account for the higher photodynamic efficacy of meso-tetra-hydroxyphenyl-chlorin vs Photofrin. *Photochemistry and Photobiology*. **2005**; 81 (4), 849-859.
- [35] A. Molinari, C. Bombelli, S. Mannino, A. Stringaro, L. Toccaceli, A. Calcabrini, M. Colone, A. Mangiola, G. Maira, P. Luciani, G. Mancini, G. Arancia. m-THPC-mediated photodynamic therapy of malignant gliomas: Assessment of a new transfection strategy. *International Journal of Cancer*. **2007**; 121 (5), 1149-1155.
- [36] A. Obwegeser, R. Jakober, H. Kostron. Uptake and kinetics of ¹⁴C-labelled meta-tetrahydroxyphenylchlorin and 5-aminolaevulinic acid in the C6 rat glioma model. *British Journal of Cancer*. **1998**; 78 (6), 733-738.
- [37] A. Zimmermann, M. Ritsch-Marte, H. Kostron. mTHPC-mediated photodynamic diagnosis of malignant brain tumors. *Photochemistry and Photobiology*. **2001**; 74 (4), 611-616.

- [38] M. P. Copper, I. B. Tan, H. Oppelaar, M. C. Ruevekamp, F. A. Stewart. Meta-tetra(hydroxyphenyl)chlorin photodynamic therapy in early-stage squamous cell carcinoma of the head and neck. *Archives of Otolaryngology - Head and Neck Surgery*. **2003**; 129 (7), 709-711.
- [39] M. G. Dilkes, E. Benjamin, S. Ovaisi, A. S. Banerjee. Treatment of primary mucosal head and neck squamous cell carcinoma using photodynamic therapy: Results after 25 treated cases. *Journal of Laryngology and Otology*. **2003**; 117 (9), 713-717.
- [40] K. F. M. Fan, C. Hopper, P. M. Speight, G. A. Buonaccorsi, S. G. Bown. Photodynamic therapy using mTHPC for malignant disease in the oral cavity. *International Journal of Cancer*. **1997**; 73 (1), 25-32.
- [41] C. Hopper, A. Kübler, H. Lewis, I. B. Tan, G. Putnam, T. Patrice, C. Beauvillain, J. Evensen, K. Butow, B. Smit, J. Brown, J. De Carpentier, J. Carruth, M. Dilkes, G. Kenyon, F. Roberts, N. Sudderick. mTHPC-mediated photodynamic therapy for early oral squamous cell carcinoma. *International Journal of Cancer*. **2004**; 111 (1), 138-146.
- [42] A. C. Kübler, J. De Carpentier, C. Hopper, A. G. Leonard, G. Putnam. Treatment of squamous cell carcinoma of the lip using Foscan-mediated photodynamic therapy. *International Journal of Oral and Maxillofacial Surgery*. **2001**; 30 (6), 504-509.
- [43] K. Kohler. *Temperature-Induced Rearrangements of Polyelectrolyte Multilayer Capsules: Mechanisms and Applications*. Potsdam: University Potsdam; 2006.
- [44] G. Decher, J. B. Schlenoff. *Multilayer thin films: Sequential assembly of nanocomposite materials*. 1 ed. Weinheim: Wiley-VCH **2003**.
- [45] H. Dautzenberg, W. Jaeger, J. Kötz, B. Philipp, C. Seidel, D. Stscherbina. *Polyelectrolytes: Formation, Characterization and Application*. Munich: Hanser Publishers **1994**.
- [46] K. N. Bakeev, V. A. Izumrudov, S. I. Kuchanov, A. B. Zezin, V. A. Kabanov. Kinetics and mechanism of interpolyelectrolyte exchange and addition reactions. *Macromolecules*. **1992**; 25 (17), 4249-4254.
- [47] G. Decher, J. D. Hong, J. Schmitt. Buildup of ultrathin multilayer films by a self-assembly process: III. Consecutively alternating adsorption of anionic and cationic polyelectrolytes on charged surfaces. *Thin Solid Films*. **1992**; 210-211 (PART 2), 831-835.
- [48] R. V. Klitzing, J. E. Wong, W. Jaeger, R. Steitz. Short range interactions in polyelectrolyte multilayers. *Current Opinion in Colloid and Interface Science*. **2004**; 9 (1-2), 158-162.

- [49] P. Bertrand, A. Jonas, A. Laschewsky, R. Legras. Ultrathin polymer coatings by complexation of polyelectrolytes at interfaces: Suitable materials, structure and properties. *Macromolecular Rapid Communications*. **2000**; 21 (7), 319-348.
- [50] M. Schönhoff. Layered polyelectrolyte complexes: Physics of formation and molecular properties. *Journal of Physics Condensed Matter*. **2003**; 15 (49).
- [51] M. Schönhoff. Self-assembled polyelectrolyte multilayers. *Current Opinion in Colloid and Interface Science*. **2003**; 8 (1-2), 86-95.
- [52] R. K. Iler. Multilayers of colloidal particles. *Journal of Colloid And Interface Science*. **1966**; 21 (6), 569-594.
- [53] K. M. Lenahan, Y. X. Wang, Y. Liu, R. O. Claus, J. R. Heflin, D. Marciu, C. Figura. Novel polymer dyes for nonlinear optical applications using ionic self-assembled monolayer technology. *Advanced Materials*. **1998**; 10 (11), 853-855.
- [54] T. Boudou, T. Crouzier, K. Ren, G. Blin, C. Picart. Multiple functionalities of polyelectrolyte multilayer films: New biomedical applications. *Advanced Materials*. **2010**; 22 (4), 441-467.
- [55] T. Crouzier, T. Boudou, C. Picart. Polysaccharide-based polyelectrolyte multilayers. *Current Opinion in Colloid and Interface Science*. **2010**; 15 (6), 417-426.
- [56] C. Picart. Polyelectrolyte multilayer film: From physico-chemical properties to the control of cellular processes. *Current Medicinal Chemistry*. **2008**; 15 (7), 685-697.
- [57] F. Lisdat, R. Dronov, H. Möhwald, F. W. Scheller, D. G. Kurth. Self-assembly of electro-active protein architectures on electrodes for the construction of biomimetic signal chains. *Chemical Communications*. **2009**; (3), 274-283.
- [58] J. F. Rusling, E. G. Hvastkovs, D. O. Hull, J. B. Schenkman. Biochemical applications of ultrathin films of enzymes, polyions and DNA. *Chemical Communications*. **2008**; (2), 141-154.
- [59] R. B. Shmueli, D. G. Anderson, J. J. Green. Electrostatic surface modifications to improve gene delivery. *Expert Opinion on Drug Delivery*. **2010**; 7 (4), 535-550.
- [60] C. M. Jewell, D. M. Lynn. Surface-mediated delivery of DNA: Cationic polymers take charge. *Current Opinion in Colloid and Interface Science*. **2008**; 13 (6), 395-402.
- [61] L. J. De Cock, S. De Koker, B. G. De Geest, J. Grooten, C. Vervaet, J. P. Remon, G. B. Sukhorukov, M. N. Antipina. Polymeric Multilayer Capsules in Drug Delivery. *Angewandte Chemie - International Edition*. **2010**; 49 (39), 6954-6973.
- [62] G. Ladam, P. Schaad, J. C. Voegel, P. Schaaf, G. Decher, F. Cuisinier. In situ determination of the structural properties of initially deposited polyelectrolyte multilayers. *Langmuir*. **2000**; 16 (3), 1249-1255.

- [63] P. Lavalle, V. Vivet, N. Jessel, G. Decher, J. C. Voegel, P. J. Mesini, P. Schaaf. Direct evidence for vertical diffusion and exchange processes of polyanions and polycations in polyelectrolyte multilayer films. *Macromolecules*. **2004**; 37 (3), 1159-1162.
- [64] M. Salomäki, I. A. Vinokurov, J. Kankare. Effect of temperature on the buildup of polyelectrolyte multilayers. *Langmuir*. **2005**; 21 (24), 11232-11240.
- [65] C. Porcel, P. Lavalle, V. Ball, G. Decher, B. Senger, J. C. Voegel, P. Schaaf. From Exponential to Linear Growth in Polyelectrolyte Multilayers. *Langmuir*. **2006**; 22 (9), 4376-4383.
- [66] R. V. Klitzing, H. Möhwald. Proton concentration profile in ultrathin polyelectrolyte films. *Langmuir*. **1995**; 11 (9), 3554-3559.
- [67] J. B. Schlenoff, H. Ly, M. Li. Charge and mass balance in polyelectrolyte multilayers. *Journal of the American Chemical Society*. **1998**; 120 (30), 7626-7634.
- [68] R. Steitz, V. Leiner, R. Siebrecht, R. V. Klitzing. Influence of the ionic strength on the structure of polyelectrolyte films at the solid/liquid interface. *Colloids and Surfaces A: Physicochemical and Engineering Aspects*. **2000**; 163 (1), 63-70.
- [69] I. Estrela-Lopis, S. Leporatti, S. Moya, A. Brandt, E. Donath, H. Möhwald. SANS studies of polyelectrolyte multilayers on colloidal templates. *Langmuir*. **2002**; 18 (21), 7861-7866.
- [70] M. Lösche, J. Schmitt, G. Decher, W. G. Bouwman, K. Kjaer. Detailed structure of molecularly thin polyelectrolyte multilayer films on solid substrates as revealed by neutron reflectometry. *Macromolecules*. **1998**; 31 (25), 8893-8906.
- [71] T. Farhat, G. Yassin, S. T. Dubas, J. B. Schlenoff. Water and ion pairing in polyelectrolyte multilayers. *Langmuir*. **1999**; 15 (20), 6621-6623.
- [72] R. V. Klitzing, H. Möhwald. A realistic diffusion model for ultrathin polyelectrolyte films. *Macromolecules*. **1996**; 29 (21), 6901-6906.
- [73] R. V. Klitzing, H. Möhwald. Transport through ultrathin polyelectrolyte films. *Thin Solid Films*. **1996**; 284-285, 352-356.
- [74] L. Krasemann, B. Tieke. Composite membranes with ultrathin separation layer prepared by self-assembly of polyelectrolytes. *Materials Science and Engineering C*. **1999**; 8-9, 513-518.
- [75] W. Jin, A. Toutianoush, B. Tieke. Size- and charge-selective transport of aromatic compounds across polyelectrolyte multilayer membranes. *Applied Surface Science*. **2005**; 246 (4), 444-450.
- [76] L. Krasemann, B. Tieke. Highly efficient composite membranes for ethanol-water pervaporation. *Chemical Engineering and Technology*. **2000**; 23 (3), 211-213.
- [77] L. Krasemann, B. Tieke. Selective ion transport across self-assembled alternating multilayers of cationic and anionic polyelectrolytes. *Langmuir*. **2000**; 16 (2), 287-290.

- [78] R. V. Klitzing, B. Tieke. Polyelectrolyte Membranes. *Advances in Polymer Science* 2004:177-210.
- [79] S. T. Dubas, J. B. Schlenoff. Factors controlling the growth of polyelectrolyte multilayers. *Macromolecules*. **1999**; 32 (24), 8153-8160.
- [80] R. Steitz, W. Jaeger, R. V. Klitzing. Influence of charge density and ionic strength on the multilayer formation of strong polyelectrolytes. *Langmuir*. **2001**; 17 (15), 4471-4474.
- [81] M. Salomäki, P. Tervasmäki, S. Areva, J. Kankare. The Hofmeister anion effect and the growth of polyelectrolyte multilayers. *Langmuir*. **2004**; 20 (9), 3679-3683.
- [82] K. Glinel, A. Moussa, A. M. Jonas, A. Laschewsky. Influence of polyelectrolyte charge density on the formation of multilayers of strong polyelectrolytes at low ionic strength. *Langmuir*. **2002**; 18 (4), 1408-1412.
- [83] B. Schoeler, G. Kumaraswamy, F. Caruso. Investigation of the influence of polyelectrolyte charge density on the growth of multilayer thin films prepared by the layer-by-layer technique. *Macromolecules*. **2002**; 35 (3), 889-897.
- [84] J. Choi, M. F. Rubner. Influence of the degree of ionization on weak polyelectrolyte multilayer assembly. *Macromolecules*. **2005**; 38 (1), 116-124.
- [85] S. S. Shiratori, M. F. Rubner. pH-dependent thickness behavior of sequentially adsorbed layers of weak polyelectrolytes. *Macromolecules*. **2000**; 33 (11), 4213-4219.
- [86] E. Poptoshev, B. Schoeler, F. Caruso. Influence of solvent quality on the growth of polyelectrolyte multilayers. *Langmuir*. **2004**; 20 (3), 829-834.
- [87] K. Büscher, K. Graf, H. Ahrens, C. A. Helm. Influence of adsorption conditions on the structure of polyelectrolyte multilayers. *Langmuir*. **2002**; 18 (9), 3585-3591.
- [88] H. L. Tan, M. J. McMurdo, G. Pan, P. G. Van Patten. Temperature Dependence of Polyelectrolyte Multilayer Assembly. *Langmuir*. **2003**; 19 (22), 9311-9314.
- [89] M. Gopinadhan, H. Ahrens, J. U. Günther, R. Steitz, C. A. Helm. Approaching the precipitation temperature of the deposition solution and the effects on the internal order of polyelectrolyte multilayers. *Macromolecules*. **2005**; 38 (12), 5228-5235.
- [90] Y. Lvov, G. Decher, H. Möhwald. Assembly, structural characterization, and thermal behavior of layer-by-layer deposited ultrathin films of poly(vinyl sulfate) and poly(allylamine). *Langmuir*. **1993**; 9 (2), 481-486.
- [91] S. T. Dubas, J. B. Schlenoff. Polyelectrolyte multilayers containing a weak polyacid: Construction and deconstruction. *Macromolecules*. **2001**; 34 (11), 3736-3740.
- [92] Z. Sui, D. Salloum, J. B. Schlenoff. Effect of molecular weight on the construction of polyelectrolyte multilayers: Stripping versus sticking. *Langmuir*. **2003**; 19 (6), 2491-2495.

- [93] R. Kügler, J. Schmitt, W. Knoll. The swelling behavior of polyelectrolyte multilayers in air of different relative humidity and in water. *Macromolecular Chemistry and Physics*. **2002**; 203 (2), 413-419.
- [94] J. E. Wong, F. Rehfeldt, P. Hanni, M. Tanaka, R. V. Klitzing. Swelling behavior of polyelectrolyte multilayers in saturated water vapor. *Macromolecules*. **2004**; 37 (19), 7285-7289.
- [95] M. Müller, S. Heinen, U. Oertel, K. Lunkwitz. Adsorption of poly(N-ethyl-4-vinyl pyridinium bromide) onto Langmuir-Blodgett films built up from amphiphilic polymers. *Macromolecular Symposia*. **2001**; 164, 145-158.
- [96] L. Zhai, A. J. Nolte, R. E. Cohen, M. F. Rubner. PH-Gated porosity transitions of polyelectrolyte multilayers in confined geometries and their application as tunable Bragg reflectors. *Macromolecules*. **2004**; 37 (16), 6113-6123.
- [97] J. Hiller, M. F. Rubner. Reversible molecular memory and pH-switchable swelling transitions in polyelectrolyte multilayers. *Macromolecules*. **2003**; 36 (11), 4078-4083.
- [98] S. T. Dubas, J. B. Schlenoff. Swelling and smoothing of polyelectrolyte multilayers by salt. *Langmuir*. **2001**; 17 (25), 7725-7727.
- [99] R. A. McAloney, V. Dudnik, M. C. Goh. Kinetics of salt-induced annealing of a polyelectrolyte multilayer film morphology. *Langmuir*. **2003**; 19 (9), 3947-3952.
- [100] R. Steitz, V. Leiner, K. Tauer, V. Khrenov, R. V. Klitzing. Temperature-induced changes in polyelectrolyte films at the solid-liquid interface. *Applied Physics A: Materials Science and Processing*. **2002**; 74 (SUPPL.I).
- [101] H. Ahrens, K. Büscher, D. Eck, S. Förster, C. Luap, G. Papastavrou, J. Schmitt, R. Steitz, C. A. Helm. Poly(styrene sulfonate) self-organization: Electrostatic and secondary interactions. *Macromolecular Symposia*; 2004; 2004. p. 93-105.
- [102] G. Schneider, G. Decher. Functional core/shell nanoparticles via layer-by-layer assembly. Investigation of the experimental parameters for controlling particle aggregation and for enhancing dispersion stability. *Langmuir*. **2008**; 24 (5), 1778-1789.
- [103] R. Bawa, S. R. Bawa, S. B. Maebius, T. Flynn, C. Wei. Protecting new ideas and inventions in nanomedicine with patents. *Nanomedicine: Nanotechnology, Biology, and Medicine*. **2005**; 1 (2), 150-158.
- [104] N. C. Institute. Nanoparticles. In: N. C. Institute, ed. *Dictionary of Cancer Terms* 2011.
- [105] M. Auffan, J. Rose, J. Y. Bottero, G. V. Lowry, J. P. Jolivet, M. R. Wiesner. Towards a definition of inorganic nanoparticles from an environmental, health and safety perspective. *Nature Nanotechnology*. **2009**; 4 (10), 634-641.

- [106] Y. Malam, M. Loizidou, A. M. Seifalian. Liposomes and nanoparticles: nanosized vehicles for drug delivery in cancer. *Trends in Pharmacological Sciences*. **2009**; 30 (11), 592-599.
- [107] B. S. Sekhon, S. R. Kamboj. Inorganic nanomedicine-Part 2. *Nanomedicine: Nanotechnology, Biology, and Medicine*. **2010**; 6 (5), 612-618.
- [108] M. Yezhelyev, R. Yacoub, R. O'Regan. Inorganic nanoparticles for predictive oncology of breast cancer. *Nanomedicine*. **2009**; 4 (1), 83-103.
- [109] Z. P. Xu, Q. H. Zeng, G. Q. Lu, A. B. Yu. Inorganic nanoparticles as carriers for efficient cellular delivery. *Chemical Engineering Science*. **2006**; 61 (3), 1027-1040.
- [110] H. Maeda, G. Y. Bharate, J. Daruwalla. Polymeric drugs for efficient tumor-targeted drug delivery based on EPR-effect. *European Journal of Pharmaceutics and Biopharmaceutics*. **2009**; 71 (3), 409-419.
- [111] S. Parveen, S. K. Sahoo. Polymeric nanoparticles for cancer therapy. *Journal of Drug Targeting*. **2008**; 16 (2), 108-123.
- [112] E. M. Pridgen, R. Langer, O. C. Farokhzad. Biodegradable, polymeric nanoparticle delivery systems for cancer therapy. *Nanomedicine*. **2007**; 2 (5), 669-680.
- [113] G. N. C. Chiu, M. Y. Wong, L. U. Ling, I. M. Shaikh, K. B. Tan, A. Chaudhury, B. J. Tan. Lipid-based nanoparticulate systems for the delivery of anti-cancer drug cocktails: Implications on pharmacokinetics and drug toxicities. *Current Drug Metabolism*. **2009**; 10 (8), 861-874.
- [114] S. Mukherjee, S. Ray, R. S. Thakur. Solid lipid nanoparticles: A modern formulation approach in drug delivery system. *Indian Journal of Pharmaceutical Sciences*. **2009**; 71 (4), 349-358.
- [115] A. J. Almeida, E. Souto. Solid lipid nanoparticles as a drug delivery system for peptides and proteins. *Advanced Drug Delivery Reviews*. **2007**; 59 (6), 478-490.
- [116] T. Kaasgaard, T. L. Andresen. Liposomal cancer therapy: Exploiting tumor characteristics. *Expert Opinion on Drug Delivery*. **2010**; 7 (2), 225-243.
- [117] R. M. Schiffelers, G. Storm. Liposomal nanomedicines as anticancer therapeutics: Beyond targeting tumor cells. *International Journal of Pharmaceutics*. **2008**; 364 (2), 258-264.
- [118] R. Fanciullino, J. Ciccolini. Liposome-encapsulated anticancer drugs: Still waiting for the magic bullet? *Current Medicinal Chemistry*. **2009**; 16 (33), 4361-4373.
- [119] D. B. Fenske, P. R. Cullis. Liposomal nanomedicines. *Expert Opinion on Drug Delivery*. **2008**; 5 (1), 25-44.
- [120] A. Samad, Y. Sultana, M. Aqil. Liposomal drug delivery systems: An update review. *Current Drug Delivery*. **2007**; 4 (4), 297-305.

- [121] L. A. Bentolila, Y. Ebenstein, S. Weiss. Quantum dots for in vivo small-animal imaging. *Journal of Nuclear Medicine*. **2009**; 50 (4), 493-496.
- [122] A. M. Smith, H. Duan, A. M. Mohs, S. Nie. Bioconjugated quantum dots for in vivo molecular and cellular imaging. *Advanced Drug Delivery Reviews*. **2008**; 60 (11), 1226-1240.
- [123] S. R. Ji, C. Liu, B. Zhang, F. Yang, J. Xu, J. Long, C. Jin, D. L. Fu, Q. X. Ni, X. J. Yu. Carbon nanotubes in cancer diagnosis and therapy. *Biochimica et Biophysica Acta - Reviews on Cancer*. **2010**; 1806 (1), 29-35.
- [124] H. Xu, J. Meng, H. Kong. What are carbon nanotubes' roles in anti-tumor therapies? *Science China Chemistry*. **2010**; 53 (11), 2250-2256.
- [125] Y. Cheng, Z. Xu, M. Ma, T. Xu. Dendrimers as drug carriers: Applications in different routes of drug administration. *Journal of Pharmaceutical Sciences*. **2008**; 97 (1), 123-143.
- [126] S. Svenson, D. A. Tomalia. Dendrimers in biomedical applications - Reflections on the field. *Advanced Drug Delivery Reviews*. **2005**; 57 (15), 2106-2129.
- [127] P. P. Adiseshiaiah, J. B. Hall, S. E. McNeil. Nanomaterial standards for efficacy and toxicity assessment. *Wiley Interdisciplinary Reviews: Nanomedicine and Nanobiotechnology*. **2010**; 2 (1), 99-112.
- [128] R. Duncan. The dawning era of polymer therapeutics. *Nature Reviews Drug Discovery*. **2003**; 2 (5), 347-360.
- [129] M. Wang, M. Thanou. Targeting nanoparticles to cancer. *Pharmacological Research*. **2010**; 62 (2), 90-99.
- [130] J. D. Byrne, T. Betancourt, L. Brannon-Peppas. Active targeting schemes for nanoparticle systems in cancer therapeutics. *Advanced Drug Delivery Reviews*. **2008**; 60 (15), 1615-1626.
- [131] E. E. Connor, J. Mwamuka, A. Gole, C. J. Murphy, M. D. Wyatt. Gold nanoparticles are taken up by human cells but do not cause acute cytotoxicity. *Small*. **2005**; 1 (3), 325-327.
- [132] Y.-S. Chen, Y.-C. Hung, I. Liau, G. S. Huang. Assessment of the In Vivo Toxicity of Gold Nanoparticles. *Nanoscale Research Letters*. **2009**; 4 (8), 858-864.
- [133] A. C. Templeton, W. P. Wuelfing, R. W. Murray. Monolayer-protected cluster molecules. *Accounts of Chemical Research*. **2000**; 33 (1), 27-36.
- [134] H. I. Labouta, M. Schneider. Tailor-made biofunctionalized nanoparticles using layer-by-layer technology. *International Journal of Pharmaceutics*. **2010**; 395 (1-2), 236-242.

- [135] S. D. Perrault, C. Walkey, T. Jennings, H. C. Fischer, W. C. W. Chan. Mediating tumor targeting efficiency of nanoparticles through design. *Nano Letters*. **2009**; 9 (5), 1909-1915.
- [136] M. Brust, M. Walker, D. Bethell, D. J. Schiffrin, R. Whyman. Synthesis of thiol-derivatised gold nanoparticles in a two-phase liquid-liquid system. *Journal of the Chemical Society, Chemical Communications*. **1994**; (7), 801-802.
- [137] J. Turkevich, P. C. Stevenson, J. Hillier. A study of the nucleation and growth processes in the synthesis of colloidal gold. *Discussions of the Faraday Society*. **1951**; 11, 55-75.
- [138] L. M. Liz-Marzan. Nanometals: Formation and color. *Materials Today*. **2004**; 7 (2), 26-31.
- [139] P. Ghosh, G. Han, M. De, C. K. Kim, V. M. Rotello. Gold nanoparticles in delivery applications. *Advanced Drug Delivery Reviews*. **2008**; 60 (11), 1307-1315.
- [140] P. K. Jain, I. H. ElSayed, M. A. El-Sayed. Au nanoparticles target cancer. *Nano Today*. **2007**; 2 (1), 18-29.
- [141] M. M. C. Cheng, G. Cuda, Y. L. Bunimovich, M. Gaspari, J. R. Heath, H. D. Hill, C. A. Mirkin, A. J. Nijdam, R. Terracciano, T. Thundat, M. Ferrari. Nanotechnologies for biomolecular detection and medical diagnostics. *Current Opinion in Chemical Biology*. **2006**; 10 (1), 11-19.
- [142] N. L. Rosi, C. A. Mirkin. Nanostructures in biodiagnostics. *Chemical Reviews*. **2005**; 105 (4), 1547-1562.
- [143] C. M. Niemeyer, C. A. Mirkin. *Nanobiotechnology*. Weinheim: Wiley-VCH **2004**.
- [144] T. Laaksonen. *Monolayer Protected Clusters: Electrostatics, Stability and Applications*. Helsinki: Helsinki University of Technology; 2007.
- [145] B. Mishra, B. B. Patel, S. Tiwari. Colloidal nanocarriers: a review on formulation technology, types and applications toward targeted drug delivery. *Nanomedicine: Nanotechnology, Biology, and Medicine*. **2010**; 6 (1).
- [146] G. F. Schneider, V. Subr, K. Ulbrich, G. Decher. Multifunctional cytotoxic stealth nanoparticles. A model approach with potential for cancer therapy. *Nano Letters*. **2009**; 9 (2), 636-642.

4 Chapter 2: Polymer-drug complex

Non-covalent drug- polyelectrolyte complex as new approach for drug delivery of water-insoluble photosensitizers*

This chapter is prepared for publication as a journal article:

Nico Reum, Judith Pohl, Beate Röder, Marc Schneider . Non-covalent drug-polyelectrolyte complex as new approach for drug delivery of water-insoluble photosensitizers.

Abstract:

Photosensitizers are used in photodynamic therapy (PDT) as promising treatment method of solid tumors. To avoid low bioavailability as well as side effects caused by the insolubility of the photosensitizers in water, we have prepared a water soluble complex consisting of the water insoluble photosensitizer 5,10,15,20-tetrakis(3-hydroxyphenyl)chlorin (mTHPC) non-covalently attached to the polyelectrolyte poly(styrene sulfonate) sodium salt (PSS). The complex preparation with the highest drug loading was carried out by freeze-drying an ethanolic/aqueous (1:1 v/v) mixture of both compounds. The complexation efficiency determined by UV/vis measurement and CHNS elemental analysis was 11 ± 2 monomer units or 4-ethyl(styrene sulfonate) sodium salt (ESS) units of PSS to complex one mTHPC molecule independent of PSS molecular weight. The photophysical characterization resulted in a decreased singlet oxygen quantum yield of the complex compared to free mTHPC but in an increased phototoxicity. No toxicity of PSS could be observed in vitro indicating that the PSS/mTHPC complex has great prospects to become a potential drug delivery system for mTHPC, especially due to its simple and quick preparation.

4.1 Introduction

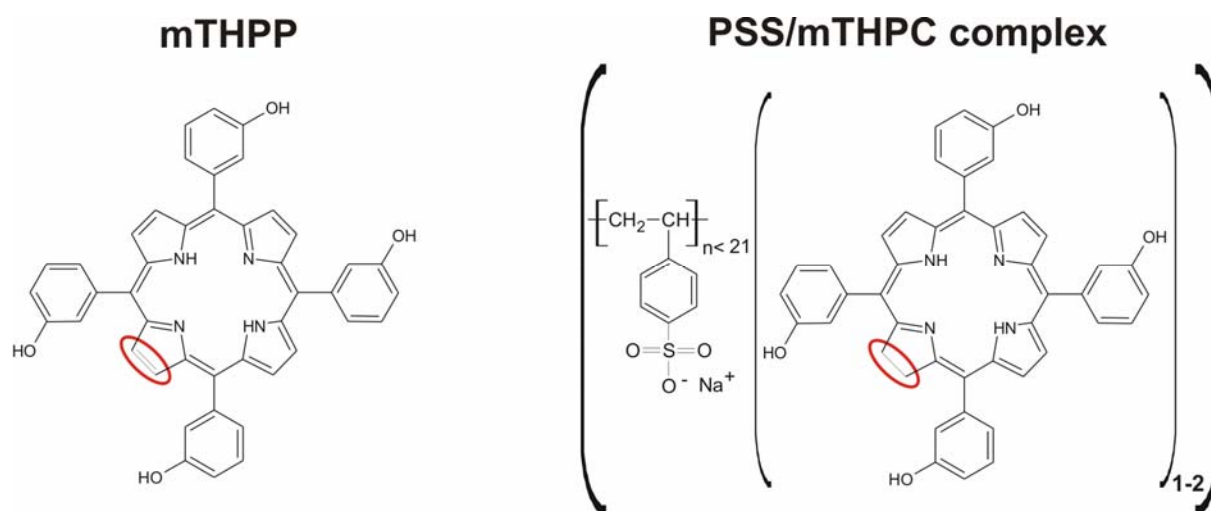
Photodynamic therapy (PDT) is an established minimally invasive therapeutic modality approved for clinical treatment of several types of cancer and non-oncological disorders [1, 2]. PDT treatment is based on the presence of a drug with photosensitizing properties (photosensitizer) combined with visible or infrared light and tissue oxygen. The activation of the photosensitizer by light generates reactive oxygen species, such as singlet oxygen, responsible for direct or indirect destruction of tumor cells. The cell death occurs mainly by the induction of apoptosis and necrosis [3, 4].

The application of PDT technique clearly requires systemic delivery of photosensitizers. Unfortunately, the extended delocalized aromatic π -electron system characterizing photosensitizers generally makes them highly hydrophobic and thus poorly water soluble and prone to aggregation and precipitation in aqueous solution [5-7]. The resulting disadvantage is the decrease of their ability to efficiently generate singlet oxygen in combination with multifarious other intrinsic drawbacks such as the poor bioavailability combined with unfavorable biodistribution, the non-selective tumor specificity, and respectively undesirable side effects such as prolonged skin phototoxicity of up to two weeks and damage to surrounding healthy tissues [8, 9].

To solve the problems, a lot of promising studies were carried out using photosensitizer conjugates [5, 10] or nanoparticles [11-14] as drug delivery systems with the aim to increase the water solubility of the photosensitizers and the specificity to the tumor tissue caused by receptor-mediated endocytosis [15] or the EPR effect [16]. Nevertheless, the elaborated and time-consuming preparation is a big disadvantage for the nanoparticulate-based approaches. Whereas, the drawback of the photosensitizer conjugates is caused by the covalent bond between the drug and the excipient resulting in a reduced drug activity and delayed release [10, 12]. For photosensitizers, a fast release is aspired to avoid side effects [13].

As a simple and novel carrier system, we formed a coadsorbate between the photosensitizer and the polyelectrolyte poly(styrene sulfonate) (PSS). The advantages of PSS are the very good water solubility in combination with the hydrophobic π -system allowing for non-covalent attachment of the photosensitizer, and the established administration for pharmaceutical applications [17]. As drug was used the second generation photosensitizer [12] 5,10,15,20-tetrakis(3-

hydroxyphenyl)chlorin (mTHPC) and its low cost model drug 5,10,15,20-tetrakis(3-hydroxyphenyl)porphyrin (mTHPP) for the physico-chemical characterization (Scheme 1). The drug was non-covalently coupled to PSS by H-bonds and π - π interaction. The preparation technique, the influence of the PSS molecular weight, the complexation efficiency, and the photophysical properties of the resulting PSS/mTHPC coadsorbates were investigated in this study. The overall preserved photosensitizing ability after complexation could be demonstrated for PSS/mTHPC *in vitro*.



Scheme 1: Structural formula of mTHPP and PSS/mTHPC complex (4.3 kDa).

4.2 Materials and methods

4.2.1 Materials

The 5,10,15,20-tetrakis(3-hydroxyphenyl)porphyrin, mTHPP, (MW 678.73 g/mol) and 5,10,15,20-tetrakis(3-hydroxyphenyl)chlorin, mTHPC, (MW 680.75 g/mol) seen in **Scheme 1** were kindly provided by biolitec AG (Jena, Germany). Poly(styrene sulfonate) sodium salt (PSS) (MW 0.21, 4.3, 13, 32.9, and 152 kDa) was purchased from Sigma-Aldrich (Steinheim, Germany). PSS with MW 1.10, and 1.92 kDa was purchased from Polymer Standards Service GmbH (Mainz, Germany). The water used in all experiments was prepared in a Millipore Milli-Q purification system (resistivity higher than 18.0 M Ω /cm).

4.2.2 Methods

4.2.2.1 PSS/mTHPP complexation efficiency

A fixed mass of mTHPP (77 μg) in 2 mL ethanol was added to different masses of PSS with molecular weight of 4.3 kDa (92, 184, 500, 922, 1844, 5001 mg) in 2 mL water, to check if complex formation occurs. After mixing, the solution was freeze-dried in a Christ Alpha 2-4 LSC (Christ GmbH, Osterode, Germany). The lyophilisate was suspended in water and centrifuged for 35 min at 16,098 g with a table centrifuge, Hettich Rotina 420 R (Hettich GmbH & Co. KG, Tuttlingen, Germany). The supernatant was filtered to remove the free mTHPP. The pellet of centrifugation, the filters and all other materials which were in contact with the complex mixture were rinsed out with ethanol, which was collected and pooled to determine the concentration of free or not complexed mTHPP. The concentration of mTHPP in ethanol was obtained by UV/vis spectroscopy (5 relevant peaks: $\lambda_{\text{ex}} \in \{416, 512, 546, 589, 645\}$ nm) (PerkinElmer Lambda 35, PerkinElmer LAS, Rodgau, Germany). The mass of mTHPP in ethanol subtracted from initial weight of mTHPP (77 μg) is the mass of the mTHPP transferred to the aqueous phase in a complex with PSS.

To determine how many monomer units (4-ethyl(benzene sulfonate) sodium salt (ESS) units) of PSS are necessary to complex one mTHPP molecule, around 50 mg of the corresponding PSS (MW 0.21, 1.10, 1.92, 4.3, 13, 32.9, and 152 kDa) was dissolved in 5 mL water. Each aqueous solution of PSS was mixed with 20 mg of mTHPP in 5 mL ethanol. The mixtures were freeze-dried and purified like described before. The efficiency of complexation was determined by UV/vis measurement.

To investigate additional procedures for successful complex formation between PSS and mTHPP further experiments were carried out. Freeze-drying with a mixture of PSS and mTHPP in water instead of a water/ethanol, simple stirring of both compounds in water and also the evaporation of an ethanolic/aqueous (1:3 v/v) solution with PSS and mTHPP were checked for their complexation efficiency.

4.2.2.2 Preparation of PSS/mTHPC complex

A similar procedure was before described by Reum et al [18] for mTHPP loaded to colloidal gold. In this study, however, we used the approved drug for head and neck cancer mTHPC. 50.14 mg (7.37 μmol) of PSS (MW = 4,300 g/mol) was dissolved in 15 mL water. 21.75 mg (31.95 μmol) of mTHPC was dissolved in 15 mL ethanol. Both solutions were mixed and freeze-dried in a Christ Alpha 2-4 LSC (Christ GmbH,

Osterode, Germany). To obtain maximum complexation, the drug mTHPC was used in excess. Hence, not all of the drug could be complexed with the PSS necessitating a purification step after the freeze-drying. Therefore, the lyophilisate was suspended in 50 mL of water and centrifuged for 35 min at 16,098 g with a table centrifuge, Hettich Rotina 420 R (Hettich GmbH & Co. KG, Tuttlingen, Germany). The supernatant was filtered and refilled with water to 50 mL. The pellet of centrifugation, the filters and all other materials which were in contact with the complex mixture were rinsed out with 50 mL ethanol which was collected to determine the concentration of free or not complexed mTHPC. The concentration of mTHPC in ethanol was obtained by UV/vis spectroscopy (5 relevant peaks: $\lambda_{\text{ex}} \in \{417, 517, 542, 597, 650\}$ nm) (PerkinElmer Lambda 35, PerkinElmer LAS, Rodgau, Germany). The mass of mTHPC in ethanol subtracted from the initial weight of mTHPC (21.75 mg) is the mTHPC mass in water complexed with PSS. The concentrations of PSS (4.3 kDa) and mTHPC complexed in water were determined directly by CHNS elemental analysis.

4.2.2.3 Characterization of PSS/mTHPC coadsorbate

4.2.2.3.1 Docking study

Molecular docking simulations were carried out to simulate, predict, and better understand the interactions between the drug (mTHPC) and the polyelectrolyte carrier (PSS). All calculations were performed on Intel(R) Core(TM) 2 Duo CPU 3.00 GHz running Linux CentOS 5.3. 3-dimensional structures of both mTHPC and PSS were generated using MOE2008.10 (Chemical Computing Group Inc., Montreal, Canada). For simplification, the PSS molecule was depicted as a nine monomer unit. The structures were energy minimized with the MMFF94 force field as implemented in MOE. Ionization states and hydrogen positions were assigned using the protonate 3D utility of MOE. AutoDock-Tools4 [19] was used for input files preparation and AutoDock Vina, version 1.0 [20] was used to dock mTHPC in the structure of PSS: 60 binding modes were produced with an exhaustiveness parameter of 100.

4.2.2.3.2 CHNS elemental analysis

The elemental analysis of freeze-dried PSS (4.3 kDa), mTHPC, and PSS/mTHPC complex was performed. Carbon, hydrogen, nitrogen, and sulfur were analyzed by universal elemental analyzer vario El III (Elementar Analysensysteme GmbH, Hanau, Germany). Samples were weighed into tin boats, compressed and taken to the auto sampler, where they are dropped into the combustion tube automatically. Calibration curves of sulfanilic acid as reference compound (C: 41.6, H: 4.1, N: 8.1 and S: 18.5 wt-%) were compiled by manufacturer and daytime factor measurements were repeated six times with weighed samples of about 5 mg. Each freeze-dried sample was measured three times. The theoretical calculation of the percentage of elements of mTHPC and PSS was done on the basis of their structural formula (Supplementary data).

4.2.2.3.3 UV-visible spectroscopy measurements

The amounts of mTHPP and mTHPC in the drug complex were determined indirectly based on UV/vis spectroscopy. Therefore, the concentration of mTHPP and mTHPC in the organic solution (ethanol) was determined (see 2.2.1. and 2.2.3.) from which the aqueous concentrations could be calculated. All measurements were carried out in 1 cm quartz cuvettes with the Perkin Elmer Lambda 35 Spectrophotometer (Perkin Elmer LAS, Rodgau, Germany).

4.2.2.3.4 Singlet oxygen measurements

Time resolved singlet oxygen luminescence measurements were carried out using a nanosecond ND³⁺-YAG laser (BM Industries, Evry Cedex, France) with an attached optical parametric oscillator (OPO, Ekspla, 420-2500 nm). For the spectral selection of the emitted light an 800 nm edge filter and a 1270 nm interference filter was used. The singlet oxygen emission was detected using a liquid nitrogen cooled Ge-PIN diode (North Coast, Inc.; Santa Rosa CA). The PSS/mTHPC complex was dissolved in D₂O and the mTHPC was dissolved in ethanol. The optical density was adjusted to 0.2 at the excitation wavelength of 548 nm. Rose Bengal served as reference standard for the determination of singlet oxygen quantum yield (QY = 0.76).

4.2.2.3.5 Photodynamic activity and cytotoxicity

To determine the phototoxicity of pure mTHPC and the polyelectrolyte complex, Jurkat cells (clone E 6-1 human acute T-cell leukaemia) were cultured in RPMI 1640 medium with L-glutamine (PAA, Pasching, Austria) supplemented with 10% fetal calf serum (FCS), 50 U/mL of penicillin and 500 µg/mL streptomycin without phenol red [21]. 1 ml Jurkat cell suspension ($\sim 2\text{--}3 \cdot 10^5$ cells/mL) per well was placed on a 24-well plate and incubated with pure mTHPC ($c_{\text{mTHPC}} = 3 \text{ µmol/L}$), the polyelectrolyte (PSS Mw = 4.3 kDa with $c_{\text{PSS}} = 1.8 \text{ µmol/L}$) equal to the PSS concentration in the complex with $c_{\text{mTHPC}} = 3 \text{ µmol/L}$, and the complex at a concentration of 3 µmol/L mTHPC. The ethanol concentration in the cell suspension was 0.3% for better solubility of the pure drug. For this value no toxicity was observed. The incubation times were 1 h, 3 h, 5 h, and 24 h.

For irradiation a laser diode with $\lambda_{\text{em}} = 668 \text{ nm}$ was used. The irradiation power was 120 mW/cm^2 . The living and dead cell numbers were counted after additional 2 h incubation using a hemocytometer under an inverse microscope CKX 41 (Olympus, Hamburg).

4.3 Results and Discussion

4.3.1 PSS/mTHPP complexation efficiency

First of all, an experiment has to be carried out to show that PSS can complex the drug mTHPP increasing the solubility in water. Therefore, different concentrated aqueous PSS ($MW_{\text{PSS}} = 4,300 \text{ g/mol}$) solutions were mixed with an ethanolic mTHPP solution of a fixed mTHPP concentration and freeze-dried. As expected, the higher the PSS concentration the higher was the mTHPP concentration determined in water (Figure 1). This effect could be explained by π - π interactions [22] between the PSS molecules with the mTHPP molecules which is an explicit hint for the successful complex formation of a water soluble complex.

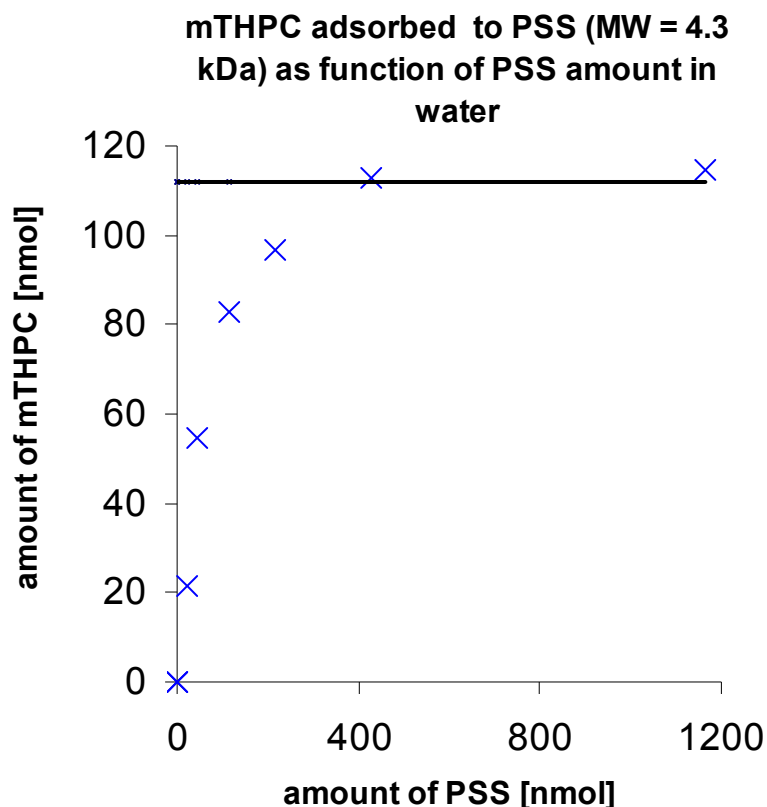


Figure 1: Solubility enhancement of mTHPP in water as function of PSS (4.3 kDa) amount added to 77 μg mTHPP, shown results after freeze drying and complex purification.

The complexation efficiency of mTHPC with PSS is defined as the needful number of monomer units (4-ethyl(styrene sulfonate) sodium salt) (ESS, MW = 208 g/mol) to complex one mTHPP molecule. PSS with a molecular weight of 4,300 g/mol is composed of 21 EES units. The aim was to find the method and the conditions for the highest complexation efficiency between PSS and mTHPP, which was used as low cost drug alternative to mTHPC.

For the determination of the complexation efficiency by UV/vis measurement the amount of substance ratio between both compounds was chosen to be 1:2.5 (PSS:mTHPP). The excess of mTHPP compared to PSS was necessary to obtain a maximum complexation of mTHPP to PSS. To control the influence of the PSS molecular weight, different chain length of PSS (MW 0.21, 1.10, 1.92, 4.3, 13, 32.9, and 152 kDa) were complexed with the drug. With the monomer of PSS (MW 0.21 kDa) it was not possible to form a complex with mTHPP. But with all other molecular weights of PSS (repeating units of PSS monomer: 5-740) a successful complex formation could be observed and the complexation efficiency was in each case

around 11 ± 2 monomer units of PSS for the complexation of one mTHPP molecule (Figure 2).

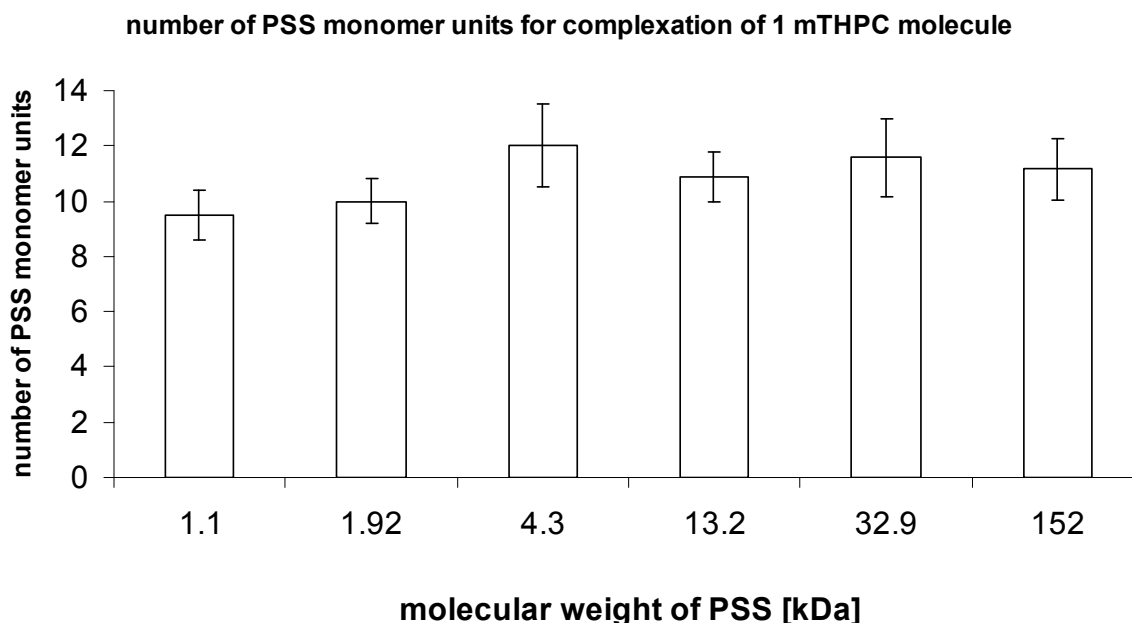


Figure 2: Complexation efficiency of different PSS molecular weights with mTHPP.

To find the highest complexation efficiency, several methods for complex formation were tested. For the evaporation of the mixture composed of ethanol/water (3:1 v/v), the complexation efficiency reached a value of 30 monomer units of PSS (Figure 3). Simple stirring of the aqueous suspension of PSS and mTHPP resulted in efficiency values dependent of the stirring time. The longer the stirring time the better was the complexation efficiency; after 12 days stirring at room temperature 142 monomers, after 22 days 67 monomers, and after 42 days 56 monomers of PSS were necessary to complex one mTHPP molecule (Figure 3). The best complexation efficiency with around 11 monomers was obtained by freeze-drying the ethanolic/aqueous mixture (1:1 v/v) followed by the evaporation method with 30 monomers but with the big disadvantage that it was necessary to evaporate the water. Therefore, a very careful handling and a long time interval for evaporation were essential. The stirring method was the most comfortable method but resulted in the worst complexation efficiency of 56 monomers, in addition, after a very long time of 42 days. Interestingly, the freeze-drying of both compounds only in water did not produce the complex because it seems to be essential that the drug is dissolved and homogeneously distributed with the polyelectrolyte during the freeze-drying process.

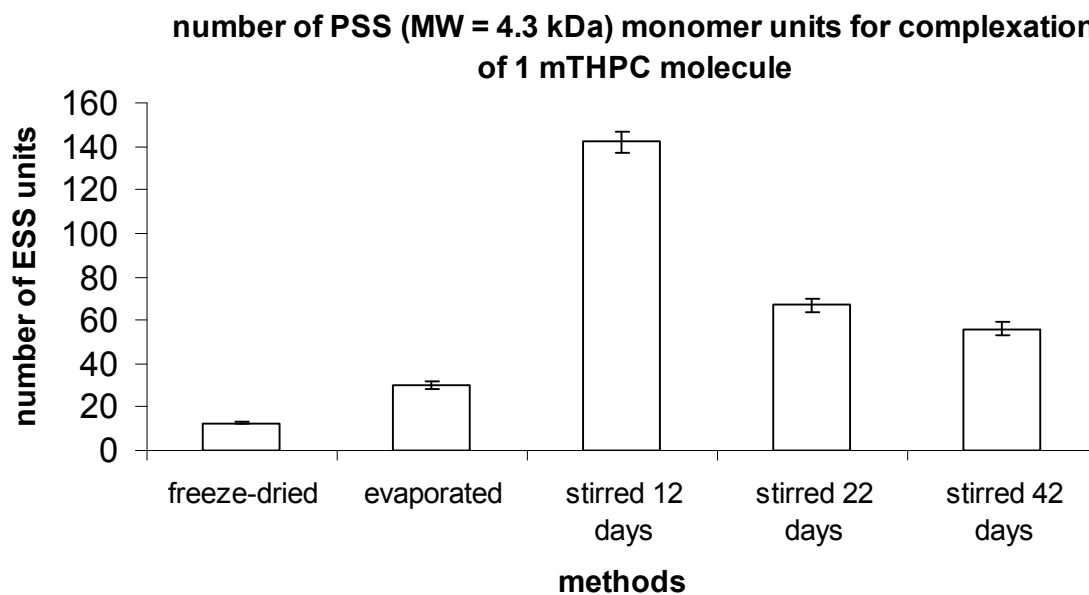


Figure 3: Complexation efficiency by different methods of complex preparation between PSS (4.3 kDa) and mTHPP.

Altogether the freeze-drying in an ethanolic/aqueous mixture was the most applicable procedure to complex the drug mTHPP to the polyelectrolyte PSS. The 4-ethyl(styrene sulfonate) sodium salt (ESS) or the monomer of the PSS could not complex the drug. For all the other different molecular weights of PSS, between 1.1 kDa and 152 kDa which is equal to 5 and 740 ESS units of the respective PSS the complexation efficiency resulted in 11 ± 2 monomers of PSS to complex one mTHPP molecule.

4.3.2 Preparation and characterization of PSS/mTHPC complex

The mTHPP which is a model substance for mTHPC was used to find the general conditions for the complexation with PSS because it is much cheaper than the mTHPC. Nevertheless, the mTHPC is the approved drug showing the needed biological activity by the high intersystem crossing yield. To enable a renal clearance of PSS, a small molecular weight of 4.3 kDa for the PSS was chosen. That is why a preparation and characterization of a complex between PSS with a molecular weight of 4.3 kDa and mTHPC were carried out.

To prepare the PSS/mTHPC complex, the freeze-drying method with the mixture of ethanol and water as the most efficient approach (determined with mTHPP) was

used. As expected only a part of mTHPC was complexed with PSS in water (pH value of 7.4) because the drug was used in excess compared to PSS to obtain a complete complexation of PSS. It seemed that more than half the mass of mTHPC could be not complexed with PSS because the mTHPC signal in ethanol has a higher absorbance compared to the mTHPC in water (Figure 4). However, the successful complex preparation was demonstrated by means of UV/vis measurement because the water solubility of mTHPC was dramatically increased. A further observation from the UV/vis spectra was the bathochromic shift (4-8 nm) of the absorption spectrum of mTHPC in water compared to that in ethanol which can be explained by the different polarity of the solvents (Figure 4).

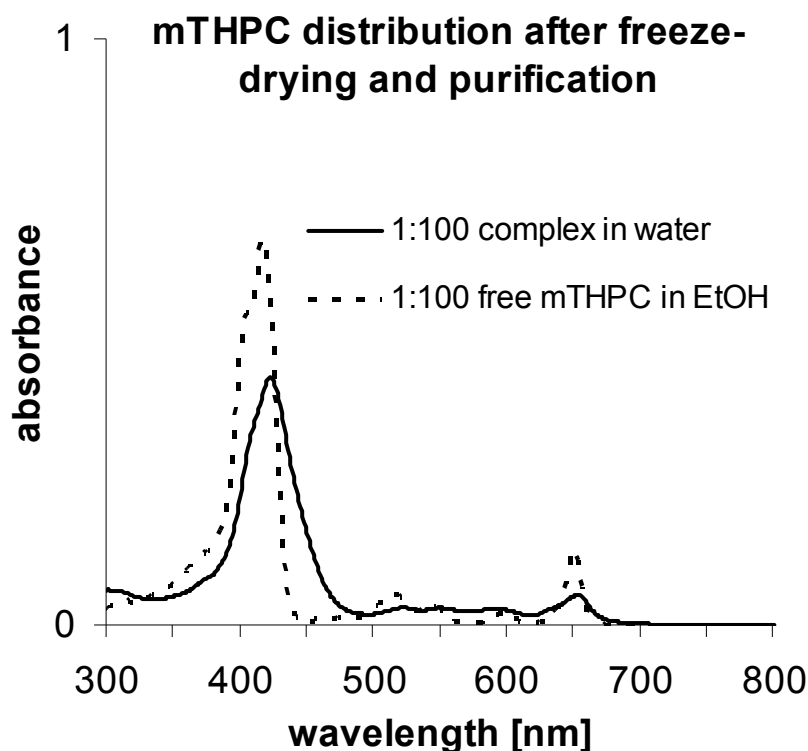


Figure 4: UV/vis spectra of complexed mTHPC in water 1:100 dilution (black solid line), free or uncomplexed mTHPC in ethanol 1:100 dilution (black dashed line); both samples after freeze-drying, centrifugation, and filtration.

As the activity depends also on the attachment of the drug to the PSS the aim was a non-covalent association of the drug to the polyelectrolyte (PE) PSS. Therefore, PSS was chosen because of its benzene rings in the molecule which can interact with the benzene rings in the mTHPC molecule [22]. To understand the interactions between

both molecules, molecular docking simulations were carried out. The first crude results were parallel displaced π - π interactions of benzene rings from PSS with the benzene- and pyrrole rings of mTHPC as well as H-bonds of OH- and NH-groups with the sulfonate groups (Figure 5) which lead to the successful complexation.

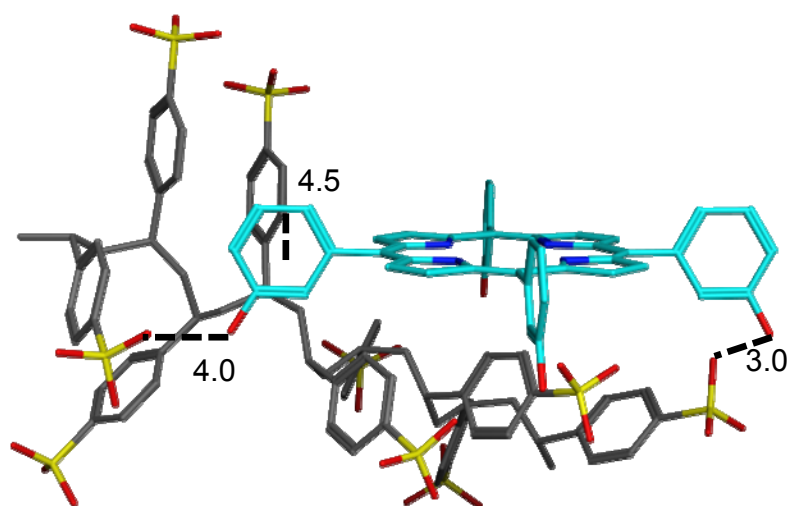


Figure 5: Docking complex between PSS (grey backbone) and mTHPC (cyan). The numbers indicate the distance between interacting groups in Angstrom.

For the complex PSS/mTHPC the determination of the complexation efficiency was also investigated. To facilitate future quantification a calculation by CHNS elemental analysis was carried out and then compared with the results obtained by UV/vis analysis. The percentage of nitrogen in the PSS/mTHPC complex allowed quantifying the amount of mTHPC and the percentage of sulfur reflects the amount of PSS. The total mass of mTHPC in the complex based on the mass percentage of the elements in the complex was determined with 12.22 mg and the total mass of PSS with 47.84 mg (Table 1). Correspondingly, the mass percentage of mTHPC in the complex was 20.34% and 79.66% of PSS respectively. The complexation efficiency determined by elemental analysis resulted in a value of 13 ESS units for

complexation of one mTHPC molecule. Compared to the complexation of mTHPP with PSS, the complex efficiency was similar but slightly lower. To our speculation the reason for that could be the reduced aromatic characteristic of the one pyrrole ring due to the hydrogenation of one double bond in the pyrrole ring of the mTHPC molecule. Therefore, the interaction between the heterocyclic ring and the benzene rings of PSS molecule could be reduced, which results in a lower complexation efficiency.

Table 1: Complex characteristics prepared with 50.14 mg PSS and 21.75 mg mTHPC by elemental analysis and UV/vis measurement (mean value \pm standard deviation (SD)).

parameter for complex	CHNS analysis	UV/vis
total mass _(mTHPC in complex) [mg] \pm SD	12.22 \pm 0.12	12.05 \pm 0.36
total mass _(PSS in complex) [mg] \pm SD	47.84 \pm 0.48	47.84 \pm 0.48
mass percentage _(mTHPC) [%] \pm SD	20.34 \pm 0.20	20.12 \pm 0.60
mass percentage _(PSS) [%] \pm SD	79.66 \pm 0.80	79.88 \pm 2.40
number of monomers pro mTHPC molecule \pm SD	12.93 \pm 0.13	13.11 \pm 0.39

A big advantage of the UV/vis measurement is the simple and cheap procedure being responsible for the omnipresence in research. The result 12.05 mg (Table 1) for the total mass of mTHPC in the complex determined by UV/vis analysis was obtained indirectly because mTHPC's insolubility in water impeded a calibration in water. Furthermore, it was not possible by UV/vis measurement to determine the PSS concentration in the complex because of overlapping absorption of PSS and mTHPC. Therefore, the total mass of PSS in the complex obtained by elemental analysis was used for further calculations. The mass percentage of mTHPC in the complex was 20.12% and of PSS 79.88%, respectively, resulting in a complexation efficiency of 13 ESS units for the complexation of one mTHPC. Hence, both analysis resulted in the same complexation efficiency of 13 ESS units. However, the CHNS elemental analysis was the more precise method because of the direct determination of PSS and mTHPC in the aqueous phase. Therefore, the PSS loss of 5.4% during

the complexation and purification procedure could be detected. Without this information, the total PSS mass used in this experiment would be used for the calculation of complexation efficiency by UV/vis analysis because PSS is not soluble in ethanol resulting in around 14 EES units for complexation of one mTHPC molecule. Nevertheless, the UV/vis method is suitable for determination of the complexation efficiency.

The challenge to prepare stable complexes with non-covalent attachment of the water insoluble drug mTHPC to the water soluble polyelectrolyte PSS to transfer the drug in aqueous medium was successfully achieved. The stability of the complexes was tested and no modifications concerning color, haze or sedimentation could be found over a period of one year. Molecular docking simulations indicated interactions between both molecules due to the π - π interactions and H-bonds. To complex one mTHPC molecule, around 13 ESS units of one PSS chain (4.3 kDa) were needed even though no molecular weight dependence was observed for the drug analogue.

4.3.3 Singlet oxygen measurements

The determination of the singlet oxygen quantum yield is essential as this value is an indication for the activity of the drug and hence, of the complex with PSS (4.3 kDa). As reference, Rose Bengal with a singlet quantum yield of 0.76 in D₂O was used [23]. The singlet oxygen quantum yield of the PSS/mTHPC complex in D₂O was 0.16 and 0.31 of free mTHPC in ethanol. The 50% reduction of the singlet oxygen quantum yield of the complex compared to the free mTHPC could be also observed for other photosensitizer-carrier systems [24] and is probably caused by interactions between the mTHPC and the polymer. Hence, the higher solubility of the complex will overcome the lower quantum yield.

4.3.4 Photodynamic activity and cytotoxicity

Besides the production of singlet oxygen the activity in biological systems is the most relevant parameter for a potential application. Therefore, the phototoxicity of the complex to Jurkat cells was ascertained. Compared to the reference (untreated cells) the PE carrier PSS (4.3 kDa) alone did not induce toxic effects (Figure 6). This beneficial result allowed the usage of PSS as drug carrier system. The phototoxicity of the free mTHPC and the complexed mTHPC was equal with around 45% survival

rate after 3 hours. After 5 hours incubation time, the free mTHPC showed an increased phototoxicity of 62%. The complex did not show such an increase in phototoxicity remaining at the 3 hours incubation level. However, 24 h after irradiation the highest phototoxicity was induced by the complex (79% compared to the free mTHPC with only 69%). Apoptosis and necrosis could be observed both contributing to the overall toxicity. Further detailed analysis is ongoing to better understand the mechanism of the complex interaction.

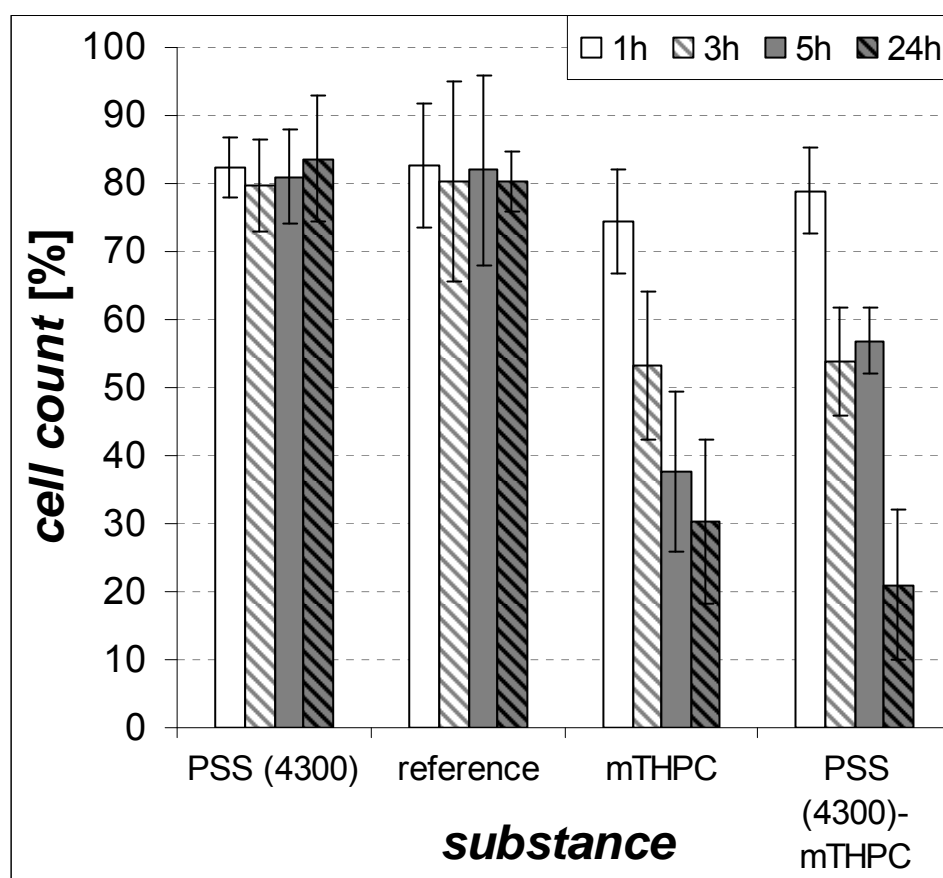


Figure 6: Survival rate of Jurkat cells after 1, 3, 5, and 24 hours incubation time with 3 μM mTHPC and PSS/mTHPC complex followed by irradiation with white light: Light source: Exposure time: 1 min; Light dose: 2 mJ/cm^2 . Error bars represent the standard deviation of nine measurements ($n = 9$).

4.4 Conclusion

Poly(styrene sulfonate) sodium salt (PSS) is a non-toxic drug delivery system for Jurkat cells (clone E 6-1 human acute T-cell leukemia). The successful preparation of the water soluble and non-covalent linked PSS/mTHPC complex was achieved with a complexation efficiency of around 13 monomer units (4-ethyl(styrene sulfonate) sodium salt) of PSS, independent of the PSS molecular weight, to complex one mTHPC molecule. The freeze-drying method of an ethanolic/aqueous (1:1 v/v) mixture with both compounds resulted in the highest complexation efficiency compared to other techniques, like just stirring or evaporation. The complex showed a lower singlet oxygen quantum yield in water than the free mTHPC in ethanol. The improved water solubility allowed however, an improved phototoxicity. This non-toxic polyelectrolyte (PE) carrier in combination with its ability to improve the water solubility of the photosensitizer mTHPC showed a very promising phototoxicity. Hence, this simply prepared PSS/mTHPC complex facilitates a potential application in photodynamic therapy. However, the biochemical stability, the immune reaction to the polyelectrolyte, and *in vivo* PDT effects still need to be investigated.

4.5 Supporting information

Table S1: UV/vis calibration of mTHPP in ethanol

Table S2: UV/vis calibration of mTHPC in ethanol

Figure S1: CHNS elemental analysis of PSS (n=3) with set point as theoretical value and with measurement as measured value.

Figure S2: CHNS elemental analysis mTHPC (n=3) with set point as theoretical value and with measurement as measured value.

Table S1: UV/vis calibration of mTHPP in ethanol

λ [nm]	$A = \varepsilon \cdot c \cdot d$, $\varepsilon \cdot d = x$ [$\mu\text{g/mL}$]	Correlation factor	Measurement range [$\mu\text{g/mL}$]
416.0	0.83128	0.9999	0.01 - 1
512.4	0.03019	0.9999	0.2 - 50
546.0	0.01082	0.9999	1.0 - 100
587.7	0.00871	0.9999	5.0 - 100
644.5	0.00493	0.9999	10.0 - 100

Table S2: UV/vis calibration of mTHPC in ethanol

lambda [nm]	$A = \varepsilon \cdot c \cdot d$, $\varepsilon \cdot d = x$ [$\mu\text{g/mL}$]	correlation factor	Measurement range [$\mu\text{g/mL}$]
417	0.28301	0.9999	0.1 - 5
517	0.06151	0.9999	2.0 - 50
542	0.02341	0.9999	5.0 - 50
597	0.01583	0.9999	10.0 - 100
650	0.00886	0.9999	10.0 - 20

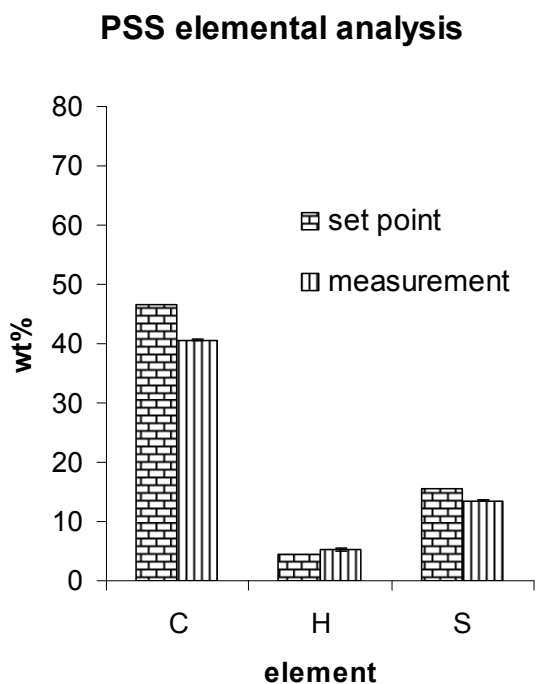


Figure S1: CHNS elemental analysis of PSS (n=3) with set point as theoretical value and with measurement as measured value.

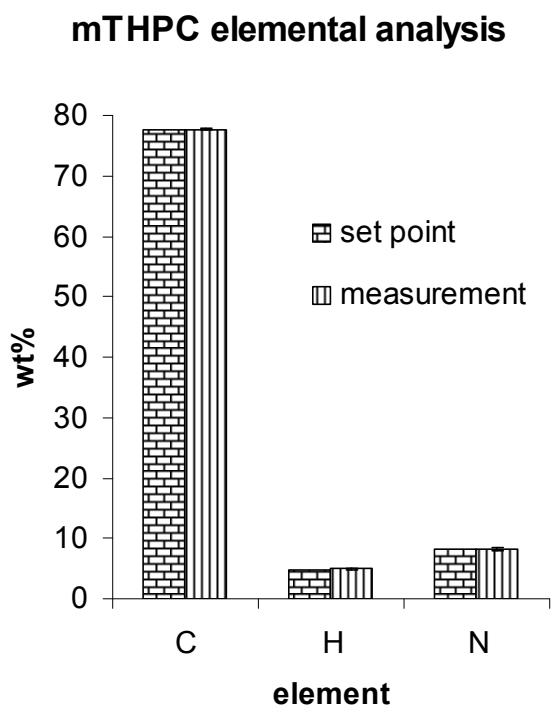


Figure S2: CHNS elemental analysis of mTHPC (n=3) with set point as theoretical value and with measurement as measured value.

References:

- [1] A. Juarranz, P. Jaèn, F. Sanz-Rodríguez, J. Cuevas, S. González. Photodynamic therapy of cancer. Basic principles and applications. *Clinical and Translational Oncology*. **2008**; 10 (3), 148-154.
- [2] A. C. Kübler. Photodynamic therapy. *Medical Laser Application*. **2005**; 20 (1), 37-45.
- [3] G. Monfrecola, G. Fabbrocini, P. C. Pinton. Photodynamic therapy for non-melanoma skin cancers. *Current Cancer Therapy Reviews*. **2009**; 5 (4), 271-280.
- [4] A. P. Castano, T. N. Demidova, M. R. Hamblin. Mechanisms in photodynamic therapy: Part two - Cellular signaling, cell metabolism and modes of cell death. *Photodiagnosis and Photodynamic Therapy*. **2005**; 2 (1 SPEC. ISS.), 1-23.
- [5] S. A. Sibani, P. A. McCarron, A. D. Woolfson, R. F. Donnelly. Photosensitizer delivery for photodynamic therapy. Part 2: Systemic carrier platforms. *Expert Opinion on Drug Delivery*. **2008**; 5 (11), 1241-1254.
- [6] F. Ricchelli. Photophysical properties of porphyrins in biological membranes. *Journal of Photochemistry and Photobiology B: Biology*. **1995**; 29 (2-3), 109-118.
- [7] R. W. Boyle, D. Dolphin. Structure and biodistribution relationships of photodynamic sensitizers. *Photochemistry and Photobiology*. **1996**; 64 (3), 469-485.
- [8] Y. N. Konan, R. Gurny, E. Allemann. State of the art in the delivery of photosensitizers for photodynamic therapy. *Journal of Photochemistry and Photobiology B: Biology*. **2002**; 66 (2), 89-106.
- [9] S. B. Brown, E. A. Brown, I. Walker. The present and future role of photodynamic therapy in cancer treatment. *Lancet Oncology*. **2004**; 5 (8), 497-508.
- [10] T. Oba. Photosensitizer nanoparticles for photodynamic therapy. *Current Bioactive Compounds*. **2007**; 3 (4), 239-251.
- [11] D. Bechet, P. Couleaud, C. Frochot, M. L. Viriot, F. Guillemin, M. Barberi-Heyob. Nanoparticles as vehicles for delivery of photodynamic therapy agents. *Trends in Biotechnology*. **2008**; 26 (11), 612-621.
- [12] D. K. Chatterjee, L. S. Fong, Y. Zhang. Nanoparticles in photodynamic therapy: An emerging paradigm. *Advanced Drug Delivery Reviews*. **2008**; 60 (15), 1627-1637.
- [13] J. Schwiertz, A. Wiehe, S. Gräfe, B. Gitter, M. Epple. Calcium phosphate nanoparticles as efficient carriers for photodynamic therapy against cells and bacteria. *Biomaterials*. **2009**; 30 (19), 3324-3331.
- [14] M. Wacker, K. Chen, A. Preuss, K. Possemeyer, B. Roeder, K. Langer. Photosensitizer loaded HSA nanoparticles. I: Preparation and photophysical properties. *International Journal of Pharmaceutics*. **2010**; 393 (1-2), 253-262.

- [15] N. Solban, I. Rizvi, T. Hasan. Targeted photodynamic therapy. *Lasers in Surgery and Medicine*. **2006**; 38 (5), 522-531.
- [16] R. Duncan. The dawning era of polymer therapeutics. *Nature Reviews Drug Discovery*. **2003**; 2 (5), 347-360.
- [17] R. H. Sterns, M. Rojas, P. Bernstein, S. Chennupati. Ion-exchange resins for the treatment of hyperkalemia: Are they safe and effective? *Journal of the American Society of Nephrology*. **2010**; 21 (5), 733-735.
- [18] N. Reum, C. Fink-Straube, T. Klein, R. W. Hartmann, C. M. Lehr, M. Schneider. Multilayer coating of gold nanoparticles with drug-polymer coadsorbates. *Langmuir*. **2010**; 26 (22), 16901–16908.
- [19] G. M. Morris, H. Ruth, W. Lindstrom, M. F. Sanner, R. K. Belew, D. S. Goodsell, A. J. Olson. Software news and updates AutoDock4 and AutoDockTools4: Automated docking with selective receptor flexibility. *Journal of Computational Chemistry*. **2009**; 30 (16), 2785-2791.
- [20] O. Trott, A. J. Olson. Software news and update AutoDock Vina: Improving the speed and accuracy of docking with a new scoring function, efficient optimization, and multithreading. *Journal of Computational Chemistry*. **2010**; 31 (2), 455-461.
- [21] F. Rancan, M. Helmreich, A. Mölich, N. Jux, A. Hirsch, B. Röder, C. Witt, F. Böhm. Fullerene-porphyrin complexes as sensitizer for photodynamic therapy: Uptake and photo-induced cytotoxicity on Jurkat cells. *Journal of Photochemistry and Photobiology B: Biology*. **2005**; 80 (1), 1-7.
- [22] E. A. Meyer, R. K. Castellano, F. Diederich. Interactions with aromatic rings in chemical and biological recognition. *Angewandte Chemie - International Edition*. **2003**; 42 (11), 1210-1250.
- [23] R. W. Redmond, J. N. Gamlin. A compilation of singlet oxygen yields from biologically relevant molecules. *Photochemistry and Photobiology*. **1999**; 70 (4), 391-475.
- [24] K. Chen, A. Preuß, S. Hackbarth, M. Wacker, K. Langer, B. Röder. Novel photosensitizer-protein nanoparticles for Photodynamic therapy: Photophysical characterization and in vitro investigations. *Journal of Photochemistry and Photobiology B: Biology*. **2009**; 96 (1), 66-74.

5 Chapter 3: Drug-multilayer coating of AuNP

Multilayer coating of gold nanoparticles with drug-polymer coadsorbates*

***This chapter has been published in:**

N. Reum, C. Fink-Straube, T. Klein, R. W. Hartmann, C. M. Lehr and M. Schneider.
(2010) Multilayer coating of gold nanoparticles with drug-polymer coadsorbates.
Langmuir, 26, 16901-16908.

Abstract

The aim of our present study was the development of a drug multilayer-based carrier system for delivery of water-insoluble drugs. As drug, we applied the anticancer drug 5,10,15,20-tetrakis(hydroxyphenyl)porphyrin, mTHPP which is a model photosensitizer for photodynamic therapy. Gold nanoparticles with a diameter of 14.5 ± 0.9 nm were prepared and used as template for the layer-by-layer approach. The drug and the negatively charged polyelectrolyte [1] poly(styrene sulfonate) sodium salt (PSS) were complexed with a new developed method using freeze-drying. The complexation efficiency was determined to be ~11-12 monomers PSS per mTHPP molecule by CHNS analysis and UV/vis measurement. Molecular docking simulations revealed π - π interactions and H-bonding to be the responsible mechanisms. A drug multilayer system based on the layer-by-layer (LbL) technique utilized the water-soluble complex as anionic layer material and poly(allylamine hydrochloride) (PAH) as cationic layer. The modified AuNP were characterized by different physicochemical techniques such as UV/vis, ζ -potential, ICP-OES and TEM. To the best of our knowledge we could demonstrate for the first time the adsorption of three drug layers to a nanoparticulate system. Furthermore, the adaptation of the LbL-technique resulted in drastically increased drug deposition efficiency (factor of one 100). Furthermore, we developed a new and comfortable way to solubilize water-insoluble drugs in water.

5.1 Introduction

The photosensitizer mTHPP is a model anticancer drug best suited for mTHPC (tetra (hydroxyphenyl)chlorin) used as second-generation photosensitizer [2] in photodynamic therapy [3]. The drug is practically insoluble in water and must be intravenously administered, e.g., in ethanolic solution, causing local pain to patients [4]. Besides, the mTHPP molecules are only slowly released or degraded, because they tend to accumulate in the amphiphilic cell membrane[5]. As a huge disadvantage, the patients show a prolonged strong light sensitivity of up to two weeks after treatment due to the nonselective accumulation inside the tissue damaging both healthy and malignant cells by irradiation [4].

To overcome this obstacle, the usage of nanoparticles is a promising approach [6]. Chatterjee et al. divided the nanoparticle delivery systems for photodynamic therapy (PDT) in passive and active carriers for photosensitizer excitation [2]. Our focus is on passive carriers which are nonbiodegradable and metallic. Furthermore, the usage of such nanoparticles results in different advantages such as uptake into cells without being recognized by efflux systems (e.g., P-glycoprotein) resulting in the increased intracellular concentration of drugs [7]. A key advantage is the transport of hydrophobic drugs in the body, avoiding photosensitizer aggregation and inducing loss of activity. Additionally, they can show a minimum of immunogenicity and can also be designed to be resistant to microbial attack [2, 6]. The coating with poly(ethylene glycol) increases blood circulation time resulting in accumulation in cancer tissue by the so-called EPR effect [8, 9]. Hence, the intravenously administered drug delivery systems can increase the tumor concentration of antitumor drugs up to 70-fold [9, 10]. They can be synthesized in different sizes and can act as multifunctional platforms through (I) a shell volume in which photosensitizers can be encapsulated or coupled, (II) a surface that can be functionalized to attach targeting groups for cancer specific drug accumulation, and (III) a contrast agent that can be incorporated for diagnostic reasons [2, 6].

To ensure maximum flexibility for the drug carrier, modular systems are most suited. An intriguing approach is based on the layer-by-layer (LbL) technique introduced by Decher et al. [11] The LbL technique offers an endless variety of polyelectrolyte material and hence the preparation of tailor-made surfaces. Although it was originally performed on planar surfaces, Sukhorukov et al. [1] transferred the LbL technique on microparticles by coating a template core. This template ascertains the size of the

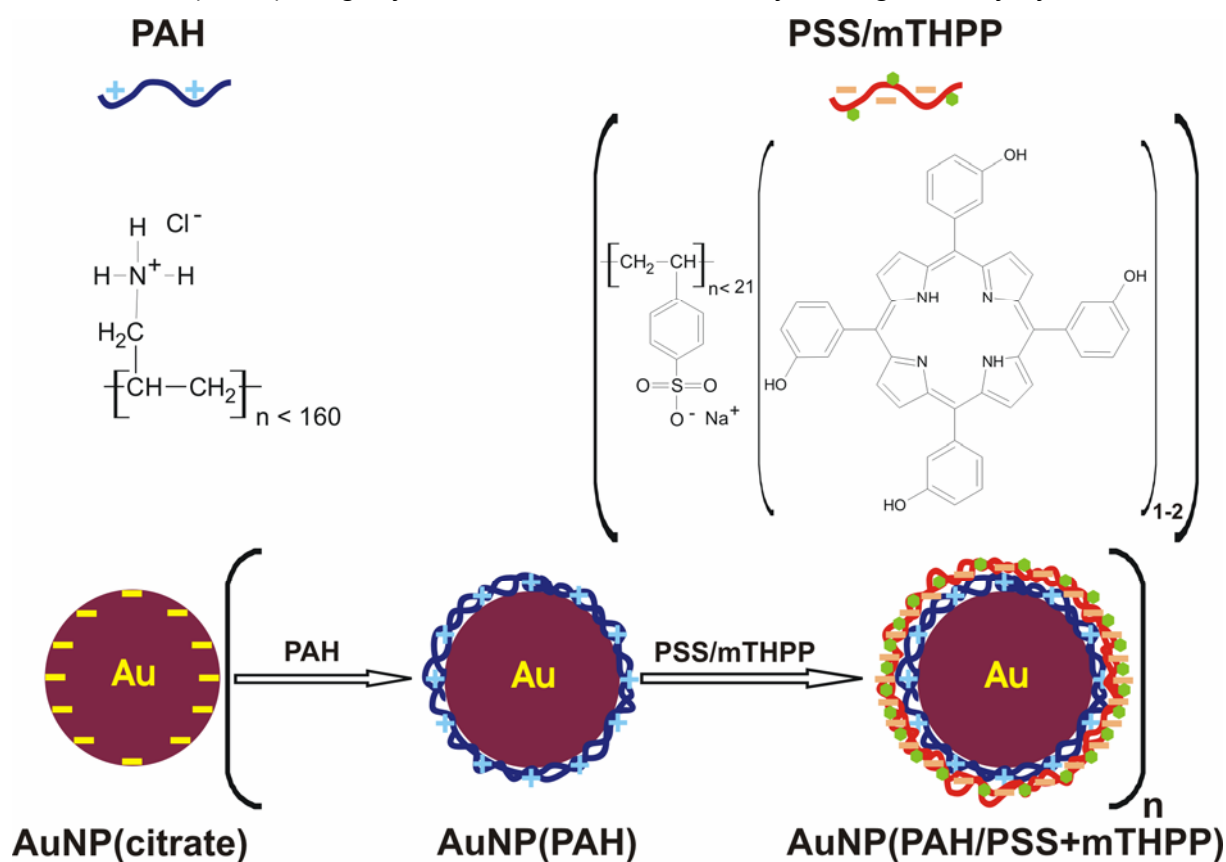
particulate system, i.e., the drug carrier. Since then, a lot of work has been published mainly about microparticles and LbL self-assembly [12-15]. However, for cellular targeting and uptake nanosized particles are favorable.

As a core material, colloidal gold was chosen because of its optical properties, the intriguing size range in which monodispers particles can be obtained, and its high chemical stability [16]. With respect to PDT, AuNP were also found to positively influence the singlet oxygen yield [17]. Furthermore, applying gold nanoparticles (AuNP) as a drug delivery system reduces and suppresses adverse effects due to particle toxicity. The usage of nanoparticles can also improve therapeutic efficiency and biodistribution, and overcomes the problems of solubility, stability, and pharmacokinetics of drugs [18, 19]. Furthermore, geometry and surface physicochemical properties affect the transport and biodistribution of particles at the vascular level and the strength of adhesion and the internalization rate at the cellular level [20]. The diameter and shape of AuNP can be easily diversified by application of different methods of AuNP preparation [21, 22]. Although the surface modification of AuNP was already carried out by Gittins and Caruso in 2000 [23], nanoparticles have up to now not been used intensively for coating by the LbL technique [24].

The kind of drug attachment to nanoparticles is constricted by the chemical structure of the drug molecule, the solubility, the stability, and the mechanism of action of drug, and furthermore dispersion medium, stability, size, and surface material of nanoparticles. To load the AuNP with drug, several methods have been published. Obvious is the attachment of siRNA and DNA as negatively charged polyelectrolytes by ionic interactions based on the LbL technique [25, 26]. Because of the structure of mTHPP, this principle is not available for mTHPP. Other possibilities for drug attachment to AuNP were carried out by coordinate-covalent bonding [27] and covalent bonding [28, 29]. The disadvantage for a covalent bonding of mTHPP can be the reduced drug efficiency through a lower singlet oxygen quantum yield.[2] Drug attachment by nitrogen-Au bonding systems [30] allows only one drug layer, reducing the dosing flexibility. Hence, a promising strategy for mTHPP attachment to AuNP surface is adsorption caused by interactions between the drug and the layer material as excipient.

Our aim was the development of a nanoscale model for multilayer drug delivery system based on AuNP as templates allowing adjustment of the drug dose. The dose adjustment by varying the number of drug layers rather than the amount of particles

would improve the applicability. So far, most LbL systems in the nanorange are based on drug monolayers [24]. As layer material, we have applied two model polyelectrolytes for AuNP coating, PAH and PSS [31]. To avoid a strong reduction of the drug effect by covalent binding of mTHPP to AuNP surface, a coadsorbate of the water-insoluble mTHPP and the polyelectrolyte was formed by π - π interactions [32] and H-bonds resulting in a water-soluble polymer drug complex. The negatively charged complex consisting of PSS/mTHPP was applied as a layer material in combination with PAH (Scheme 1). Herein, for the first time AuNP coating is reported with several (three) drug layers to obtain a real multilayer drug delivery system.



Scheme 1: Principle of mTHPP loaded AuNP manufacture using standard LbL method.

5.2 Materials and methods

5.2.1 Materials

The 5,10,15,20-tetrakis(3-hydroxyphenyl)porphyrin (mTHPP) seen in Scheme 1 was kindly provided by Biolitec AG (Jena, Germany). Gold(III) chloride hydrate

($\text{HAuCl}_4 \cdot 3\text{H}_2\text{O}$), trisodium citrate-2-hydrate ($\text{Na}_3\text{C}_6\text{H}_5\text{O}_7 \cdot 2\text{H}_2\text{O}$), poly(styrene sulfonate) sodium salt (PSS) (MW 4.3 kDa), and poly(allylamine hydrochloride) (PAH) (MW 15.0 kDa) were purchased from Sigma-Aldrich (Steinheim, Germany). The water used in all experiments was prepared in a Millipore Milli-Q purification system (resistivity higher than $18.0 \text{ M}\Omega \text{ cm}^{-1}$).

5.2.2 Methods

5.2.2.1 Preparation of PSS/mTHPP complex

86.0 mg (20.0 μmol) of PSS was dissolved in 15 mL water. 27.0 mg (39.7 μmol) of mTHPP was dissolved in 15 mL ethanol. Both solutions were mixed and freeze-dried in a Christ Alpha 2-4 LSC (Christ GmbH, Osterode, Germany). The lyophilizate was suspended in 20 mL of water and centrifuged for 35 min at 16,098 g with a table centrifuge, Hettich Rotina 420 R (Hettich GmbH & Co. KG, Tuttlingen, Germany). The supernatant was filtered and refilled with water to 25 mL. The pellet of centrifugation, the filters, and all other materials that were in contact with the complex mixture were rinsed out with ethanol, which was collected to determine the concentration of free or uncomplexed mTHPP. The concentration of mTHPP in ethanol was obtained by UV/vis spectroscopy (5 relevant peaks: $\lambda_{\text{ex}} \in \{416, 512, 546, 589, 645\} \text{ nm}$) (PerkinElmer Lambda 35, PerkinElmer LAS, Rodgau, Germany) and the concentration of PSS and mTHPP in water by CHNS analysis (Elementar Analysensysteme GmbH, Hanau, Germany).

5.2.2.2 Characterization of PSS/mTHPP coadsorbate

5.2.2.2.1 Docking study

Molecular docking simulations were carried out to simulate, predict, and better understand the interactions between the drug (mTHPP) and the polyelectrolyte carrier (PSS). All calculations were performed on Intel Core2 Duo CPU 3.00 GHz running *Linux CentOS 5.3*. Tridimensional structures of both mTHPP and PSS were generated using *MOE2008.10* (Chemical Computing Group Inc., Montreal, Canada). For simplification, the PSS molecule was depicted as a nine monomer unit. The structures were energy-minimized with the MMFF94 force field as implemented in MOE. Ionization states and hydrogen positions were assigned using the Protonate

3D utility of MOE. AutoDock-Tools4 [33] was used for input files preparation and AutoDock *Vina*, version 1.0 [34] was used to dock mTHPP in the structure of PSS: 60 binding modes were produced with an exhaustiveness parameter of 100.

5.2.2.2.2 CHNS elemental analysis

The determination of CHNS contents of drug complexes was carried out by universal elemental analyzer vario El III (Elementar Analysensysteme GmbH, Hanau, Germany). The basic principle of quantitative CHNS analysis is high-temperature combustion of organic solid or liquid samples. Programmable control of the direct oxygen jet injection during high-temperature combustion guarantees complete combustion. The gaseous combustion products are purified, separated into their components by special adsorption traps, and sequentially analyzed with universally used thermoconductivity detector (TCD).

Samples were weighed into tin boats, compressed, and taken to the auto sampler, where they are dropped into the combustion tube automatically. Calibration curves of sulfanilic acid as reference compound (C, 41.6; H, 4.1; N, 8.1; and S, 18.5 wt %) were compiled by manufacturer, and daytime factor measurements were repeated six times with weighed samples of about 5 mg. The aqueous solution of PSS/mTHPP complex was freeze-dried with Christ Alpha 2-4 LSC (Christ GmbH, Osterode, Germany). Freeze-dried drug polymer coadsorbate analysis was repeated three times with weighed samples of about 3 mg. The temperatures of combustion tube, reduction tube, CO₂ column, H₂O column, and SO₂ column amounted to 1150, 850, 190, 150, and 210°C, respectively.

5.2.2.2.3 UV-visible spectroscopy measurements

The amount of mTHPP in the drug complex was determined indirectly based on UV/vis spectroscopy. Therefore, the concentration of mTHPP in the organic solution (ethanol) was calculated (see Results and Discussion). All measurements were carried out in 1 cm quartz cuvettes with the Perkin-Elmer Lambda 35 spectrophotometer (PerkinElmer LAS, Rodgau, Germany).

5.2.2.3 Synthesis of AuNP

Colloidal gold was prepared following a method introduced by Turkevich et al. [35] by the reduction of gold ions with citrate ions [36]. A volume of 99 mL of a tetrachlorauric acid ($\text{HAuCl}_4 \cdot 3\text{H}_2\text{O}$) solution containing 20 mg (50.8 μmol) of gold salt were refluxed and 1 mL of sodium citrate solution containing 74.7 mg (254 μmol) of $\text{Na}_3\text{C}_6\text{H}_5\text{O}_7 \cdot 2\text{H}_2\text{O}$ was added to the boiling solution. The solution was boiled for 20 min and cooled to room temperature. The resulting suspension had a gold concentration of 100 $\mu\text{g/mL}$ analyzed by ICP OES.

5.2.2.4 Preparation of PAH and PSS/mTHPP coated AuNP

5.2.2.4.1 Standard LbL method

For encapsulation of colloidal gold nanoparticles, we used an adapted method formerly described by Decher [31] and Krol [37] using PAH and drug polymer complex instead of pure polymers. To 10 mL of unwashed-citrate-stabilized gold nanoparticle solution with a gold concentration of 100 $\mu\text{g/mL}$ was added 10 mL of the PAH solution (10 mg/mL) resulting in 110,000 PAH chains per AuNP determined following Schneider et al. [38]. After stirring for 10 min, particles were separated from PAH excess by centrifugation at 23,143 g for 35 min (Hettich Rotina 420 R, Hettich GmbH & Co. KG, Tuttlingen, Germany). The centrifuged nanoparticles were redispersed in water to a volume of 10 mL. The washing step was repeated once. Ten milliliters of PAH-coated AuNP was coated with 10 mL of the drug complex solution. The drug complex was applied in water with a concentration of 111 $\mu\text{g/mL}$ PSS and 32 $\mu\text{g/mL}$ mTHPP, respectively. That means per AuNP are available 4,200 PSS chains. The quantification of mTHPP/PSS complex will be described in the results and discussion section. After incubation for 10 min, the solution was centrifuged for 35 min at 14,800 g with a table centrifuge. The supernatant was removed and replaced by the necessary volume of water to obtain 10 mL of AuNP coated with PAH and PSS/mTHPP ($\text{AuNP}(\text{PAH}/\text{PSS}+\text{mTHPP})_1$). Then, the next PE double layer was deposited, repeating the procedure.

5.2.2.4.2 Modified LbL method

Modified LbL was similar to the standard method, but instead of twice-washed AuNP(PAH), only once-washed AuNP(PAH) were used. The drug complex was applied in water at a concentration of 100 µg/mL PSS and 29 µg/mL mTHPP (per AuNP are 3,784 PSS chains available), respectively. Afterwards, a third layer of pure PSS was used again with a concentration of 3.5 mg/mL. To 10 mL of AuNP(PAH/PSS+mTHPP)₁ was added 10 mL of PSS solution (per AuNP are 450,000 PSS chains available). The modified AuNP were washed twice, and then, PAH was adsorbed as the fourth layer as described before.

5.2.2.5 Characterization of AuNP and coated AuNP

5.2.2.5.1 Transmission electron microscopy (TEM) measurements

TEM measurements of the gold nanoparticles were performed on a JOEL model JEM 2010 instrument (JOEL GmbH, Eching, Germany) operated at an accelerating voltage of 120 kV. Samples for TEM analysis were prepared by placing 12 µL of washed gold nanoparticle solution on carbon-coated 400 mesh copper grid (S160-4, Plano GmbH, Wetzlar, Germany). The suspensions were allowed to dry until the water was completely evaporated. Contrast agent was not applied.

5.2.2.5.2 Particle size analysis

The particle size analysis of TEM images was carried out of around 100 particles using *ImageJ*. The real median diameter was determined.

5.2.2.5.3 Atomic emission spectrometry with induced coupled plasma (ICP OES)

Atomic emission spectrometry with induced coupled plasma (ICP OES) was performed using an Ultima 2 (Horiba Jobin-Yvon, Longjumeau, France) with a Czerny-Turner type monochromator (focal length 1 m). HF power of 1 kW was supplied by a regulated generator at 40.68 MHz. The liquid sample is nebulized, then transferred to argon plasma. It is decomposed, atomized, and ionized whereby the atoms and ions are excited. The intensity of light emitted is measured when the atoms or ions return to a lower energy. Each element emits light at characteristic

wavelengths, and these lines can be used for quantitative analysis (Supporting Information Table S1).

Standard solutions were prepared from single-element stock solutions (1.000 g/L) obtained from Alfa Aesar GmbH and Co KG (Karlsruhe, Germany). Ultrapure water was used for dilution of standards. Calibration was performed using aqueous standard solutions of 0, 5, and 10 mg/L and led to calibration coefficients of 0.999 in the case of Au. In contrast to the typical procedure, we have not dissolved the AuNP in aqua regia but the colloidal Au solutions were diluted 1:10 with ultrapure water for analysis. All measurements were done in triplicate.

5.2.2.5.4 ζ -potential measurements

The ζ -potential of uncoated, coated, and mTHPP-loaded AuNP was determined by the principle of laser Doppler velocimetry with a Malvern Zetasizer Nano ZS (Malvern Instruments GmbH, Herrenberg, Germany). Measurements were realized in triplicate at 25 °C with the model of Smoluchowski.

5.2.2.5.5 UV-visible spectroscopy measurements

UV/vis spectroscopy was carried out to check the successful polyelectrolyte and drug adsorption to AuNP surface. Furthermore, the adsorbed mTHPP mass to AuNP surfaces was determined. All measurements were carried out in 1 cm quartz cuvettes with the Perkin-Elmer Lambda 35 Spectrophotometer (PerkinElmer LAS, Rodgau, Germany).

5.3 Results and discussion

5.3.1 Preparation of PSS/mTHPP complex

The aim was the noncovalent attachment of drug to the polyelectrolyte (PE) PSS. The advantage of drug adsorption to PSS is the direct coating of AuNP with the PSS/mTHPP complex. PSS was chosen because of its benzene rings in the molecule which can interact with the benzene rings in the mTHPP molecule. The water solubility of mTHPP coadsorbed with PSS is remarkably enhanced, which is a

clear hint for successful complex formation between both compounds (Supporting Information Figure S1).

To understand the interactions between both molecules, a molecular docking simulation was carried out. The first crude results were parallel displaced π - π interactions of benzene rings from PSS with the benzene and pyrrole rings of mTHPP as well as H-bonds of OH- and NH-groups with the sulfonate groups (Supporting Information Figure S2) which lead to the successful complexation. The π - π interactions also resulted in a red shift of the mTHPP absorption spectrum of the complex in water, as expected (Figure 1).

An intriguing aspect is the complexation ratio between the drug and the PSS molecules. CHNS elemental analysis was carried out to determine the mass fraction of both compounds in the complex. The results of CHNS elemental analysis of PSS and mTHPP in mass percentage C, H, N, and S were found to yield a very small standard deviation (Supporting Information Figure S3). The recovery rate of PSS relating to carbon and sulfur is only 86% because of the impurities (unspecified by producer) reducing the actual content of PSS [39]. The recovery rate of mTHPP relating to carbon and hydrogen is 97%, for nitrogen, it is 91%. For determination of complexation ratio, the recovery rate of PSS and mTHPP has to be considered.

To determine the mTHPP concentration in the complex in water, a fixed volume of 10 mL of the aqueous complex solution was freeze-dried and analyzed by elemental analysis. On the basis of the mass percentage of the elements in the complex (Supporting Information Table S2), the amount of complex in the aqueous phase was 105.7 mg, indicating that 6.5% of the PSS/mTHPP coadsorbate is transferred into the ethanolic phase (total mass = 86 mg PSS and 27 mg mTHPP = 113 mg). This result fits the visual observations clearly including mTHPP in ethanol due to the red/brown discoloration of ethanol after contact with the PSS/mTHPP mixture. In the aqueous phase, 77.85% PSS and 22.78% mTHPP were determined with an excellent rate of recovery (Supporting Information Table S2). One PSS molecule ($\sim 4,300$ g/mol) consists of around 21 monomer units (206.18 g/mol). Therefore, the result of complexation efficiency of 11 monomers units of PSS per mTHPP molecule or 2 mTHPP molecules per PSS molecule is very reliable (Table 1).

Table 1: Complex characteristics prepared from 86 mg PSS and 27 mg mTHPP by elemental analysis and UV/vis measurement (mean value \pm standard deviation (SD)).

parameter for complex	CHNS analysis	UV/vis
$m_{(\text{free mTHPP in ethanol})}$ [mg] \pm SD	2.92 ± 0.180	2.95 ± 0.330
$m_{(\text{mTHPP in complex in water})}$ [mg] \pm SD	24.08 ± 0.180	24.05 ± 0.330
$m_{(\text{PSS in complex})}$ [mg] \pm SD	82.29 ± 1.069	86.00 ± 0.000
$m_{(\text{complex})}$ [mg] \pm SD	106.37 ± 1.181	110.05 ± 0.330
number of monomers per mTHPP molecule \pm SD	11.25 ± 0.062	11.80 ± 0.039

To facilitate the determination of the complexation ratio, an approach based on UV/vis was investigated. The determination of complex concentration by UV/vis spectroscopy would offer a simple and cheap method to be carried out in all laboratories. A disadvantage of UV/vis measurement is that the calibration of mTHPP is not possible in the aqueous phase, because the drug is practically insoluble in water (a UV/vis calibration in water cannot be performed). Due to complex preparation and purification, the free mTHPP is dissolved in ethanol, whereas free PSS is insoluble in ethanol. However, an indirect determination of mTHPP concentration in water can be carried out in ethanol. As the PSS/mTHPP complex is insoluble in ethanol, only the unbound mTHPP can be in the ethanol phase. The concentration of complexed mTHPP in water ($c_{(\text{mTHPP})}$) can be determined with equation (1) with $m_{(\text{total})}$ as the total mass of mTHPP for complex preparation, $m_{(\text{ethanol})}$ as the free or uncomplexed mTHPP mass in ethanol determined by UV/vis measurement, and V as the volume of water with the PSS/mTHPP coadsorbate:

$$C_{(\text{mTHPP})} = \frac{m_{(\text{total})} - m_{(\text{ethanol})}}{V} \quad (1)$$

Drug mass in water or complexed mTHPP mass is the mass of mTHPP used for complexation minus mass of mTHPP in ethanol assuming that there is no loss of mTHPP during the complexation procedure. The UV/vis spectrum of mTHPP in ethanol indicates five peaks as seen in Figure 1. For all calibration curves was obtained a very high linearity of around 0.9999. Samples can be measured in a broad range between 10 ng/mL and 100 $\mu\text{g/mL}$ due to selection of different measurement

wavelengths. In Table 1, one can find the total mass of free or uncomplexed mTHPP in ethanol, which is 2.95 mg. That means 24.05 mg of the used drug mass was complexed by 86 mg PSS (Table 1). With the help of the knowledge about the mass of mTHPP and PSS in the complex solution, a complexation efficiency of twelve monomer units of PSS for one mTHPP molecule was calculated based on UV/vis spectroscopy.

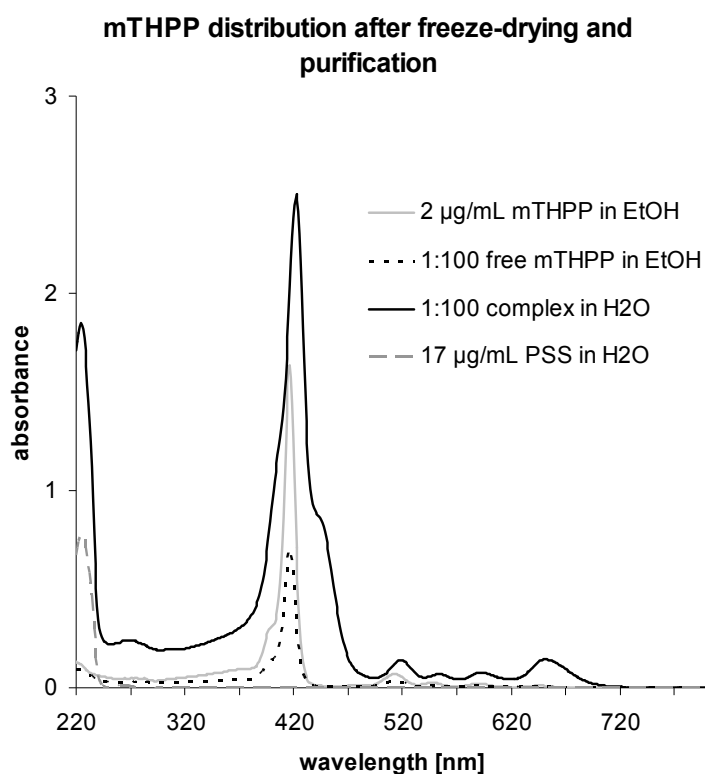


Figure 1: UV/vis spectra of complexed mTHPP in water 1:100 dilution (black solid line), free or uncomplexed mTHPP in ethanol 1:100 dilution (black dashed line) – both samples after freeze-drying, centrifugation, and filtration; 2 µg/mL mTHPP in ethanol (gray solid line) and PSS $C_{(PSS)} = 17$ µg/mL (gray dashed line) in water.

The total volume of the aqueous complex solution was 25 mL and the pH value was 7.4. The total volume of the free, uncomplexed mTHPP was also 25 mL but with ethanol as solvent. In Figure 1, one can see the absorption of 1:100 diluted PSS/mTHPP complex in water (black solid line) and of 1:100 diluted free mTHPP in ethanol (black dashed line). As a comparison to the free mTHPP of the complexation procedure, the solid gray line indicates mTHPP concentration of 2.0 µg/mL in ethanol (Figure 1). The adsorption spectra allowed identification of the drug. PSS with a concentration of 17 µg/mL in water (gray dashed line) is characterized by a peak

near 225 nm as shown in Figure 1. This peak can only be found in the water phase, whereas PSS was not detected in the organic phase (PSS not soluble in ethanol).

Comparing the results of the elemental analysis with those of the UV/vis measurements indicates the similar complexation efficiencies between PSS and mTHPP (Table 1). The mTHPP mass was the same for both measurements ($m_{\text{THPP}} = 24.1$ mg). PSS could only be detected by elemental analysis (82.29 mg indicating a loss of 3.71 mg or 4.3%) because of the overlapping UV/vis signal of PSS and mTHPP at $\lambda = 225$ nm. As PSS is not soluble in ethanol, all PSS ($m_{\text{PSS}} = 86$ mg) is assumed to be in the aqueous phase. The results of elemental analysis indicate differences most likely due to the adsorption of PSS to the membrane material of the filters or to the surface of the equipment. With elemental analysis, a value of 11.3 monomer units (4-ethylbenzenesulfonate sodium salt, 206.2 g/mol) of PSS (4,300 g/mol) was calculated to complex 1 mTHPP molecule and by UV/vis measurement, it was 11.8 monomer units of PSS. The fewer monomer units necessary to complex 1 mTHPP molecule, the better the complexation efficiency is. The more precise method from the direct determination of PSS and mTHPP in aqueous phase (elemental analysis) leads to higher complexation efficiency than the UV/vis method. Nevertheless, the UV/vis method is suitable for determination of complexation efficiency. To test the complexation efficiency, the mass ratio between mTHPP and PSS was changed. However, 11 monomer units of PSS for 1 mTHPP molecule was the most effective result relating to the highest complexation efficiency.

The stability of such complexes was also checked, and no modifications concerning color, haze, or sedimentation could be found over a period of one year. The idea to form stable complexes of the water-soluble polymer PSS with the water-insoluble drug mTHPP to transfer the drug in aqueous medium was successfully achieved. Molecular docking simulations could indicate interactions between both molecules due to the π - π interactions and H-bonds. For complexation of 1 mTHPP molecule, around 11 monomers of the PSS chain were needed.

5.3.2 Synthesis of gold nanoparticles (AuNP)

Colloidal gold prepared from trisodium citrate-2-hydrate was characterized by TEM and showed a monodisperse size distribution with a median particle diameter of 14.5 nm and a standard deviation of 0.9 nm (Figure 2). As expected, the ζ -potential

of citrate stabilized AuNP has shown a negative value because of the citrate ions on the surface of AuNP [38]. With the help of the equation (2) from Haiss et al. [40] and the UV/vis data, we could also calculate the AuNP diameter, obtaining a value of (14.1 ± 0.8) nm which is equal to the result by TEM measurement.

$$d = \left(\frac{A_{SPR} (5.89 \times 10^{-6})}{c_{Au} \exp(C_1)} \right)^{\frac{1}{C_2}} \quad (2)$$

With d the diameter of the particles in nanometer (for $5 \text{ nm} \leq d \leq 30 \text{ nm}$), c_{Au} the gold concentration (mol/L), A_{SPR} the absorbance at the surface plasmon resonance of AuNP solution, and $C_1 = -4.75$, $C_2 = 0.314$ being specific constants.

The concentration of gold in the freshly prepared AuNP suspension was determined by ICP-OES. In comparison to the typically described procedure in literature [41], it was not necessary to dissolve the AuNP in aqua regia before ICP-OES measurement. A 100% transformation of gold cations to AuNP could be observed, as UV/vis measurement indicated no gold salt after redox reaction. In combination with the ICP-OES results, the number of waters of crystallization in the tetrachlorauric acid compound was determined to be 3.

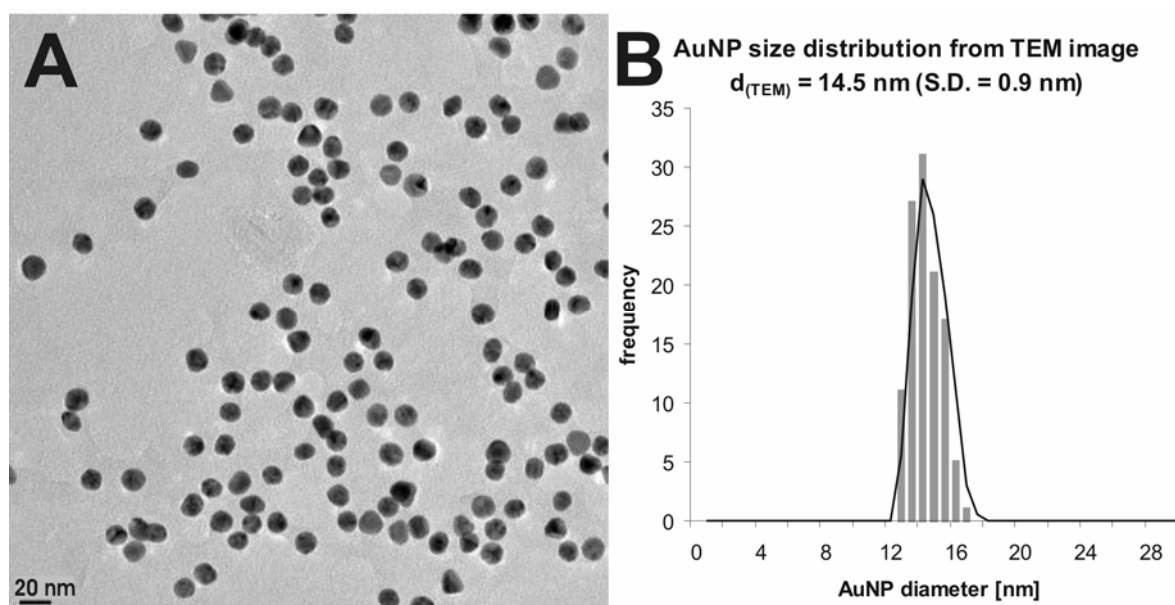


Figure 2: A) TEM image of citrate-stabilized AuNP. B) Size distribution of citrate-stabilized AuNP (analysis of the TEM image with Image J software).

5.3.3 Preparation of PAH and PSS/mTHPP coated AuNP

5.3.3.1 Standard LbL method

Scheme 1 depicts the principle of mTHPP loaded AuNP preparation with the layer-by-layer deposition technique. As first layer, PAH was adsorbed; therefore, the ζ -potential changed from negative values with citrate-stabilized AuNP to positive charges (Supporting Information Table S4) [38]. In Figure 3 is shown the typical absorption spectrum of citrate-stabilized AuNP (black solid line) and AuNP(PAH) (black dashed line). The peak near 520 nm is caused by surface plasmon resonance (SPR) of AuNP [19]. The adsorption of PAH leads to a little red shift of the AuNP peak of 1 – 2 nm due to interactions of electrons from the surface of AuNP with the adsorbed polyelectrolyte PAH and a broadening of the peak on the right side (black dashed line in Figure 3). Via washing steps, the excess PAH was removed resulting in the pH increase of the colloidal solution from 3.7 to 4.9.

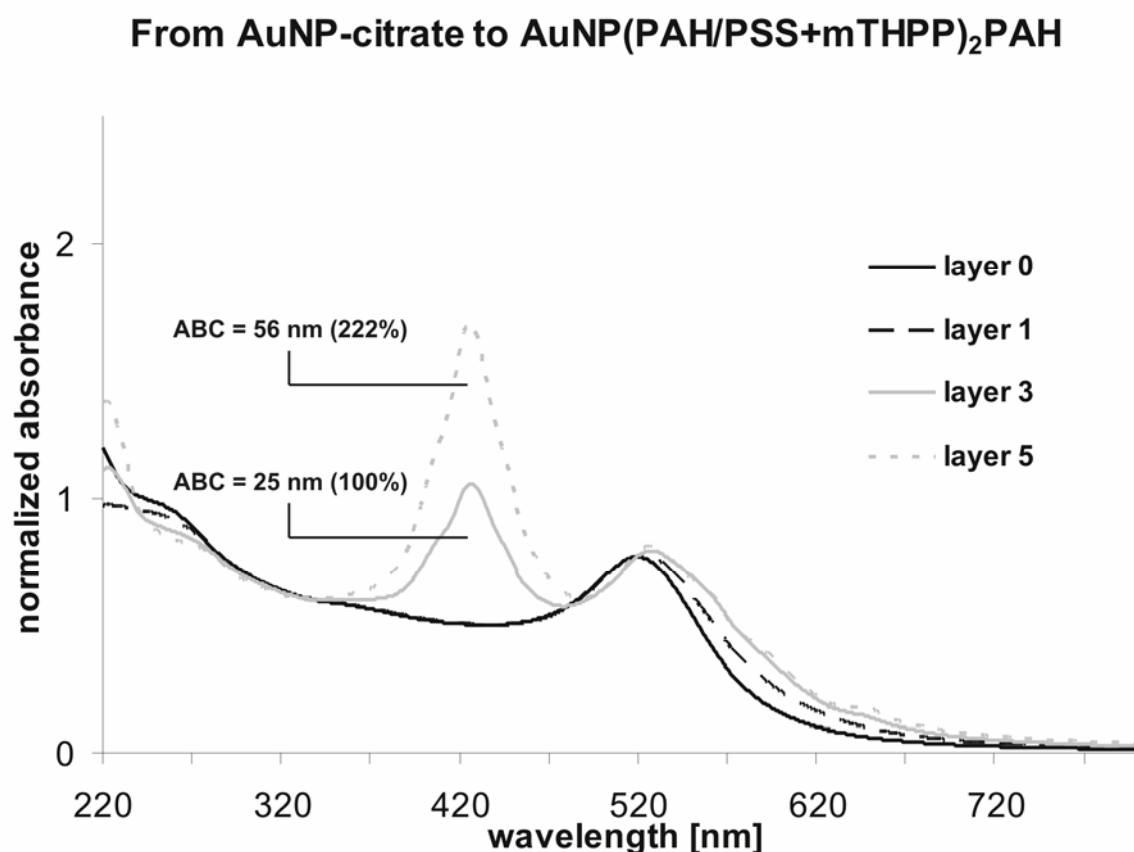


Figure 3: UV/vis spectra with ABC between 338 and 519 nm of the standard LbL method from AuNP-citrate to AuNP (PAH/ PSS+mTHPP)₂PAH: black solid line = layer 0 \triangleq unwashed citrate-stabilized AuNP; black dashed

line = layer 1 \triangleq twice-washed AuNP with PAH as first layer; gray solid line = layer 3 \triangleq twice-washed AuNP with PAH as first layer, PSS/mTHPP complex as second layer, and PAH as third and last layer (AuNP(PAH/PSS+mTHPP/PAH)₁); gray dotted line = layer 5 \triangleq twice-washed AuNP with PAH as first layer, PSS/mTHPP complex as second layer, PAH as third layer, PSS/mTHPP complex as fourth layer, and PAH as fifth and last layer AuNP(PAH/PSS+mTHPP)₂PAH.

The complex composed of PSS and mTHPP was adsorbed as second layer. Schneider et al. [38] identified that 60,000 PE chains per AuNP resulted in the highest single, non-aggregated AuNP yield. Here, however, only 4,200 PSS chains were available per AuNP. The idea behind this was to reduce the excess material and to increase deposition efficiency. Both procedures resulted in the same drug loading onto the AuNP, hence increasing the loading efficiency. Adsorbing the polyelectrolyte drug coadsorbate changed the ζ -potential to a negative value. As third layer, we have deposited PAH again, reversing the ζ -potential to positive values. The absorption spectrum of twice-washed AuNP(PAH/PSS+mTHPP/PAH)₁ is also presented in Figure 3. We could observe again a small red shift of AuNP peak of 2 - 3 nm due to the two further layers in comparison to AuNP(PAH)₁. More interestingly, the spectrum indicates an additional peak near 420 nm originating from mTHPP deposited as a complex on the AuNP surface.

Furthermore, adjusting the dose would require tuning the drug amount on the carrier. Therefore, additional layers were added. The absorption spectrum was always recorded after two washing steps. Whereas the AuNP peak was altered only marginally (Figure 3), the peak of mTHPP increased considerably, and that is a cogent hint for a second mTHPP layer adsorbed onto AuNP surface. The colloidal solutions of AuNP(PAH/PSS+mTHPP)₂PAH have not indicated agglomerated AuNP being stable for at least three months. The flocculation level, a stability parameter introduced by Weisbecker et al. [42], did not show differences between the citrate-stabilized AuNP and the coated AuNP. The calculation of the area between the curves (ABC) between 338 nm and 519 nm of AuNP(PAH)₁, AuNP(PAH/PSS+mTHPP/PAH)₁, and AuNP(PAH/PSS+mTHPP)₂PAH (Figure 3) allows determination of the increase of mTHPP molecules adsorbed onto the AuNP

surface. The ABC of AuNP with the first mTHPP layer is defined as 100% value (Figure 3). After adsorbing the second mTHPP layer, one could expect to slightly exceed doubling the ABC ($ABC_{mTHPP-2} \triangleq 222\%$). The reason for that might be the longer perimeter due to two further polyelectrolyte layers (+21% assuming a layer thickness of 0.8 nm). With our experimental data, we could show for the first time the preparation of AuNP surfaces modified by the so-called LbL technique with repetitive drug layers due to complex formation between the water-insoluble mTHPP and the negatively charged polyelectrolyte PSS.

So far, it was possible to transfer the water-insoluble drug due to complexation with PSS into aqueous solution. The deposition of the complex onto the surface of AuNP(PAH) via layer-by-layer technology could also be successfully achieved. That means we can apply the drug polymer coadsorbate of PSS and mTHPP like PSS alone regarding the layer-by layer technique. Zhifei Dai et al. published in 2001 the incorporation of dyes into layers of microparticles but due to ionic interactions of dyes and polyelectrolytes [43]. The formation of such a polymer drug complex is a new and comfortable method for drug incorporation into the layers, which is even working for coatings of nanoparticles.

5.3.3.2 Modified LbL method

To reduce the number of aggregated AuNP during the LbL coating, a modified LbL procedure was developed. Therefore, once- and twice-washed AuNP(PAH)- and different complex concentrations were mixed together. After centrifugation of the mixture, the yield of AuNP was determined by UV/vis. Surprisingly, the highest yield (92%) was obtained with once-washed AuNP(PAH) solution with a gold concentration of 50 $\mu\text{g/mL}$ and with a PSS concentration of 50 $\mu\text{g/mL}$, which corresponds to 3,784 PSS molecules for 1 AuNP.

The ζ -potential changed from +62 mV with (AuNP(PAH)) to +50 mV with (AuNP(PAH/PSS+mTHPP)) (Figure 4) in contrast to the standard method. The reason for the incomplete charge reversal could be either a lower amount of adsorbed drug complex or a complex formed between the mTHPP/PSS coadsorbate and unbound PAH in solution. In either case, as a consequence the AuNP surface has to be modified with additional PSS for charge reversal of the coated AuNP before

adsorption of the successive PAH layer is possible. PSS coating resulted in a ζ -potential of -54 mV.

In Figure 4 are depicted the ζ -potentials and pH values during the coating procedure. Both values are very important for cell experiments or nanoparticle stability in a medium requiring enough stability at physiological pH. PAH is a weak PE with a strong chloride anion as counterion, and that is why the pH values are low, ca. 3.8 after addition of PAH. PSS is a strong PE with a strong sodium cation as counter-ion, and after addition of PSS to modified AuNP solution, the pH values are between 6 and 7. AuNP with PAH as the outer layer indicate a positive ζ -potential, while with PSS as the outermost layer a negative ζ -potential was obtained. AuNP with drug complex as the outer layer always showed only a decrease of ζ -potentials from 60 mV to 40 mV as described above for the first adsorbed layer.

pH values and zeta-potential of modified AuNP

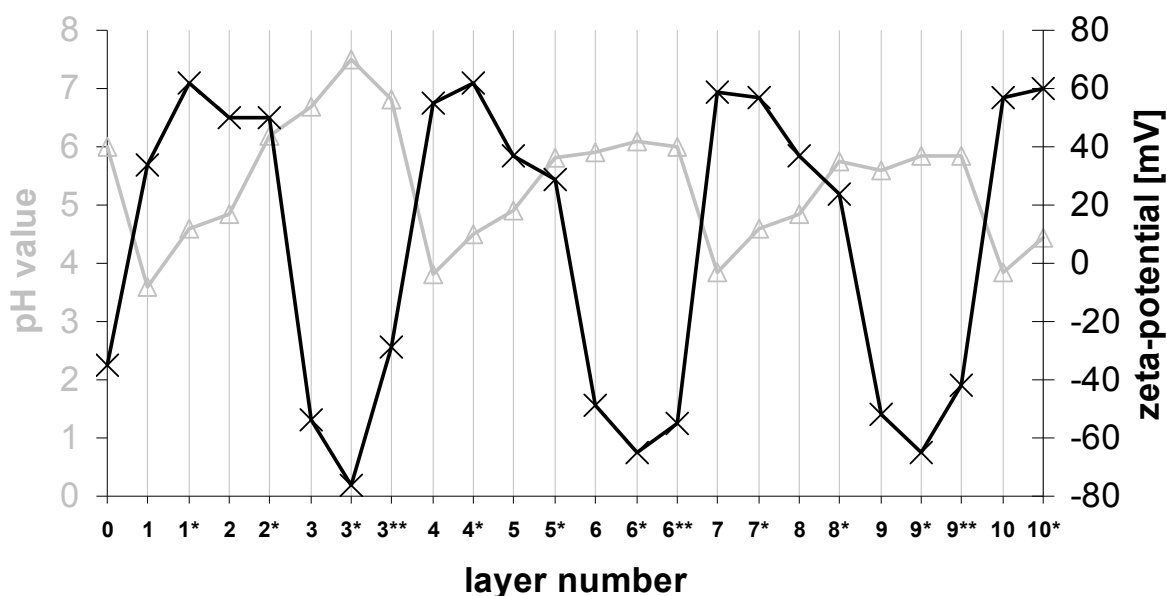


Figure 4: Changes of pH value and ζ -potential of surface-modified AuNP by modified LbL method (unwashed, *once washed, **twice washed).

UV/vis spectra indicate definitely that three complex layers could be adsorbed to the AuNP surface using the LbL technique (Figure 5). Spectra of AuNP, AuNP(PAH), and AuNP with one complex layer are described in section 3.3.1. In comparison to the mTHPP peak near 420 nm of the standard method (Figure 3) the mTHPP peak of AuNP with one drug layer in Figure 5 was narrower in width and therefore higher.

The peak of 225 nm caused by PSS was clearly higher in Figure 5 than in Figure 3. That is an indication for a higher concentration of PSS adsorbed to AuNP in the modified method because of the additional PSS layer compared to the standard method. The increase of the mTHPP peak with the second drug layer was smaller in the modified procedure than in the standard procedure. The third drug layer caused a similar increase as the second adsorbed mTHPP layer (increase of ABC of 70%).

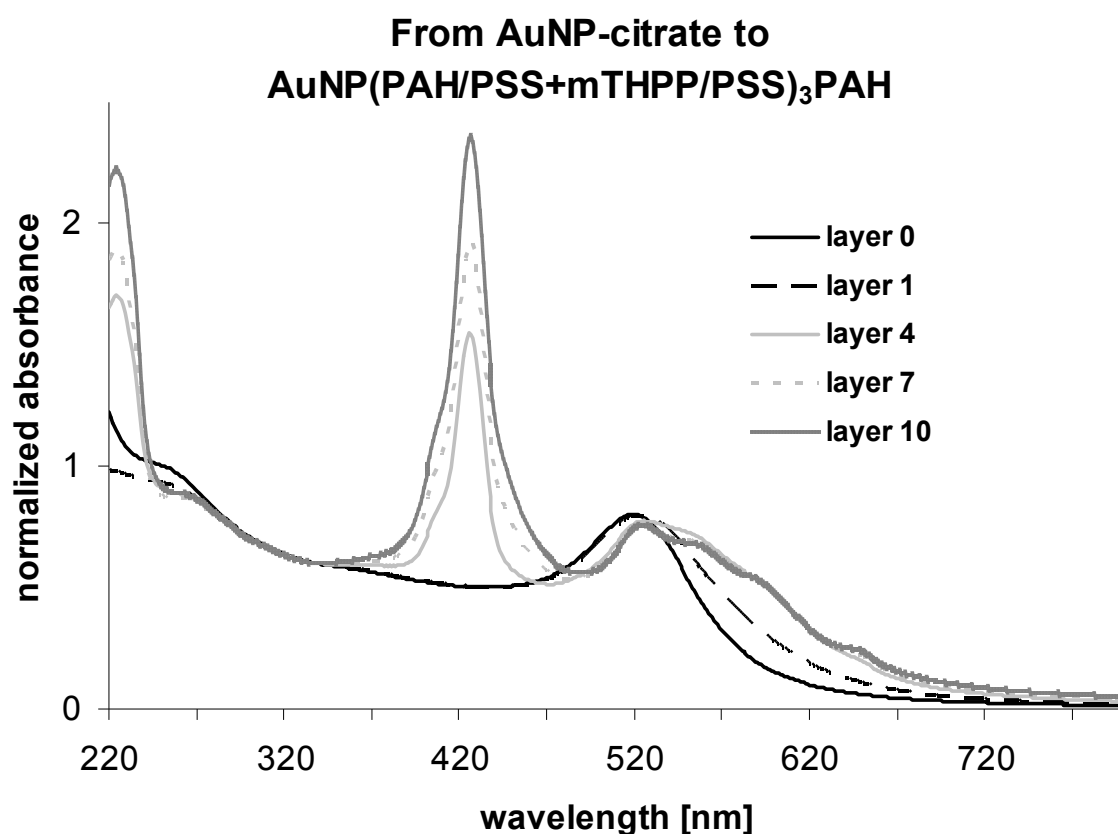


Figure 5: UV/vis spectra of modified LbL method from AuNP-citrate to AuNP(PAH/PSS+mTHPP/PSS)₃PAH: black solid line = layer 0 \triangleq unwashed citrate-stabilized AuNP; black dashed line = layer 1 \triangleq twice-washed AuNP with PAH as first layer; gray solid line = layer 4 \triangleq twice-washed AuNP with PAH as first layer, PSS/mTHPP complex as second layer, PSS as third layer, and PAH as fourth and last layer (AuNP(PAH/PSS+mTHPP/PSS/PAH)₁); gray dotted line = layer 7 \triangleq twice-washed AuNP with PAH as first layer, PSS/mTHPP complex as second layer, PSS as third layer, PAH as fourth layer, PSS/mTHPP

complex as fifth layer, PSS as sixth layer, and PAH as seventh and last layer (AuNP(PAH/PSS+mTHPP/ PSS)₂PAH)₁; black spotted line = layer 10 \triangleq twice-washed AuNP with PAH as first layer, PSS/mTHPP complex as second layer, PSS as third layer, PAH as fourth layer, PSS/mTHPP complex as fifth layer, PSS as sixth layer, PAH as seventh layer, PSS/mTHPP complex as eighth layer, PSS as ninth layer, and PAH as tenth and outer layer material (AuNP(PAH/PSS+mTHPP/PSS)₃PAH)₁.

To determine more precisely the number of adsorbed mTHPP molecules to AuNP surface, the ABC were calculated as before. ABC of one drug layer with standard method was 25 nm (Figure 3) and with modified method 24 nm (Figure 5). This is a clear hint that all uncomplexed mTHPP molecules were removed completely by washing steps. Complex layer two caused an increase of the ABC to 40 nm, and that corresponds to an increase of ABC of only 168%. The ABC of AuNP with three complex layers was 58 nm or 244% (Figure 5) compared to the first drug layer with 24 nm or 100% (Figure 5). That means the total increase of ABC with three mTHPP layers was a little bit higher than the increase of ABC with two drug layers. However, compared to the standard method the AuNP loss during the washing steps was reduced by this modified procedure. Therefore, it was possible to enhance the number of drug layers adsorbed to the AuNP surface.

As the overall amount of material on the particles is of interest, the number of adsorbed PSS molecules onto the AuNP was estimated by two approaches: the projected surface area of 1) a PSS random coil ($M_w = 4,300$ g/mol; $r = 0.573$ nm) $A_{(rc)} = 1.03$ nm² and of 2) a stretched PSS molecule (cylinder geometry) $A_{(cg)} = 4.03$ nm² was calculated. Together with the available surface area of the AuNP ($d = 14.5$ nm; $C_{(AuNP)} = 50$ μ g/mL, PAH layer of 0.4 nm thickness determined by TEM) 8 μ g/mL random coiled PSS or 2 μ g/mL stretched PSS molecules would be necessary for complete coverage of the available AuNP surface. From the complexation efficiency, the adsorbed amount of mTHPP was found to be 2.28 μ g/mL for random coiled PSS or 0.57 μ g/mL for stretched PSS.

Analyzing the $AUC_{(338-519\text{ nm})}$ of the mTHPP peak furthermore allowed a determination based on the experimental results. Therefore, the $AUC_{(338-519\text{ nm})}$ of free mTHPP in ethanol was assumed to be equal to the $ABC_{(338-519\text{ nm})}$ of mTHPP adsorbed to AuNP in water resulting in equal mTHPP concentrations. The $AUC_{(338-519\text{ nm})}$ of mTHPP correlated linearly with the concentration of mTHPP in ethanol solution. Calculated

results of ABC (Table 2) are in the same range as the values determined over the surface area. With around 2.1 $\mu\text{g/mL}$ mTHPP adsorbed to AuNP surface for the first drug layer (is equal to 1035 mTHPP molecules to 1 gold nanoparticle with a diameter of 14.5 nm), the concentration is close to the calculated value with the random coiled PSS molecule structure, which was 2.28 $\mu\text{g/mL}$. Therefore, it seems that most of the PSS molecules are adsorbed in a random coiled structure. Because of the strong polyelectrolyte characteristic of PSS, a more stretched structure was expected. However, the previously mentioned complex formation of coadsorbate and unbound PAH would lead to a lower charged complex with a nonstretched architecture supporting the estimation based on a random coil. With three complex layers of modified LbL procedure, the mTHPP concentration adsorbed to the AuNP surface was increased to 4.8 $\mu\text{g/mL}$. In this study, the drug mTHPP is applied as a model drug for the active pharmaceutical ingredient mTHPC (*meta*-tetra(hydroxyphenyl)chlorin). Typical tissue concentrations tested on several carcinoma cell lines for efficient tumor treatment with mTHPC are around 1.0 $\mu\text{g/mL}$ indicating that the concentration on the particles would be high enough for application [44-46]. To summarize, the quantification of mTHPP adsorbed to AuNP based on UV/vis spectroscopy was well in accordance with the theoretical estimation of the adsorbed drug amount. Furthermore, the model used for estimation allowed us to conclude that the polymer seems to be adsorbed mainly as PAH-coadsorbate complex.

Table 2: Quantification by UV/vis spectroscopy of mTHPP adsorbed to AuNP surface with $c_{(\text{Au})} = 50 \mu\text{g/mL}$ and AuNP diameter of 14.5 nm.

mTHPP layer number	$c_{(\text{mTHPP})} [\mu\text{g/mL}]$	
	standard method	modified method
1	2.11	2.06
2	4.73	3.30
3	-----	4.79

5.4 Conclusion

The aim was the preparation of surface-modified gold nanoparticles (AuNP) based on the LbL deposition technique with incorporation of the water-insoluble anticancer model drug mTHPP applied for PDT. For successful coating, a water-soluble

mTHPP/PSS complex was established remarkably increasing the solubility of the practical water-insoluble drug mTHPP by complex formation with the strong anionic polyelectrolyte PSS. By elemental analysis and by UV/vis spectroscopy, we could determine the number of PSS monomers (eleven) required for complexation of one mTHPP molecule. The mechanism behind the formation of stable drug polymer complexes was indicated by docking studies resulting in π - π interactions of benzene rings from PSS with the benzene and pyrrole rings of mTHPP, as well as H-bonds of OH- and NH-groups with the sulfonate groups.

The LbL method was applied with PAH as the positively charged layer and the polyelectrolyte drug coadsorbate as the negatively charged layer. Five layers, three PAH and two complex layers, were adsorbed to the AuNP surface with the standard LbL method. A modified LbL procedure was developed to reduce the AuNP loss during the washing steps allowing for ten layers. The coating process was characterized by pH value determination, ζ -potential measurement, and recording of UV/vis spectra. The calculation of $ABC_{(338-519 \text{ nm})}$ allowed us to determine the adsorbed mTHPP concentration for one, two, and three adsorbed mTHPP layers. Regarding the gold concentration of 50 $\mu\text{g/mL}$, the mTHPP concentration of around 2.1 $\mu\text{g/mL}$ was adsorbed to the AuNP surface with the first complex layer which is equal to 1035 mTHPP molecules to 1 gold nanoparticle with a diameter of 14.5 nm. Surprisingly, it seems that the PAH coadsorbate complex was attached to the AuNP surface mainly as a random coiled structure and not the PSS/mTHPP coadsorbate in the stretched modification. An increase of ABC caused by mTHPP of at least 68% compared to the first drug layer adsorbed to AuNP surface could be clearly shown for every additional complex layer. All results have confirmed that mTHPP was successfully adsorbed onto the AuNP. The coating procedure developed allowed for the first time a drug-multilayer delivery system based on nanoparticles. Consequently, the drug concentration can be adjusted not only by the overall number of AuNP, but also by the number of repetitions of the complex layer. In this context, the formulation of the drug polyelectrolyte complex offered a completely new and comfortable method for drug incorporation in multilayer-coated nanoparticles. In comparison to the LbL technique, with pure PSS the PSS concentration used for coating with complex could be decreased considerably. This decrease yielded a 100 fold increase of drug deposition efficiency.

5.5 Supporting information

Table S1: Instrument parameters used for ICP OES measurements of colloidal gold solutions.

Table S2: Complex characterization calculated with the obtained CHNS elemental analysis results in mass percentage [%] for carbon 48.68 ± 0.362 , hydrogen 4.31 ± 0.113 , nitrogen 1.72 ± 0.038 , and sulfur 10.37 ± 0.263 (mean value \pm standard deviation (S.D.)).

Table S3: UV/Vis calibration of mTHPP in ethanol.

Table S4: pH-value (mean value of pH-value, standard deviation (S.D.)) and ζ -potential (mean value of zeta potential, standard deviation (S.D.)) of colloidal AuNP and surface modified AuNP solutions prepared by standard LbL method.

Figure S1: Solubility enhancement of mTHPP in water as function mass of PSS added to 0.2 mg mTHPP, shown results after freeze drying and complex purification.

Figure S2: Docking complex between PSS and mTHPP.

Figure S3: CHNS elemental analysis (n=3) with setpoint as expected value and with measurement as measured value: A) of PSS, B) mTHPP.

Figure S4: Calibration of AUC of mTHPP between 338 nm and 519 nm as function of mTHPP concentration in ethanol.

Table S1: Instrument parameters used for ICP OES measurements of colloidal gold solutions.

plasma gas	nebu- lizer gas	nebu- lizer	spray cham-ber	injector tube dia- meter	Slit	Ana- lysis mode	Inte- gration time	Wave- length
[L/min]	[L/min]			[mm]	[μ m]		[s]	[nm]
12	0.68	Mira Mist	cyclonic	3	20x15	Gauss	0.5	242.795

Table S2: Complex characterization calculated with the obtained CHNS elemental analysis results in mass percentage [%] for carbon 48.68 ± 0.362 , hydrogen 4.31 ± 0.113 , nitrogen 1.72 ± 0.038 , and sulfur 10.37 ± 0.263 (mean value \pm standard deviation (SD)).

parameter for complex	values
$m_{(\text{complex in 25 mL})}$ [mg] \pm SD	105.70 ± 0.885
mass percentage PSS [%] \pm SD	77.85 ± 1.011
mass percentage mTHPP [%] \pm SD	22.78 ± 0.170
recovery rate [%] \pm SD	100.64 ± 1.181
number of monomers pro mTHPP molecule \pm SD	11.25 ± 0.062

Table S3: UV/vis calibration of mTHPP in ethanol.

lambda [nm]	$A = \epsilon \cdot c \cdot d$, $\epsilon \cdot d = x$ [$\mu\text{g}/\text{mL}$]	Coefficient of determination	Measurement range [$\mu\text{g}/\text{mL}$]
416.0	0.83128	0.9999	0.01 - 1
512.4	0.03019	0.9999	0.2 - 50
546.0	0.01082	0.9999	1.0 - 100
587.7	0.00871	0.9999	5.0 - 100
644.5	0.00493	0.9999	10.0 - 100

Table S4: pH-value (mean value of pH-value, standard deviation (SD)) and ζ -potential (mean value of zeta potential, standard deviation (SD)) of colloidal AuNP and surface modified AuNP solutions prepared by standard LbL method.

Sample (unwashed)	pH-value \pm SD	ζ -potential [mV] \pm SD
AuNP	6.1 \pm 0.1	-39 \pm 1
AuNP(PAH) ₁	3.7 \pm 0.1	+33 \pm 6
AuNP(PAH/PSS+mTHPP) ₁	6.4 \pm 0.1	-60 \pm 2
AuNP(PAH/PSS+mTHPP) ₁ PAH	3.9 \pm 0.1	+58 \pm 3
AuNP(PAH/PSS+mTHPP) ₂	6.2 \pm 0.1	-49 \pm 1
AuNP(PAH/PSS+mTHPP) ₂ PAH	3.8 \pm 0.1	+56 \pm 3

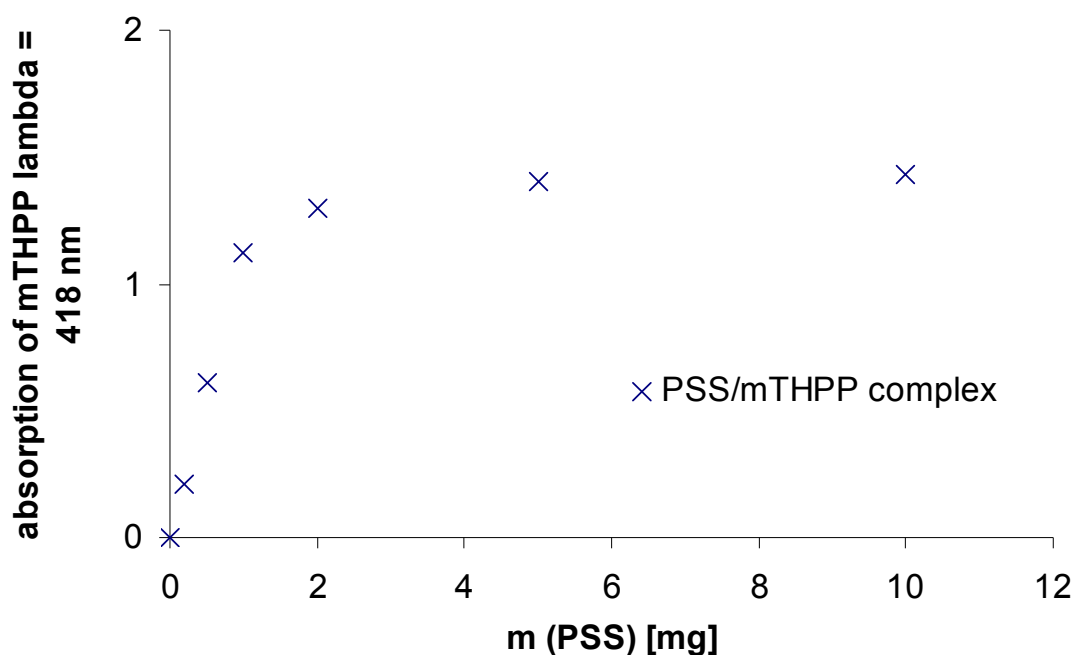


Figure S1: Solubility enhancement of mTHPP in water as function mass of PSS added to 0.2 mg mTHPP, shown results after freeze drying and complex purification.

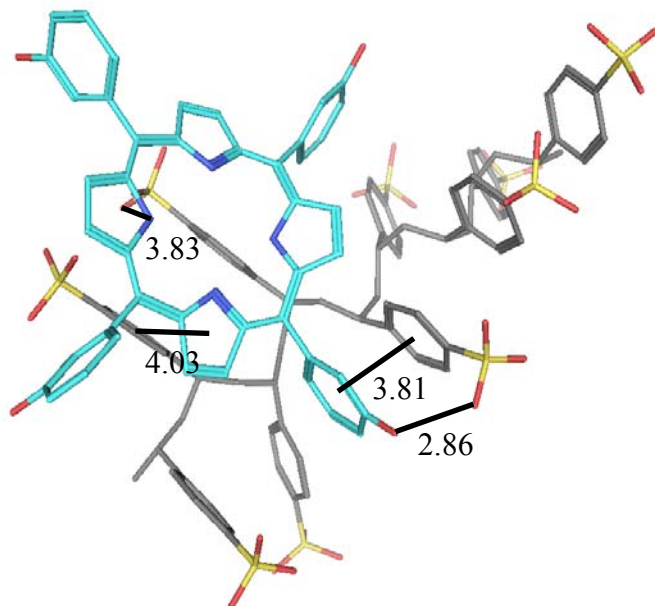


Figure S2: Docking complex between PSS (grey) and mTHPP (cyan). Hydrogen bonds and π - π interactions are drawn in black lines and distances are expressed in Å. Figures generated with MOE (Chemical Computing Group Inc., Montreal, Canada).

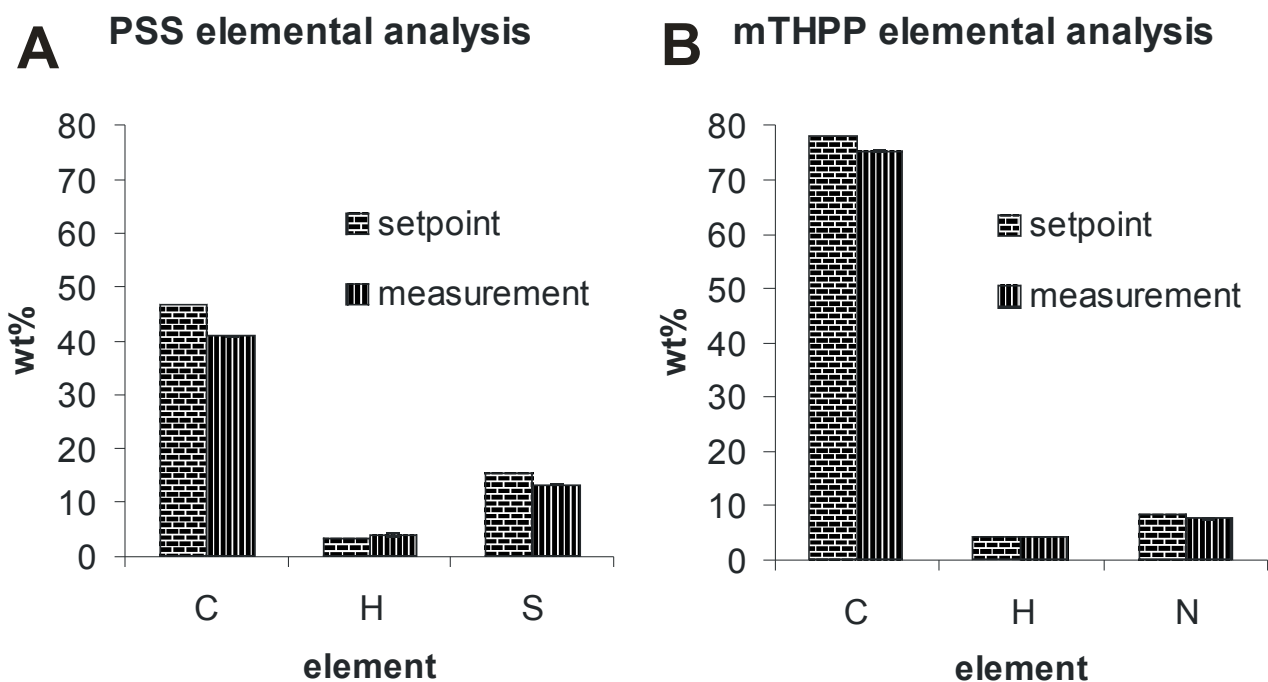


Figure S3: CHNS elemental analysis (n=3) with setpoint as expected value and with measurement as measured value: A) of PSS, B) mTHPP.

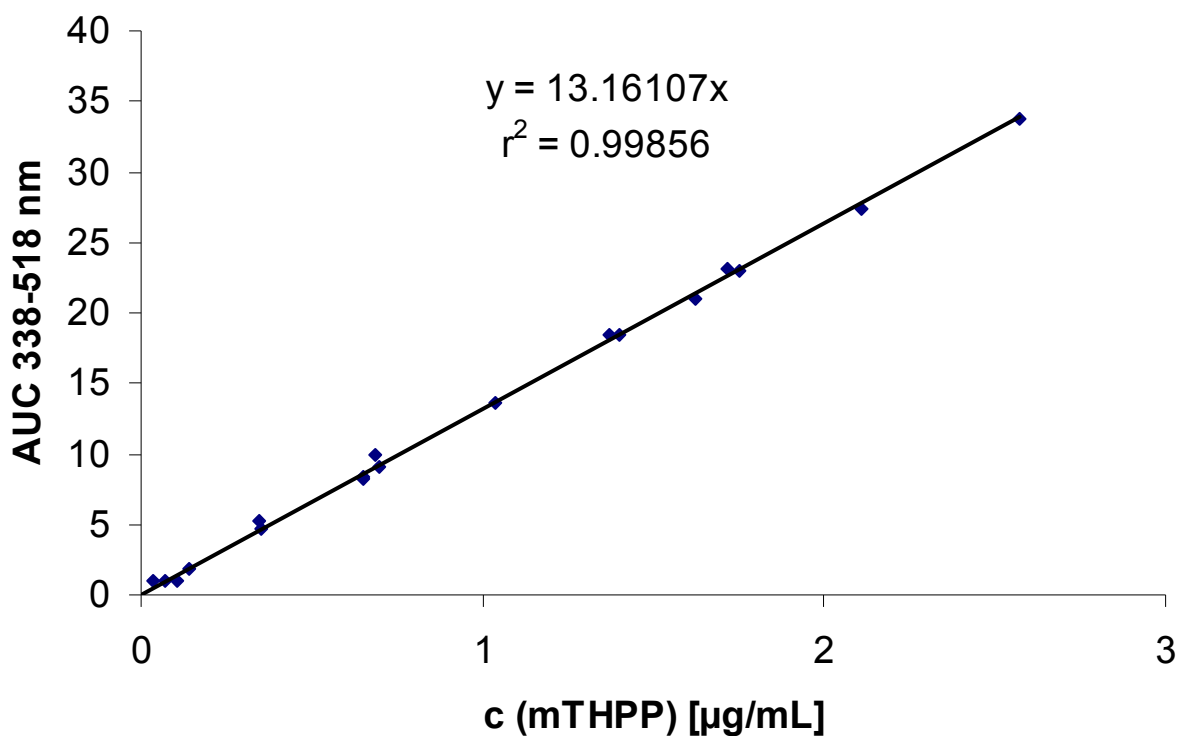


Figure S4: Calibration of AUC of mTHPP between 338 nm and 519 nm as function of mTHPP concentration in ethanol.

References:

- [1] G. B. Sukhorukov, E. Donath, H. Lichtenfeld, E. Knippel, M. Knippel, A. Budde, H. Möhwald. Layer-by-layer self assembly of polyelectrolytes on colloidal particles. *Colloids and Surfaces A: Physicochemical and Engineering Aspects*. 1998; 137 (1-3), 253-266.
- [2] D. K. Chatterjee, L. S. Fong, Y. Zhang. Nanoparticles in photodynamic therapy: An emerging paradigm. *Advanced Drug Delivery Reviews*. 2008; 60 (15), 1627-1637.
- [3] A. Juarranz, P. Jaèn, F. Sanz-Rodríguez, J. Cuevas, S. González. Photodynamic therapy of cancer. Basic principles and applications. *Clinical and Translational Oncology*. 2008; 10 (3), 148-154.
- [4] Y. N. Konan, R. Gurny, E. Allemann. State of the art in the delivery of photosensitizers for photodynamic therapy. *Journal of Photochemistry and Photobiology B: Biology*. 2002; 66 (2), 89-106.
- [5] M. Ochsner. Photophysical and photobiological processes in the photodynamic therapy of tumours. *Journal of Photochemistry and Photobiology B: Biology*. 1997; 39 (1), 1-18.
- [6] D. Bechet, P. Couleaud, C. Frochot, M. L. Viriot, F. Guillemin, M. Barberi-Heyob. Nanoparticles as vehicles for delivery of photodynamic therapy agents. *Trends in Biotechnology*. 2008; 26 (11), 612-621.
- [7] K. Cho, X. Wang, S. Nie, Z. Chen, D. M. Shin. Therapeutic nanoparticles for drug delivery in cancer. *Clinical Cancer Research*. 2008; 14 (5), 1310-1316.
- [8] Y. Matsumura, H. Maeda. A new concept for macromolecular therapeutics in cancer chemotherapy: Mechanism of tumorotropic accumulation of proteins and the antitumor agent smancs. *Cancer Research*. 1986; 46 (12 I), 6387-6392.
- [9] R. Duncan. The dawning era of polymer therapeutics. *Nature Reviews Drug Discovery*. 2003; 2 (5), 347-360.
- [10] H.-B. Ris, H. J. Altermatt, R. Inderbitzi, R. Hess, B. Nachbur, J. C. M. Stewart, Q. Wang, C. K. Lim, R. Bonnett, M. C. Berenbaum, U. Althaus. Photodynamic therapy with chlorins for diffuse malignant mesothelioma: Initial clinical results. *British Journal of Cancer*. 1991; 64 (6), 1116-1120.
- [11] G. Decher, J. D. Hong, J. Schmitt. Buildup of ultrathin multilayer films by a self-assembly process: III. Consecutively alternating adsorption of anionic and cationic polyelectrolytes on charged surfaces. *Thin Solid Films*. 1992; 210-211 (PART 2), 831-835.
- [12] I. L. Radtchenko, G. B. Sukhorukov, S. Leporatti, G. B. Khomutov, E. Donath, H. Möhwald. Assembly of alternated multivalent ion/polyelectrolyte layers on colloidal particles. Stability of the multilayers and encapsulation of macromolecules into

- polyelectrolyte capsules. *Journal of Colloid and Interface Science*. 2000; 230 (2), 272-280.
- [13] I. L. Radtchenko, G. B. Sukhorukov, H. Möhwald. A novel method for encapsulation of poorly water-soluble drugs: Precipitation in polyelectrolyte multilayer shells. *International Journal of Pharmaceutics*. 2002; 242 (1-2), 219-223.
- [14] K. Köhler, G. B. Sukhorukov. Heat treatment of polyelectrolyte multilayer capsules: A versatile method for encapsulation. *Advanced Functional Materials*. 2007; 17 (13), 2053-2061.
- [15] M. F. Bédard, S. Sadasivan, G. B. Sukhorukov, A. Skirtach. Assembling polyelectrolytes and porphyrins into hollow capsules with laser-responsive oxidative properties. *Journal of Materials Chemistry*. 2009; 19 (15), 2226-2233.
- [16] R. Sardar, A. M. Funston, P. Mulvaney, R. W. Murray. Gold Nanoparticles: Past, Present, and Future. *Langmuir*. 2009; 25 (24), 13840-13851.
- [17] M. E. Wieder, D. C. Hone, M. J. Cook, M. M. Handsley, J. Gavrilovic, D. A. Russell. Intracellular photodynamic therapy with photosensitizer-nanoparticle conjugates: Cancer therapy using a 'Trojan horse'. *Photochemical and Photobiological Sciences*. 2006; 5 (8), 727-734.
- [18] T. Ganesh. Improved biochemical strategies for targeted delivery of taxoids. *Bioorganic and Medicinal Chemistry*. 2007; 15 (11), 3597-3623.
- [19] E. Boisselier, D. Astruc. Gold nanoparticles in nanomedicine: Preparations, imaging, diagnostics, therapies and toxicity. *Chemical Society Reviews*. 2009; 38 (6), 1759-1782.
- [20] P. Decuzzi, R. Pasqualini, W. Arap, M. Ferrari. Intravascular delivery of particulate systems: Does geometry really matter? *Pharmaceutical Research*. 2009; 26 (1), 235-243.
- [21] Z. Wang, L. Ma. Gold nanoparticle probes. *Coordination Chemistry Reviews*. 2009; 253 (11-12), 1607-1618.
- [22] V. Sharma, K. Park, M. Srinivasarao. Colloidal dispersion of gold nanorods: Historical background, optical properties, seed-mediated synthesis, shape separation and self-assembly. *Materials Science and Engineering R: Reports*. 2009; 65 (1-3), 1-38.
- [23] D. I. Gittins, F. Caruso. Multilayered polymer nanocapsules derived from gold nanoparticle templates. *Advanced Materials*. 2000; 12 (24), 1947-1949.
- [24] H. I. Labouta, M. Schneider. Tailor-made biofunctionalized nanoparticles using layer-by-layer technology *International Journal of Pharmaceutics* 2010.
- [25] S. H. Lee, K. H. Bae, S. H. Kim, K. R. Lee, T. G. Park. Amine-functionalized gold nanoparticles as non-cytotoxic and efficient intracellular siRNA delivery carriers. *International Journal of Pharmaceutics*. 2008; 364 (1), 94-101.

- [26] S. R. Bhattarai, R. B. K.C., S. Aryal, N. Bhattarai, S. Y. Kim, H. K. Yi, P. H. Hwang, H. Y. Kim. Hydrophobically modified chitosan/gold nanoparticles for DNA delivery. *Journal of Nanoparticle Research*. 2008; 10 (1), 151-162.
- [27] Y.-H. Chen, C.-Y. Tsai, P.-Y. Huang, M.-Y. Chang, P.-C. Cheng, C.-H. Chou, D.-H. Chen, C.-R. Wang, A.-L. Shiau, C.-L. Wu. Methotrexate conjugated to gold nanoparticles inhibits tumor growth in a syngeneic lung tumor model. *Molecular Pharmaceutics*. 2007; 4 (5), 713-722.
- [28] M. Prabakaran, J. J. Grailer, S. Pilla, D. A. Steeber, S. Gong. Gold nanoparticles with a monolayer of doxorubicin-conjugated amphiphilic block copolymer for tumor-targeted drug delivery. *Biomaterials*. 2009; 30 (30), 6065-6075.
- [29] G. F. Schneider, V. Subr, K. Ulbrich, G. Decher. Multifunctional cytotoxic stealth nanoparticles. A model approach with potential for cancer therapy. *Nano Letters*. 2009; 9 (2), 636-642.
- [30] Y. Cheng, A. C. Samia, J. D. Meyers, I. Panagopoulos, B. Fei, C. Burda. Highly efficient drug delivery with gold nanoparticle vectors for in vivo photodynamic therapy of cancer. *Journal of the American Chemical Society*. 2008; 130 (32), 10643-10647.
- [31] G. Schneider, G. Decher. From functional core/shell nanoparticles prepared via layer-by-layer deposition to empty nanospheres. *Nano Letters*. 2004; 4 (10), 1833-1839.
- [32] E. A. Meyer, R. K. Castellano, F. Diederich. Interactions with aromatic rings in chemical and biological recognition. *Angewandte Chemie - International Edition*. 2003; 42 (11), 1210-1250.
- [33] G. M. Morris, H. Ruth, W. Lindstrom, M. F. Sanner, R. K. Belew, D. S. Goodsell, A. J. Olson. Software news and updates AutoDock4 and AutoDockTools4: Automated docking with selective receptor flexibility. *Journal of Computational Chemistry*. 2009; 30 (16), 2785-2791.
- [34] O. Trott, A. J. Olson. Software news and update AutoDock Vina: Improving the speed and accuracy of docking with a new scoring function, efficient optimization, and multithreading. *Journal of Computational Chemistry*. 2010; 31 (2), 455-461.
- [35] J. Turkevich, P. C. Stevenson, J. Hillier. A study of the nucleation and growth processes in the synthesis of colloidal gold. *Discussions of the Faraday Society*. 1951; 11, 55-75.
- [36] C. A. Mirkin. Invited contribution from recipient of ACS award in pure chemistry: Programming the assembly of two- and three-dimensional architectures with DNA and nanoscale inorganic building blocks. *Inorganic Chemistry*. 2000; 39 (11), 2258-2272.
- [37] M. Chanana, A. Gliozzi, A. Diaspro, I. Chodnevskaja, S. Huewel, V. Moskalenko, K. Ulrichs, H.-J. Galla, S. Krol. Interaction of polyelectrolytes and their composites with living cells. *Nano Letters*. 2005; 5 (12), 2605-2612.

- [38] G. Schneider, G. Decher. Functional core/shell nanoparticles via layer-by-layer assembly. Investigation of the experimental parameters for controlling particle aggregation and for enhancing dispersion stability. *Langmuir*. 2008; 24 (5), 1778-1789.
- [39] C. Herms. Sigma-Aldrich Chemie GmbH, 82024 Taufkirchen, Germany. In: G. Taufkirchen, ed. Taufkirchen, Germany: Sigma-Aldrich Chemie GmbH 2009.
- [40] W. Haiss, N. T. K. Thanh, J. Aveyard, D. G. Fernig. Determination of size and concentration of gold nanoparticles from UV-Vis spectra. *Analytical Chemistry*. 2007; 79 (11), 4215-4221.
- [41] Y. Liu, M. K. Shipton, J. Ryan, E. D. Kaufman, S. Franzen, D. L. Feldheim. Synthesis, stability, and cellular internalization of gold nanoparticles containing mixed peptide-poly(ethylene glycol) monolayers. *Analytical Chemistry*. 2007; 79 (6), 2221-2229.
- [42] C. S. Weisbecker, M. V. Merritt, G. M. Whitesides. Molecular self-assembly of aliphatic thiols on gold colloids. *Langmuir*. 1996; 12 (16), 3763-3772.
- [43] Z. Dai, A. Voigt, S. Leporatti, E. Donath, L. Dähne, H. Möhwald. Layer-by-layer self-assembly of polyelectrolyte and low molecular weight species into capsules. *Advanced Materials*. 2001; 13 (17), 1339-1342.
- [44] W. N. Leung, X. Sun, N. K. Mak, C. M. N. Yow. Photodynamic effects of mTHPC on human colon adenocarcinoma cells: Photocytotoxicity, subcellular localization and apoptosis. *Photochemistry and Photobiology*. 2002; 75 (4), 406-411.
- [45] C. M. N. Yow, J. Y. Chen, N. K. Mak, N. H. Cheung, A. W. N. Leung. Cellular uptake, subcellular localization and photodamaging effect of Temoporfin (mTHPC) in nasopharyngeal carcinoma cells: Comparison with hematoporphyrin derivative. *Cancer Letters*. 2000; 157 (2), 123-131.
- [46] O. Bourdon, V. Mosqueira, P. Legrand, J. Blais. A comparative study of the cellular uptake, localization and phototoxicity of meta-tetra (hydroxyphenyl) chlorin encapsulated in surface-modified submicronic oil/water carriers in HT29 tumor cells. *Journal of Photochemistry and Photobiology B: Biology*. 2000; 55 (2-3), 164-171.

6 Chapter 4: Drug-loaded AuNP for PDT

Gold nanoparticles as drug delivery systems for photodynamic therapy: Preparation, characterization and cellular investigations*

*** This chapter is prepared for publication as a journal article:**

Karin Löw¹, Nico Reum¹, Sylvia Wagner, Hagen von Briesen, and Marc Schneider.
Gold nanoparticles as drug delivery systems for photodynamic therapy: Preparation, characterization and cellular investigations.

¹ These authors contributed equally to this work

Abstract

Many applied photosensitizers are characterized by a strong hydrophobicity and the induction of unrequested adverse reactions. The photosensitizer 5,10,15,20-tetrakis(m-hydroxyphenyl)chlorin (mTHPC) is an approved anti-cancer drug for head-and-neck cancer causing some adverse effects due to its formulation. Furthermore, mTHPC is known to be effective against a variety of tumor cells *in vitro* indicating future potential. Therefore, the administration and the following treatment are accompanied by severe difficulties including application problems. To overcome these kind of problems, the photosensitizer can be delivered by nanoparticles. In the present study, modified gold nanoparticles (mAuNP) were prepared by surface modification of citrate stabilized gold nanoparticles (AuNP) using the layer-by-layer (LbL) technique based on standard polyelectrolytes. The mAuNP and drug-loaded mAuNP with a size of 14 nm respectively were characterized regarding their physico-chemical properties as well as the drug loading efficiency. The cellular characterization excluded a potential cytotoxicity of the unloaded mAuNP even at high concentrations. Furthermore, the cellular accumulation of unloaded and mTHPC-loaded mAuNP was shown and a drug release into the cells was assessed. Additionally, the activity of mTHPC-loaded mAuNP compared to free mTHPC was investigated. After illumination, the mTHPC-loaded mAuNP treated cells showed a decreased viability. First and foremost, dark toxic effects of the free photosensitizer could be reduced using mAuNP as drug carrier. To sum up, mAuNP are promising drug delivery systems for the hydrophobic photosensitizer mTHPC.

6.1 Introduction

Photodynamic therapy (PDT) combines the administration of a photoinducable drug (photosensitizer) and the activation with light of a certain wavelength leading to cell death [1]. PDT facilitates a topical or local treatment of patients bearing different malignancies which often are tumors. After illumination highly reactive oxygen species, e.g., singlet oxygen ($^1\text{O}_2$) are generated destroying the surrounding tissue by apoptosis or necrosis. To achieve high rates of apoptosis efficient singlet oxygen quantum yields are needed. Therefore, high amount of photosensitizer must accumulate within the targeted tissue reaching effective and therapeutic intracellular concentrations. Nevertheless, PDT possesses certain administrable challenges and can cause burns, swelling, and pain [2].

The second generation photosensitizer 5,10,15,20-tetrakis(m-hydroxyphenyl)chlorin (mTHPC), which has been approved by the EMA in October 2001 for the palliative treatment of advanced head-and-neck-cancer [3], is characterized by a strong phototoxicity against a variety of human cancer cell lines *in vitro* [4]. Besides, it is known, that mTHPC possess a limited dark toxicity and can cause adverse effects especially caused by precipitation due to its strong hydrophobicity as well as its unspecific cellular accumulation [5, 6].

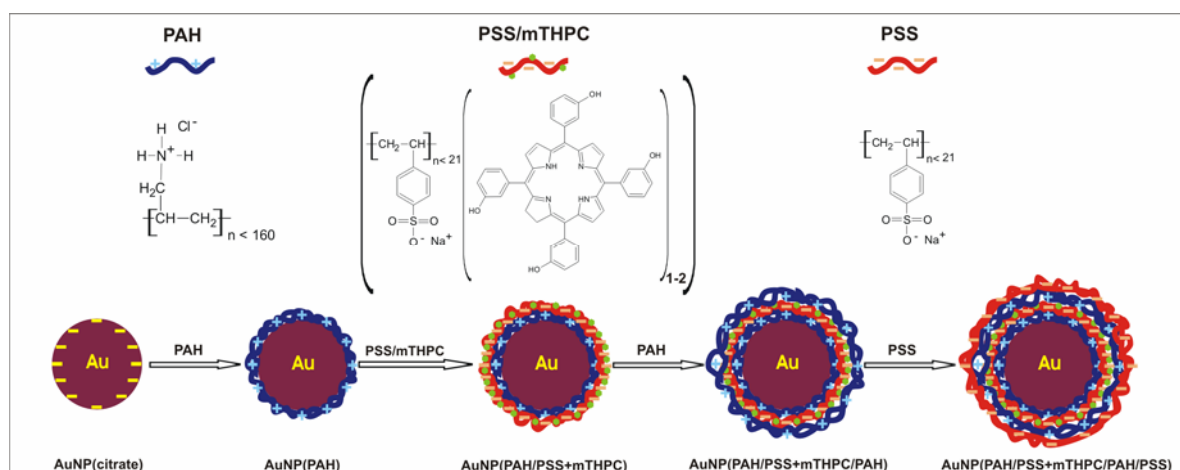
To enhance PDT efficiency and to overcome this obstacle, the usage of nanoparticulate systems is highly investigated [7]. Chatterjee et al. divided nanoparticle delivery systems for photodynamic therapy (PDT) in passive and active carriers for photosensitizer excitation[8]. Our focus is on passive carriers which are non-biodegradable and metallic. The usage of such nanoparticles results in different advantages such as well controlled synthesis, simple characterization techniques as well as uptake into cells without being recognized by efflux systems (e.g., P-glycoprotein) resulting in an increased intracellular drug concentration [9]. A key advantage is the transport of hydrophobic drugs in the body, avoiding photosensitizer aggregation and loss of activity. Furthermore, the intravenously administered drug delivery systems can increase the tumor concentration of anti-tumor drugs up to 70-fold due to the so-called enhanced permeability and retention effect (EPR effect) [10, 11]. Nanoparticles as drug delivery systems offer several advantages including high drug-loading rates with marginal premature drug release as well as an efficient uptake by cancer cells through the EPR effect [12]. Tumors are characterized by leaky vasculature with pores of a size between 200 to 600 nm in diameter following

the fast hypervascularization, a decreased pH value and a weak lymphatic drainage compared to normal tissue [13]. All these properties enable high accumulation of nanoparticles and their retention in tumor tissue.

Nanoparticles for PDT can be synthesized in different sizes and can act as multifunctional platforms through (I) a shell volume in which photosensitizers can be encapsulated or coupled, (II) a surface that can be functionalized to attach targeting groups for cancer specific drug accumulation, and (III) a contrast agent that can be incorporated for diagnostic reasons [7, 8].

To ensure maximum flexibility for the drug carrier, modular systems are most appreciated. An intriguing approach is based on the layer-by-layer (LbL) technique introduced by Decher et al. [14]. The LbL technique offers an endless variety of polyelectrolyte material and hence the preparation of tailored surfaces. As a core material, colloidal gold was chosen because of its optical properties, the intriguing size range in which monodisperse particles can be obtained, and its high chemical stability [15]. With respect to PDT, AuNP were also found to positively influence the singlet oxygen yield [16].

Here we described the preparation, characterization and cellular testing of mTHPC-loaded modified gold nanoparticles (mAuNP) (Scheme 1). In this connection, the photosensitizer was complexed with poly(styrene sulfonate) sodium salt (PSS) and adsorbed onto the nanoparticle surface. First, the unloaded and mTHPC-loaded mAuNP were subjected to a physico-chemical characterization. Following, a potential cytotoxicity was investigated regarding high mAuNP concentrations, later the cellular binding and accumulation was proofed. Furthermore, we investigated the drug release into the cells and the efficiency of the mTHPC-loaded nanoparticles.



Scheme 1: Layer-by-layer preparation of AuNP(PAH/PSS+mTHPC/PAH/PSS), PAH (MW 15.0 kDa), PSS (MW 4.3 kDa).

6.2 Materials and methods

6.2.1 Materials

The 5,10,15,20-tetrakis(m-hydroxyphenyl)chlorin, mTHPC (M_r 680.75 g mol⁻¹), seen in Scheme 1 was kindly provided by biolitec AG (Jena, Germany). Gold (III) chloride hydrate (HAuCl₄*3H₂O), tri-sodium citrate-2-hydrate (Na₃C₆H₅O₇*2H₂O), poly(styrene sulfonate) sodium salt (PSS) (MW 4.3 kDa) and poly(allylamine hydrochloride) (PAH) (MW 15.0 kDa) were purchased from Sigma-Aldrich (Steinheim, Germany). The water used in all experiments was prepared in a Millipore Milli-Q purification system (resistivity higher than 18.0 MΩ cm⁻¹).

6.2.2 Methods

6.2.2.1 Preparation and characterization of PSS/mTHPC complex

PSS/mTHPC complex was synthesized, purified, and characterized according to the procedure of Reum et al.[17] In brief, the complex was prepared by freeze-drying a liquid mixture of both compounds. The purification of the complex was realized by a combination of centrifugation and filtration. H-bonds and π – π interactions were the responsible forces of complex formation. For complexation of one mTHPC molecule, around 13 monomer units (4-ethylbenzenesulfonate sodium salt, 206.2 g mol⁻¹) of one PSS (4300 g mol⁻¹) molecule were necessary.

6.2.2.2 Synthesis of AuNP

Colloidal gold was synthesized as described before by the reduction of gold ions with citrate ions.[18] A volume of 99 mL of a tetrachlorauric acid (HAuCl₄*3H₂O) solution containing 20 mg (50.8 μmol) of gold salt were refluxed and 1 mL of sodium citrate solution containing 74.7 mg (254 μmol) of Na₃C₆H₅O₇*2H₂O was added to the boiling solution. The solution was boiled for 20 min and cooled to room temperature. AuNP diameter determined by TEM with volume was 14 nm. The resulting suspensions had gold concentrations of 100 μg mL⁻¹.

6.2.2.3 Preparation of PAH/PSS coated AuNP

For encapsulation of colloidal gold nanoparticles, we used a slightly modified method formerly described by Decher[19] and Krol[20] using PAH and PSS. To 30 mL of the PAH solution (2.0 mg mL^{-1}) was added 10 mL of unwashed-citrate-stabilized gold nanoparticle solution with a gold concentration of $100 \text{ } \mu\text{g mL}^{-1}$, resulting in 136,500 PAH chains per AuNP determined following Schneider et al.[21] After stirring for 10 min, particles were separated from PAH excess by centrifugation at 8,515 g for 15 h (Hettich Rotina 420 R, Hettich GmbH & Co. KG, Tuttlingen, Germany). The centrifuged nanoparticles were redispersed in water to a volume of 10 mL. The washing step was repeated once. Ten milliliters of PAH-coated AuNP were coated with 20 mL of PSS solution (1.17 mg mL^{-1}) resulting in 91,000 PSS chains per AuNP. After incubation for 10 min, a sterile filtration (pore size: $0.2 \text{ } \mu\text{m}$, membrane material: cellulose acetate) was carried out with the AuNP(PAH/PSS) solution. Then the solution was centrifuged for 5 h at 9,612 g with a table centrifuge. Under a laminar flow cabinet the supernatant (29.850 mL) was removed and replaced by 3.350 mL of HT29 cell culture medium with 10% FCS to obtain a total volume of 3.50 mL of AuNP(PAH/PSS) solution with an Au concentration of around $150 \text{ } \mu\text{g mL}^{-1}$ and a pH value of 7.5 (Table 1), applicable for *in vitro* cell testing.

6.2.2.4 Preparation of (PAH/PSS+mTHPC/PAH/PSS) coated AuNP

Similar to preparation of PAH/PSS coated AuNP, but as second layer instead of PSS, a complex consisting of PSS/mTHPC was used. The drug complex was applied in water at a concentration of $77.4 \text{ } \mu\text{g mL}^{-1}$ PSS and $20.1 \text{ } \mu\text{g mL}^{-1}$ mTHPC. To 20 mL of PSS/mTHPC complex was added 10 mL of AuNP(PAH), resulting in 15,000 PSS chains per AuNP. After stirring for 10 min the third polyelectrolyte layer (PAH) was adsorbed to AuNP(PAH/PSS+mTHPC). Therefore, to 20 mL of PAH solution with a concentration of 3.7 mg mL^{-1} was added the 30 mL of AuNP(PAH/PSS+mTHPC) solution, resulting in 206,000 PAH chains per AuNP. After stirring for 10 min, particles were separated from PAH excess by centrifugation at 24,400 g for 20 min (Hettich Rotina 420 R, Hettich GmbH & Co. KG, Tuttlingen, Germany). The centrifuged nanoparticles were redispersed in water to a volume of 25 mL. The washing step was repeated once and the nanoparticles were redispersed in water to a total volume of 10 mL. PSS was used as last layer material with a concentration of 1.2 mg mL^{-1} . To

20 mL of PSS solution was added 10 mL of AuNP(PAH/PSS+mTHPC/PAH) solution (per AuNP are 233,200 PSS chains available). After incubation for 10 min, a sterile filtration (pore size: 0.2 μm , membrane material: cellulose acetate) was carried out with the AuNP(PAH/PSS+mTHPC/PAH/PSS) solution. Then the solution was centrifuged for 20 min at 24,400 g with a table centrifuge. Under a laminar flow cabinet the supernatant (29.915 mL) was removed and replaced by 0.915 mL of HT29 cell culture medium with 10% FCS to obtain a total volume of 1.0 mL of AuNP(PAH/PSS+mTHPC/PAH/PSS) solution with an Au concentration of around 300 $\mu\text{g mL}^{-1}$ and a pH value of 7.5 (Table 1), applicable for *in vitro* tests.

6.2.2.5 Transmission electron microscopy (TEM) measurements

TEM measurements of the gold nanoparticles were performed on a JOEL model JEM 2010 instrument (JOEL GmbH, Eching, Germany) operated at an accelerating voltage of 120 kV. Samples for TEM analysis were prepared by placing 12 μL of washed gold nanoparticle solution on a carbon-coated 400 mesh copper grid (S160-4, Plano GmbH, Wetzlar, Germany). The suspensions were allowed to dry until the water was completely evaporated. Contrast agent was not applied.

6.2.2.6 Particle size analysis

The particle size analysis of TEM images was carried on ~ 100 particles using *Image J*. The real median diameter was determined.

6.2.2.7 ζ -potential measurements

The ζ -potential of uncoated, coated, and mTHPC loaded AuNP was determined by the principle of laser Doppler velocimetry with a Malvern Zetasizer Nano ZS (Malvern Instruments GmbH, Herrenberg, Germany). Measurements were realized in triplicate at 25 $^{\circ}\text{C}$ with the model of Smoluchowski.

6.2.2.8 UV-visible spectroscopy measurements

UV/Vis spectroscopy was carried out to check the successful polyelectrolyte and drug adsorption to AuNP surfaces. Furthermore, the adsorbed mTHPC mass to AuNP

surface was determined from the area between the curves (ABC). All measurements were carried out in 1 cm quartz cuvettes with the Perkin-Elmer Lambda 35 Spectrophotometer (PerkinElmer LAS, Rodgau, Germany).

6.2.2.9 Cell culture

For all experiments the human colon carcinoma cell line HT29 (kindly provided by Indivumed, Hamburg, Germany) was used. HT29 cells were cultured at 37 °C and 5 % CO₂ in McCoy's 5A medium (Promocell, Heidelberg, Germany) supplemented with 10 % fetal calf serum (PAA, Pasching, Austria) and antibiotics (50 U mL⁻¹ penicillin and 50 µg mL⁻¹ streptomycin; Invitrogen, Karlsruhe, Germany).

6.2.2.10 Determination of cell proliferation (BrdU assay)

The cell proliferation was measured using the Cell Proliferation ELISA assay (BrdU (colorimetric); Roche Diagnostics, Mannheim, Germany). 5,000 cells were cultured in 96 well plates (Greiner, Frickenhausen, Germany) and exposed to various concentrations (1, 10, 50 and 100 µg mL⁻¹) of unloaded mAuNP in cell culture medium for 4, 24, 48 and 72 h (long time incubation) or 4 h followed by different persisting recovery times (24, 48 and 72 h) at 37 °C. Subsequently, the cells were washed once with cell culture medium and the determination of the cell proliferation was carried out according to the manufacturer's instruction manual. The mean absorbance of untreated cells was defined as 100 % and the absorbance of the treated cells was related to this value. 2 % Triton X-100 treated cells were used as positive control.

6.2.2.11 Determination of cell viability (WST-1 assay)

Cell viability was determined with WST-1 assay (Cell Proliferation Reagent; Roche Diagnostics) that bases on the absorption measurement of formazan formation. 5,000 cells were cultured in 96 well plates (Greiner) and exposed to various concentrations (1, 10, 50 and 100 µg mL⁻¹) of unloaded mAuNP in cell culture medium for 4, 24, 48 and 72 h (long time incubation) or 4 h followed by different persisting recovery times (24, 48 and 72 h) at 37 °C. Subsequently, the cells were washed once with cell culture medium and the determination of cell viability was

carried out after addition of WST-1 reagent and the formazan formation was measured as described in the manufacturer's instruction manual. The mean absorbance of untreated cells was defined as 100 %; the absorbance of the treated cells was related to this value. 2 % Triton X-100 treated cells were used as positive control.

6.2.2.12 Determination of cell membrane integrity (LDH assay)

The release of lactate dehydrogenase (LDH) was monitored with the Cytotoxicity Detection Kit (LDH; Roche Diagnostics). 5,000 cells were cultured in 96 well plates (Greiner) and exposed to various concentrations (1, 10, 50 and 100 $\mu\text{g mL}^{-1}$) of unloaded mAuNP in cell culture medium for 4, 24, 48 and 72 h (long time incubation) or 4 h followed by different persisting recovery times (24, 48 and 72 h) at 37 °C. Subsequently, the cells were centrifuged (5 min, 1000 rpm, room temperature) and the supernatant was transferred into a new 96 well plate. The determination of the LDH leakage was carried out after addition of LDH substrate and the formazan formation was measured as described in the manufacturer's instruction manual. The mean absorbance of 2 % Triton X-100 treated cells was defined as 100 % and the absorbance of the treated cells was related to this value.

6.2.2.13 Determination of cellular accumulation

Cells were cultured in 24 well plates (Greiner) and incubated with unloaded mAuNP concentrations (100 $\mu\text{g mL}^{-1}$) for 24 up to 72 h at 37 °C. Following, the cells were washed twice with PBS and bright field pictures were taken of the cells.

6.2.2.14 Scanning electron microscopy (SEM)

Cells were cultured in μ -dishes (Ibidi, München, Germany) and incubated with unloaded mAuNP (100 $\mu\text{g mL}^{-1}$) up to 72 h at 37 °C. Afterwards, the cells were washed with PBS and fixed over night at 4 °C with sodium cacodylate buffer containing 2 % glutaraldehyde. Following, the cells were incubated with 2 % osmium tetroxide, 1% tannic acid and 1% uranyl acetate. The cells were dehydrated in ethanol series and a critical point drying was performed. For microscopy analysis, the

samples were sputtered with gold and examined in a LEO 435 VP electron scanning microscopy (LEO Elektronenmikroskope GmbH, Oberkochen, Germany).

6.2.2.15 Cellular uptake and intracellular distribution of free mTHPC and mTHPC-loaded mAuNP

Cellular uptake and intracellular distribution was analyzed using confocal laser scanning microscopy (CLSM) and multiphoton laser scanning microscopy (MP-LSM). 125,000 cells were seeded into chamber slides (CultureSlides, Becton Dickinson) and incubated for 24 h at 37 °C. For 24 h the cells were treated with both, free mTHPC ($3 \mu\text{g mL}^{-1}$) and two concentrations mTHPC-loaded mAuNP (mTHPC concentration: 3 and $9 \mu\text{g mL}^{-1}$) in the dark at 37 °C, respectively. Following, the cells were washed twice with PBS and the membrane was stained with concanavalin A Alexa Fluor 488 ($50 \mu\text{g mL}^{-1}$, Invitrogen). After fixation, the cells were washed again and embedded in Vectashield HardSet Mounting Medium (Axxora, Grünberg, Germany) and analyzed using a confocal laser scanning microscope (Axiovert 200 M microscope with a 510 NLO Meta device, Zeiss, Jena, Germany) with argon ion and chameleon laser (providing fs laser pulses at a repetition rate of 80 MHz at $\lambda = 800 \text{ nm}$ for AuNP excitation) and the LSM Image Examiner software.

6.2.2.16 Determination of cell viability after PDT treatment

Cell viability was determined with WST-1 assay (Cell Proliferation Reagent, Roche Diagnostics) after incubation with mTHPC-loaded mAuNP. 15,000 cells were cultured in 96 well plates (Greiner) and exposed to free and bound mTHPC ($3 \mu\text{g mL}^{-1}$) in cell culture medium for 4 and 24 h at 37 °C. Subsequently, the cells were washed once with cell culture medium and either illuminated with 5 J cm^{-2} (at a fluence rate of 10 mW cm^{-2} for 500 s) or kept in the dark as dark control. After 1 h recovery at 37 °C, the determination of cell viability was carried out as previously described.

6.3 Results and Discussion

6.3.1 Synthesis of Gold nanoparticles (AuNP)

Colloidal gold prepared by redox reaction of gold (III) chloride hydrate and tri-sodium citrate-2-hydrate was characterized by transmission electron microscopy (TEM) and showed a monodisperse size distribution with a median particle diameter of 14.1 nm and a standard deviation of 1.1 nm (Figure 1, Table 1). As expected the ζ -potentials of citrate stabilized AuNP showed negative values (-33 ± 3 mV) because of the citrate ions on the surface of AuNP [21].

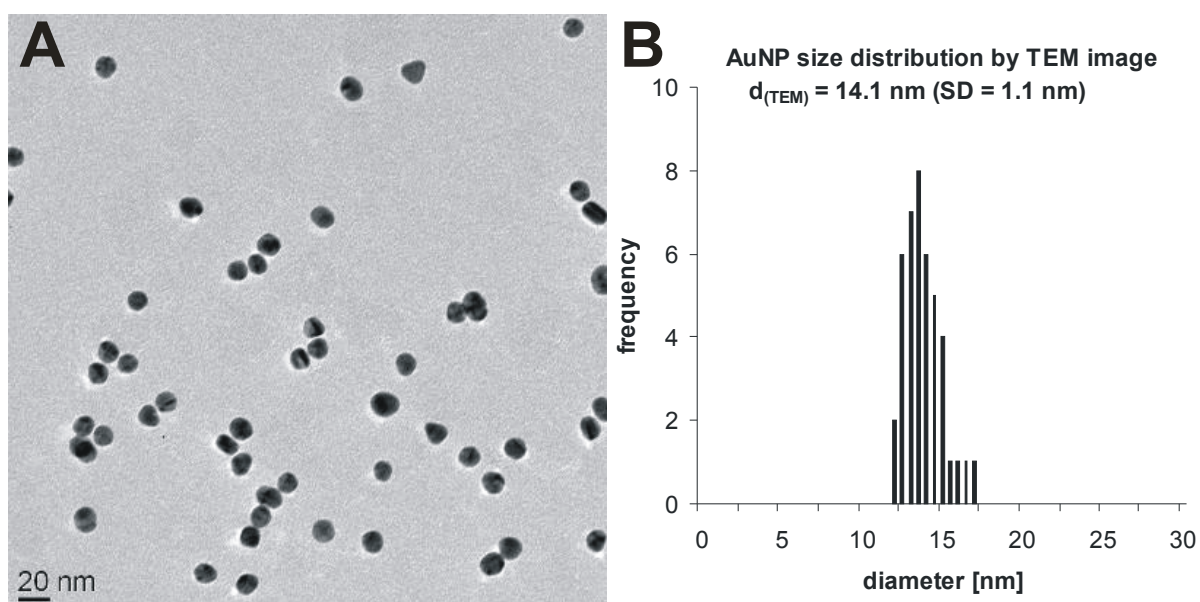


Figure 1: (A) TEM image of citrate stabilized AuNP, (B) Size distribution of citrate stabilized AuNP (analysis of the TEM image with *Image J*).

With the help of equation (1) from Haiss et al. [22], based on UV/Vis absorption data, we could also calculate the AuNP diameters obtaining a value of 13.1 ± 1.2 nm which is in very good agreement with the result by TEM measurement.

$$d = \left(\frac{A_{SPR} (5.89 \times 10^{-6})}{c_{Au} \exp(C_1)} \right)^{\frac{1}{C_2}} \quad (1)$$

with d the diameter of the particles in nanometer (for $5 \text{ nm} \leq d \leq 30 \text{ nm}$), c_{Au} the gold concentration (mol L^{-1}), A_{SPR} the absorbance at the surface plasmon resonance of AuNP solution, and $C_1 = -4.75$, $C_2 = 0.314$ being specific constants.

6.3.2 Characterization of mAuNP (AuNP(PAH/PSS))

Schema 1 depicts the principle of PAH/PSS loaded AuNP preparation with the layer-by-layer deposition technique. For the drug-free AuNP(PAH/PSS) the Schema 1 was slightly simplified because only two polyelectrolyte layers were adsorbed on the AuNP surface and instead of PSS/mTHPC complex for the second layer, pure PSS was used. As first layer, PAH was adsorbed, therefore, the ζ -potential was inverted (to positive value) with respect to the citrate-stabilized AuNP (Supporting Information) [21]. The typical absorption spectrum of citrate-stabilized AuNP (black dashed line) and the respective absorption curves after surface modification is shown in Figure 2 A. The peak near 520 nm is caused by surface plasmon resonance [20] of AuNP allowing a straightforward characterization [23]. The adsorption of PAH led to a little red shift of the AuNP peak of 1 - 2 nm due to change of the surrounding refractive index induced by the adsorbed polyelectrolyte PAH and a broadening of the peak on the right side (blue solid line in Figure 2 A). The adsorption of the second layer, PSS resulted in a negative ζ -potential of -46 mV (Supporting Information, Table 1), as expected. Sterile filtration and one centrifugation step of modified AuNP resulted still in negative ζ -potential values (-49 mV). The ζ -potential of AuNP(PAH/PSS) in medium was decreased to a value of around -10 mV caused by a higher ion concentration and proteins compared to pure water (Supporting Information, Table 1). The red shift and the broadening were obtained with every further adsorbed layer. This behavior was also found after dispersing AuNP(PAH/PSS) in cell culture medium (red to green solid line). This red shift of the plasmon peak to 528 nm is a hint for protein attachment on the nanoparticle surface [24, 25] from the cell culture medium.

6.3.3 Characterization of mAuNP_{drug} (AuNP(PAH/PSS+mTHPC/PAH/PSS))

Schema 1 depicts the principle of mTHPC-loaded mAuNP preparation with the layer-by-layer deposition technique. The complex composed of PSS and mTHPC was successfully formed [17] and was adsorbed as second layer. Schneider et al.^[17] identified that 60,000 polyelectrolyte (PE) chains per AuNP resulted in the highest single, non- aggregated mAuNP yield. Here, however, only 15,000 PSS chains were available per AuNP. The idea behind this was to reduce the excess material and to increase deposition efficiency [26]. Adsorbing the polyelectrolyte drug complex

changed the ζ -potential to a negative value of -52 mV (Supporting Information). As third layer, PAH was deposited again, reversing the ζ -potential to a positive value of 66 mV. The fourth and last PE layer was pure PSS resulting in a ζ -potential of -41 mV (Supporting Information, Table 1). Transferring the particles into cell culture medium containing fetal calf serum (FCS) resulted as before in a decrease of the ζ -potential to a value of -10 mV (Supporting Information, Table 1). This reduction of the ζ -potential is due to protein adsorption to the surface [24, 25]. However, the course of the ζ -potential values indicates that all four layers were coated to the AuNP surface.

UV/Vis spectroscopy also allowed controlling the coating steps. The absorption spectrum of AuNP(PAH/PSS+mTHPC/PAH/PSS) is presented in Figure 2 C. Compared to the UV/Vis spectrum of AuNP(PAH) a red shift of AuNP peak of 4 nm and a stronger broadening of the peak on the right side due to the three further layers were observed. More interestingly, the spectrum indicates an additional peak near 420 nm originating from mTHPC (Figure 2 B) deposited as a complex on the AuNP surface. The stability, which is crucial for application in cell culture, was controlled by the flocculation level introduced by Weisbecker et al. [27] not showing agglomeration of the modified AuNP.

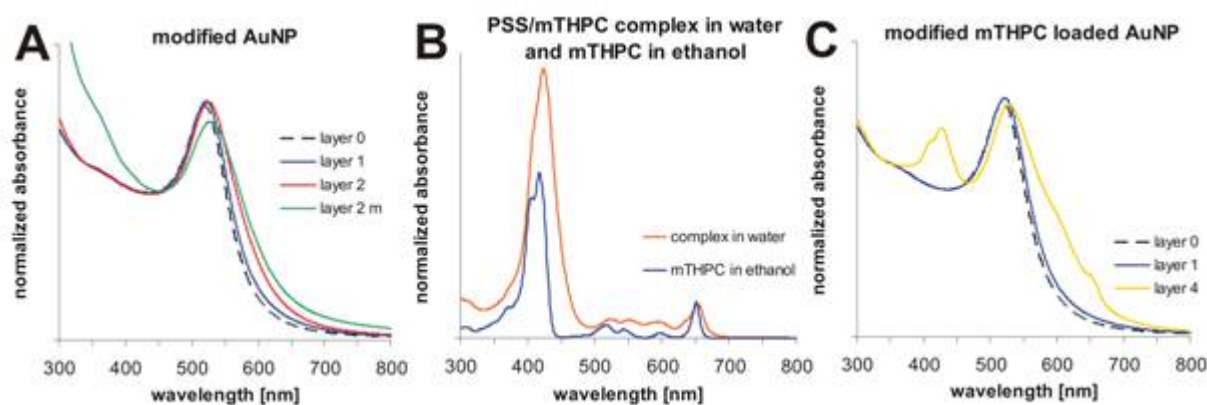


Figure 2: UV/Vis spectra in water: (A) of modified AuNP: layer 0 \triangleq citrate-stabilized AuNP; layer 1 \triangleq AuNP(PAH); layer 2 \triangleq AuNP(PAH/PSS); layer 2 medium \triangleq AuNP(PAH/PSS) in cell culture medium; (B) of PSS/mTHPC complex (orange line) and mTHPC in ethanol (blue line); (C) of modified AuNP: layer 0 \triangleq citrate-stabilized AuNP; layer 1 \triangleq AuNP(PAH); layer 4 \triangleq AuNP(PAH/PSS+mTHPC/PAH/PSS).

The knowledge about the drug concentration adsorbed to the mAuNP is essential for application. A previously developed method, based on the calculation of the area

between the curves (ABC) between 338 nm and 519 nm of AuNP(PAH) and AuNP(PAH/PSS+mTHPP/PAH/PSS), was applied to estimate the mTHPC concentration [26]. However, the method was adapted for mTHPC. For calibration of the ABC, twice washed AuNP(PAH) were added to different known concentrations of PSS/mTHPC complex (Figure 3). For calibration, the ABC of mTHPC between 338 nm and 519 nm as function of the mTHPC concentration in the drug complex in water was recorded (Figure 3B). For linearity of the calibration curve an acceptable value of $R^2 = 0.9918$ was obtained. The mTHPC concentration adsorbed to AuNP determined for a gold concentration of $50 \mu\text{g mL}^{-1}$ was $1.506 \mu\text{g mL}^{-1}$ for the AuNP(PAH/PSS+mTHPC/PAH/PSS).

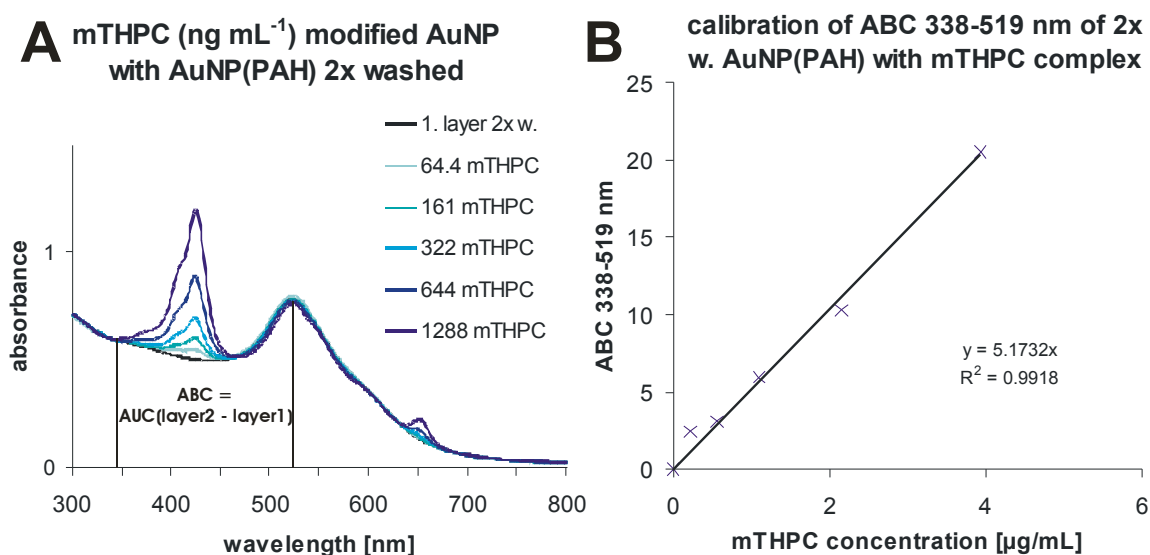


Figure 3: (A) UV/Vis spectra of mixtures of twice washed AuNP(PAH) (\triangle layer 1) and different known concentrations of PSS/mTHPC complex (\triangle layer 2) in water; (B) UV/Vis calibration of ABC of mTHPC between 338 nm and 519 nm as function of mTHPC.

To obtain higher mTHPC concentrations, the AuNP solution was concentrated by centrifugation to an Au concentration of $300 \mu\text{g mL}^{-1}$, and $9.036 \mu\text{g mL}^{-1}$ mTHPC (Table 1), respectively. A further possibility to enhance the drug concentration adsorbed to one AuNP are drug multilayers [26]. Typical tissue concentrations tested on several carcinoma cell lines for efficient tumor treatment with mTHPC are around $1.0 \mu\text{g mL}^{-1}$ indicating that the concentration on the particles would be high enough for application [28-30].

Table 1: Characterization of modified drug-free and drug-loaded AuNP with drug-free \triangleq AuNP(PAH/PSS) and drug-loaded \triangleq AuNP(PAH/PSS+mTHPC/PAH/PSS); the core diameter is the median diameter of pure AuNP determined by TEM measurement; the number of layers are the numbers of the polyelectrolytes and complex adsorbed to AuNP surface; the outer layer is the last polyelectrolyte layer adsorbed to AuNP surface; the ζ -potential in water is of the complemented layered AuNP, measured in water; the ζ -potential in cell medium is of the complemented layered AuNP, measured in HT29 cell culture medium; $c_{(Au)}$ is the Au concentration of modified AuNP in HT29 cell culture medium; $c_{(mTHPC)}$ is the mTHPC concentration adsorbed to AuNP surface of modified AuNP in HT29 cell culture medium; pH value is of the HT29 cell culture medium with the corresponding modified AuNP.

sample name (mAuNP)	(PAH/PSS)	(PAH/PSS+mTHPC/PAH/PSS)
core diameter by TEM [nm]	14	14
number of layers	2	4
outer layer	PSS	PSS
ζ -potential in water [mV]	-46	-41
ζ -potential in cell medium [mV]	-10	-10
$c_{(Au)}$ [$\mu\text{g mL}^{-1}$]	150	300
$c_{(mTHPC)}$ [$\mu\text{g mL}^{-1}$]	0	9
pH value	7.5	7.4

6.3.4 Determination of cytotoxicity after long time incubation with mAuNP

In a first cellular experiment, the effects of unloaded mAuNP following different incubation times (4-72 h) on the used human colon carcinoma cell line HT29 were analyzed. For all experiments the cells were incubated with different concentrations of unloaded mAuNP (0-100 $\mu\text{g mL}^{-1}$). Three different cytotoxicity assays (BrdU, WST-1, LDH assay) were performed with these parameters.

The cell proliferation was determined using the Cell Proliferation ELISA assay that is based on the incorporation of the base analogue BrdU (5-bromo-2-deoxyuridine) during DNA-synthesis. HT29 cells showed a time- and concentration-dependent decrease in cell proliferation leading to 40 % (72 h, 100 $\mu\text{g mL}^{-1}$) active cells for the highest AuNP concentration (c_{Au}) compared to control cells (Figure 4 A). Shorter incubation times (4 and 24 h) did not have any effects on cell proliferation. After 48 h continuous exposure of mAuNP first declines in cell proliferation could be observed.

In addition, the measured cell viability mainly remained constant during the testing phase (Figure 4 B). The used viability assay based on the reduction of the WST-1 salt by metabolic active cells leading to a formazan formation meaning the values were proportional to the amount of cells with mitochondrial activity. The cells showed minor fluctuations in cell viability caused by mAuNP and overall the cell viability was not strongly different from untreated control cells. These findings were in accordance with previous studies. Amongst others, Hauck et al. [31] tested the toxicity of different surface modified gold nanorods on HeLa cells and found that a coating with PSS had no significant influence on the cell viability.

A possible damage of the cell membrane after incubation with mAuNP was investigated using the LDH leakage assay. The presence of higher concentrations of the stable cytosolic enzyme LDH (lactate dehydrogenase) in the supernatant is only possible having reduced cell membrane integrity. HT29 cells showed nearly no effects after the nanoparticle incubation (Figure 4 C). The LDH release varied only marginally for all tested mAuNP concentrations and incubation times. Since there was no increasing LDH release, we assume that unloaded mAuNP did not disturb or destroy the cell membrane even at higher concentrations (100 $\mu\text{g mL}^{-1}$).

Our findings concerning cell viability and membrane integrity were consistent with previous studies in which PSS modified gold nanorods were shown to be non toxic [32]. Leonov et al. concluded that PSS can act as detoxification agent against

cetyltrimethyl ammonium bromide (CTAB) and shows no toxic effects on treated cells [32].

In conclusion, short time incubations (4 and 24 h) with mAuNP did not induce any cellular changes in cell viability, cell proliferation or membrane integrity. Longer incubation time had a certain effect on cell proliferation but not on cell viability and membrane integrity. Additionally, our results were in accordance with previous studies regarding the size-dependent cytotoxicity of AuNP by Pan et al. [33]. They found that 15 nm AuNP in size were non-toxic compared to smaller nanoparticles in size. It has to be mentioned that Pan et al. [33] used citrate stabilized AuNP for the trials, which were the core materials for the mAuNP.

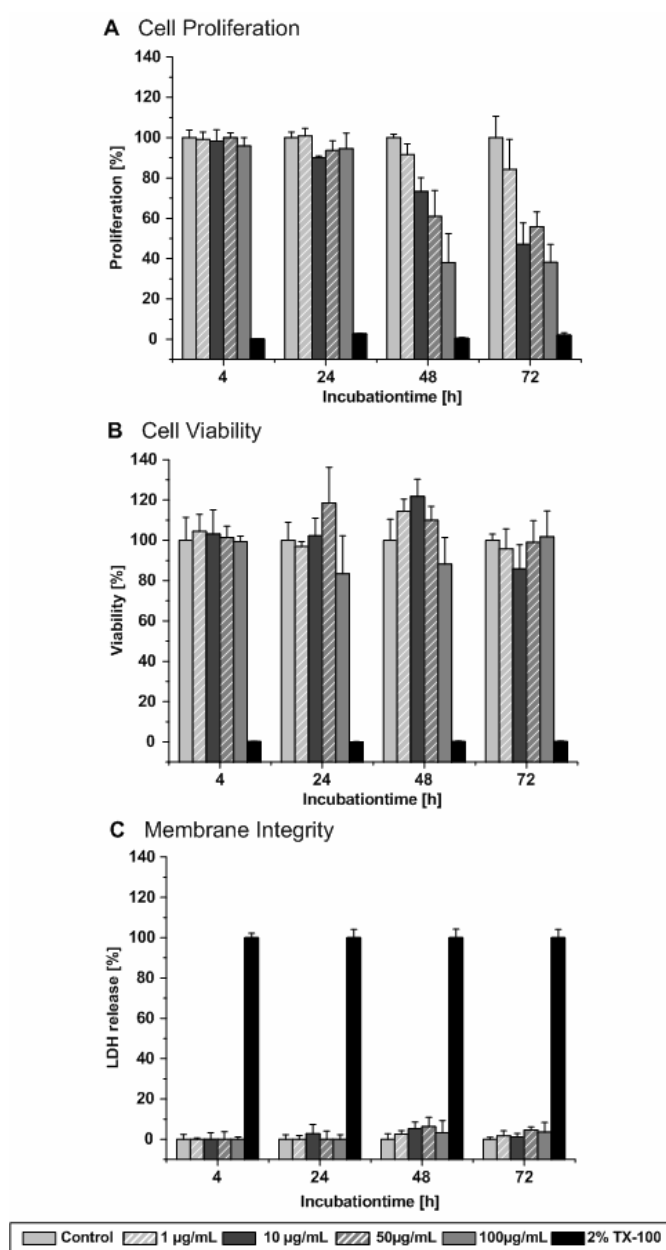


Figure 4: Determination of cytotoxic effects of unloaded mAuNP after long time incubation: HT29 cells were exposed to an increasing concentration of unloaded mAuNP (0-100 $\mu\text{g mL}^{-1}$) for 4, 24, 48 and 72 h at 37 °C. A: BrdU assay, B: WST-1 assay, C: LDH assay Each result represents the mean value \pm standard deviation (SD) of three experiments. Untreated cells were used as negative control and 2 % Triton X-100 treated cells as positive control.

6.3.5 Determination of after-effects following unloaded mAuNP incubation

After demonstration, that unloaded mAuNPs did not affect the cells even at higher concentrations, HT29 cells were tested concerning possible after-effects. Following a short incubation of 4 h (0-100 $\mu\text{g mL}^{-1}$), the cellular response after different recovery phases (24, 48 and 72 h) was tested, to see whether the cells will respond to a previous incubation. Therefore, HT29 cells were incubated with increasing unloaded mAuNP concentrations (0-100 $\mu\text{g mL}^{-1}$) and the cytotoxicity was evaluated after different rest periods. The cell proliferation (Figure 5 A) showed fluctuations after incubation with the different concentrated unloaded mAuNP. 24 h after mAuNP exposure, the cell proliferation was nearly constant for all mAuNP concentrations. An increasing cell proliferation could be detected after a rest period of 48 h. After 72 h rest period, the cell proliferation declined and reached levels comparable to the control cells.

Initially, the cell viability increased in a concentration- and time- dependent manner (Figure 5 B) but aligned with the control cells after a 72 h rest period.

HT29 cells showed nearly no effects concerning a membrane damage after the unloaded mAuNP incubation (Figure 5 C). The LDH release varied only marginally for all tested concentrations and incubation times. Only the control cells showed a slightly increased LDH leakage.

In conclusion, the results of the assays revealed no cytotoxic after-effects of the tested unloaded mAuNP after incubations times up to 72 h. A short time contact of cells with the tested nanoparticles did not cause cytotoxic effects. Therefore, an application of mAuNP with PSS as outermost layer as drug delivery system is promising with respect to their acute toxic profile.

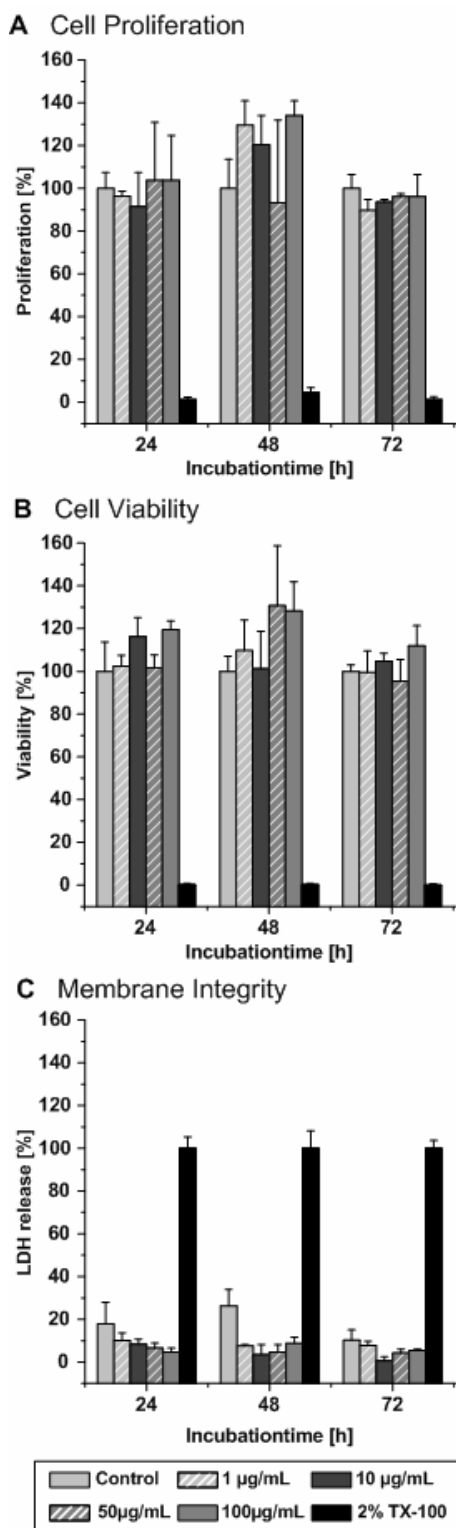


Figure 5: Determination of after-effects following unloaded mAuNP incubation. HT29 cells were exposed to an increasing concentration of unloaded mAuNPs ($0-100 \mu\text{g mL}^{-1}$) for 4 h at 37°C , followed by a rest period from 24 h up to 72 h. Cell proliferation (A; BrdU assay), cell

viability (B; WST-1 assay) and membrane integrity (C; LDH assay) were measured with the corresponding assays as described in the experimental section. Each result represents the mean value \pm standard deviation (SD) of three experiments. Untreated cells were used as negative control and 2 % Triton X-100 treated cells as positive control.

6.3.6 Cellular accumulation of unloaded mAuNP

The results of the different cytotoxicity assays revealed neither cytotoxic effects even at high mAuNP concentrations nor after-effects following short time contacts with unloaded AuNPs. Therefore, the cellular accumulation of the mAuNP was investigated. HT29 cells were incubated with the highest mAuNP concentration ($100 \mu\text{g mL}^{-1}$) for 24 to 72 h. Following, the cellular accumulation was analyzed with bright field microscopy and scanning electron microscopy (SEM).

The results of bright field microscopy revealed a time-dependent accumulation of mAuNP. HT29 cells showed over time an increasing amount of red colored clusters caused by enriched mAuNP assumedly on the cell surface (Figure 6). The incubation led to a cluster formation and red staining but the cellular localization of the nanoparticles could not be shown with this method.

Due to the high number of electrons in gold atoms the detection of AuNP with SEM is possible. Therefore, the cellular binding or accumulation respectively was determined using scanning electron microscopy (SEM). SEM analysis was performed with both secondary electrons (SE) and backscattered electrons (BSE). Accordingly, HT29 cells were incubated with mAuNP ($100 \mu\text{g mL}^{-1}$) for 24-72 h and the cellular accumulation was investigated.

Accumulated mAuNP clusters appeared as white clusters on the cell surface. After an incubation time of 24 h, mAuNP clusters on the cell surface could be detected (Figure 6). The same clusters appeared after 48 and 72 h incubation. The achieved results were consistent with bright field results. By using a SE, the achieved information was mainly pertaining to the cellular morphology. To further contrast the mAuNP clusters, a QBSD-detector was used as backscattered electrons contain information about material properties. They arise in deeper regions of the substrate and depend on the involved elements. After detection and collecting of the backscattered electrons, the clusters appeared bright white. Again, the clusters mainly arranged on the cell surface. There was no evidence that the mAuNP are

taken up by the cells. Additionally, the SEM analysis of treated HT29 cells revealed no morphological changes of HT29 cells after incubation verifying the non-toxic potential of unloaded mAuNP.

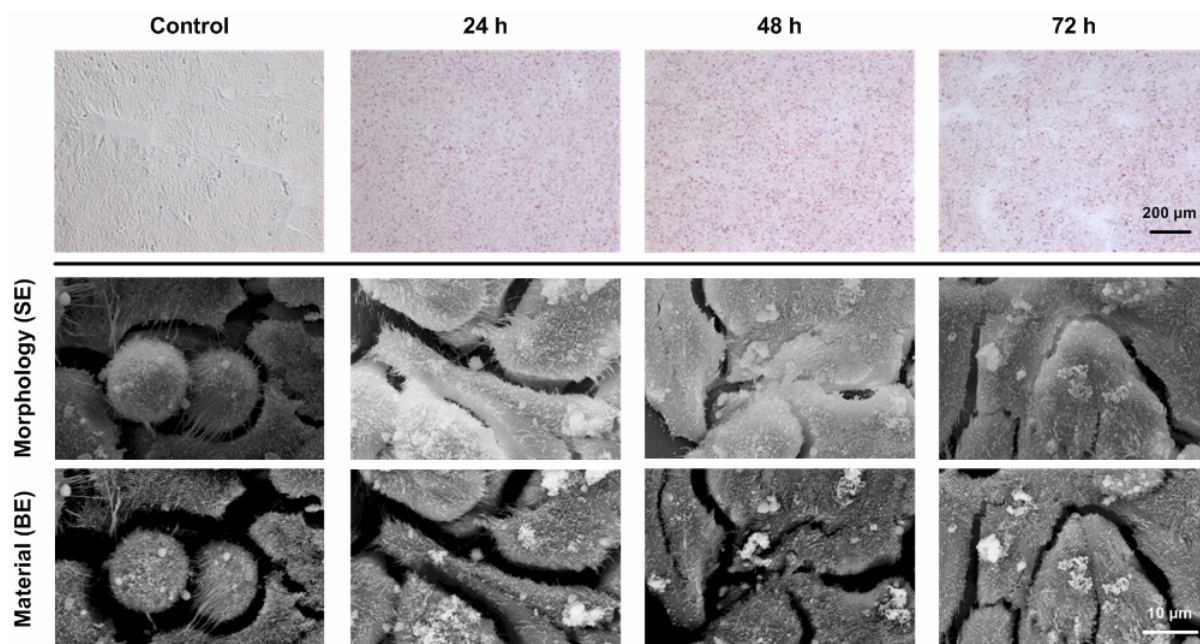


Figure 6: Determination of cellular accumulation of unloaded mAuNP ($100 \mu\text{g mL}^{-1}$) for 24 up to 72 h at 37°C . Following, bright field and scanning electron microscopy images of the cells were taken. For SEM, two detectors for visualization were used: morphology (SE; secondary electron detector) and material (BE; quadrant back scattered electron detector).

6.3.7 Cellular uptake and intracellular distribution of mAuNP

Since the previous results did not clarify the question if mAuNPs were taken up by the cells, further tests with unloaded mAuNPs were carried out. For this, the cellular uptake and intracellular accumulation was investigated using CLSM (confocal laser scanning microscopy) and MP-LSM (multiphoton laser scanning microscopy) relying on the ability of colloidal gold to be visualized by multiphoton excitation [34, 35].

Accordingly, HT29 cells were incubated with mAuNP ($100 \mu\text{g mL}^{-1}$) and mTHPC-loaded mAuNP (applied mTHPC concentration: 3 or $9 \mu\text{g mL}^{-1}$) for 24 h at 37°C . After membrane staining and fixation, the analysis was carried out.

First, the signal of accumulated unloaded mAuNP was analyzed using MP-LSM. Signals of mAuNP appeared inside of the cells (Figure 7 A). To confirm the achieved signals, phase contrast pictures were taken and the positions of the signals by MP-LSM and phase contrast were compared (Figure 7 B & C). Accumulated mAuNP

appeared as dark clusters in phase contrast and matched the position received in the multiphoton-based analysis. Consequently, it was possible to detect the accumulated mAuNP within the cells.

After demonstrating the functionality of the method, the cellular accumulation of mTHPC-loaded mAuNP was investigated to proof the release of the complexed photosensitizer. (Figure 7 D & G). Furthermore, mTHPC-loaded mAuNP were tested with regard to a cellular accumulation of the nanoparticles and mainly on the release of mTHPC into the cytoplasm (Figure 7 D & G; 3 and 9 $\mu\text{g mL}^{-1}$ mTHPC concentration) for 24 h. The release of the photosensitizer mTHPC into the cytoplasm was assessed for both concentrations (Figure 7 D & E, G & H). The incubation with both concentrations led to the typical mTHPC fluorescence within the whole cytoplasm [4, 30]. Cells incubated with 3 $\mu\text{g mL}^{-1}$ free mTHPC possessed a slightly higher fluorescence signal within the cells compared to cells treated with mTHPC-loaded mAuNP. Nevertheless, these cells were characterized by a changed morphology (Supporting Information). In some cellular regions, the characteristic AuNP-signal could be observed (arrows indicating position). The nanoparticles stuck either on the outer cell membrane as previously shown by SEM or were located within the cells. In both cases, the drug was released from the mTHPC-loaded mAuNP. Consequently, the incorporated drug was transported within the cells via the nanoparticles and there, mTHPC was released from the formulation leading to the staining of the complete cytoplasm. The morphology of the treated cells appeared unchanged. Instead, HT29 cells incubated with free mTHPC (3 $\mu\text{g mL}^{-1}$) showed also a strong intracellular mTHPC distribution, but the cells lost their typical structure. The cell shape was mostly round indicating cell death (Supporting Information) and a dissolving process of the cells started due to the toxic effects of the drug. HT29 cells incubated with the nanoparticulate formulation kept their typical morphology. No changes in the shape could be observed.

In conclusion the nanoparticulate bound drug was successfully delivered by mTHPC-loaded mAuNP into HT29 cells. There, it was released into the cytoplasm. The cellular morphology remained normal compared to cells treated with free mTHPC. The toxic effects of mTHPC on HT29 cells could be reduced by adsorbing the drug to the surface of mAuNP.

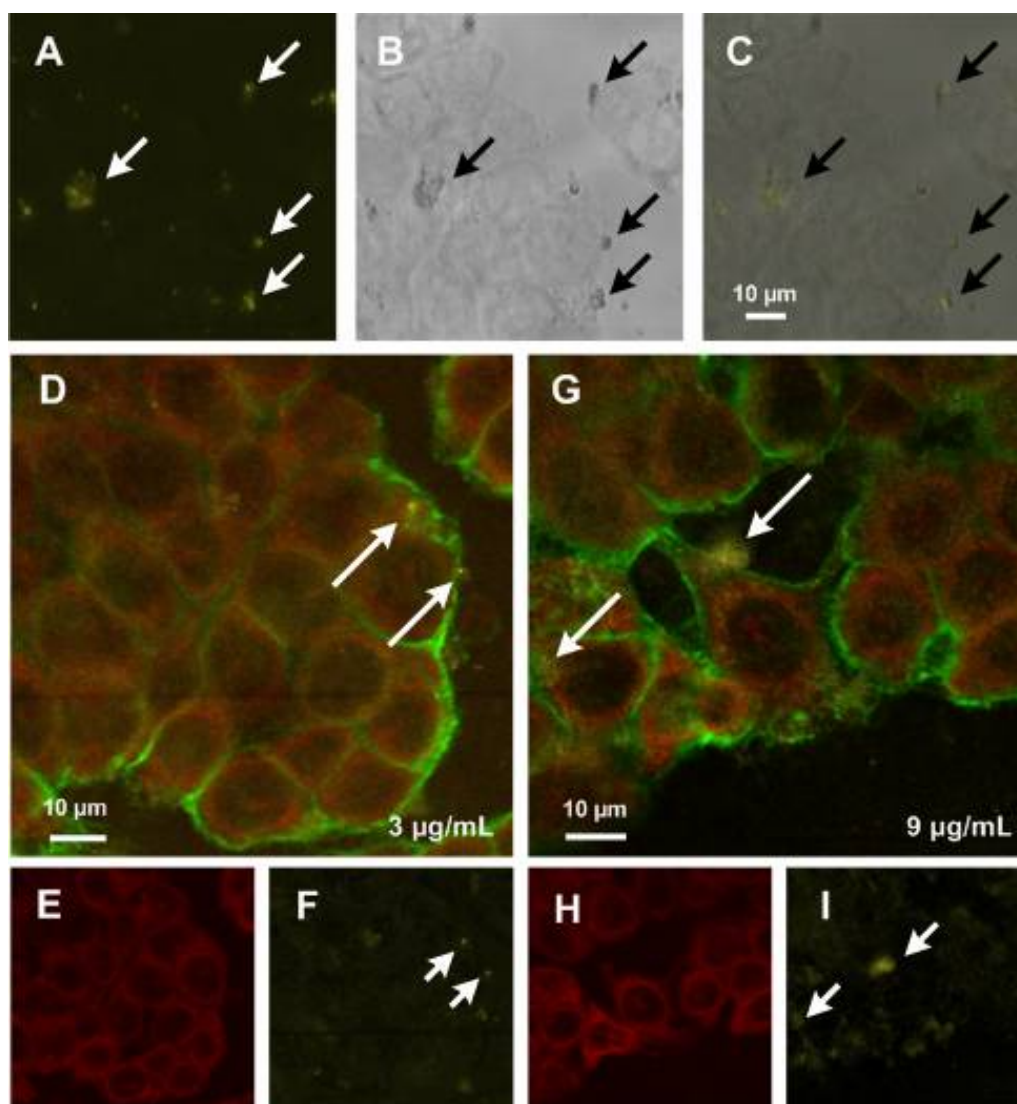


Figure 7: Cellular uptake and intracellular distribution of unloaded and mTHPC-loaded mAuNP. HT29 cells were cultured on glass slides and incubated with unloaded mAuNP (A-C: $100 \mu\text{g mL}^{-1}$) or mTHPC-loaded mAuNP (D-F: $3 \mu\text{g mL}^{-1}$ mTHPC concentration; G-I: $9 \mu\text{g mL}^{-1}$ mTHPC concentration) for 24 h at 37°C . For visualization, the cell membrane was stained with concanavalin A Alexa Fluor 488 (green). The MP-LSM based mAuNP signal was used for detection (yellow). Pictures were taken within inner sections of the cells. (A) mAuNP signal (yellow); (B) phase contrast picture of the cells, and (C) overlay of phase contrast picture and mAuNP signal. Arrows indicate mAuNP cluster. (D) Accumulation of mTHPC-loaded mAuNP, $3 \mu\text{g mL}^{-1}$ mTHPC concentration and (G) accumulation of mTHPC-loaded mAuNP, $9 \mu\text{g mL}^{-1}$ mTHPC concentration, and (E, H) accumulation of free mTHPC, and (F, I) mAuNP signal. Arrows indicate mAuNP clusters.

6.3.8 Determination of phototoxicity of free and mAuNP-bound mTHPC

In the final experiment, the *in vitro* efficiency of the mTHPC-loaded mAuNP compared with free mTHPC was determined. No further trials regarding a potential cytotoxicity of mTHPC-loaded mAuNPs were carried out because PSS was again the outermost layer. In preceding experiments, we already showed the non-toxic effects of PSS coated mAuNP. Therefore, HT29 cells were incubated either with free mTHPC ($3 \mu\text{g mL}^{-1}$) or mTHPC-loaded mAuNP (applied mTHPC concentration: $3 \mu\text{g mL}^{-1}$) for 24 h. To survey the functionality of the bound mTHPC, the cell viability was determined using the WST-1 assay after illumination (652 nm ; 5 J cm^{-2}). Dark toxic effects of both, the free drug and the nanoparticulate formulation were determined without illumination in the same experiment.

First, dark toxic effects of both drugs were analyzed. After 4 h exposure, both drugs induced a slightly increased cell viability compared to untreated control cells (Figure 8 A). By increasing the incubation time up to 24 h, dark toxic effects of the free photosensitizer could be detected indicated through reduced cell viability. The mTHPC-loaded mAuNP induced only a weak reduction in cell viability (to 83 %) even after 24 h incubation. Consequently, the nanoparticulate system reduced the dark toxicity of the drug compared to the free photosensitizer. Here, we could demonstrate that the nanoparticulate system could reduce toxic adverse effects of a drug which has been shown for another delivery system earlier [36]. Kiesslich et al. compared the efficiency and dark toxicity of free and liposomal bound mTHPC. They found a reduced dark toxicity of the liposomal formulation compared to free mTHPC. Our results concerning a reduced dark toxicity of the novel synthesized systems were consistent with these findings.

After illumination, a decrease of cell viability could be observed for both, free and nanoparticulate-bound mTHPC (Figure 8 B). Free mTHPC caused a strong decline in cell viability (to $\sim 7 \%$) after both incubation times. The nanoparticulate-bound mTHPC provoked decreased cell viability (to 48 %) only after a longer incubation time of 24 h. Four hours incubation did not effect the cells due to the structure of the nanoparticles, two polyelectrolyte layers covering the photosensitizer. The 4 h exposure time was not sufficient enough to enable cellular uptake and diffusion of mTHPC molecules from the mTHPC-loaded mAuNP into the cells. Consequently, the amount of available mTHPC was too low to affect the cells. After prolongation the exposure time up to 24 h, the viability after treatment with mTHPC-loaded mAuNP

decreased to 48 % viability indicating that many cells had been killed through photodynamic action. The cellular uptake and the local diffusion of mTHPC through the layer material enabled efficient drug release and a successful treatment. It is conceivable that after 24 h not the entire nanoparticulate-bound drug has been released into the cytoplasm leading to a reduced but not comparable reduction of cell viability. A prolongation of the exposure time could most likely increase the amount of dead cells due to an increased free drug concentration.

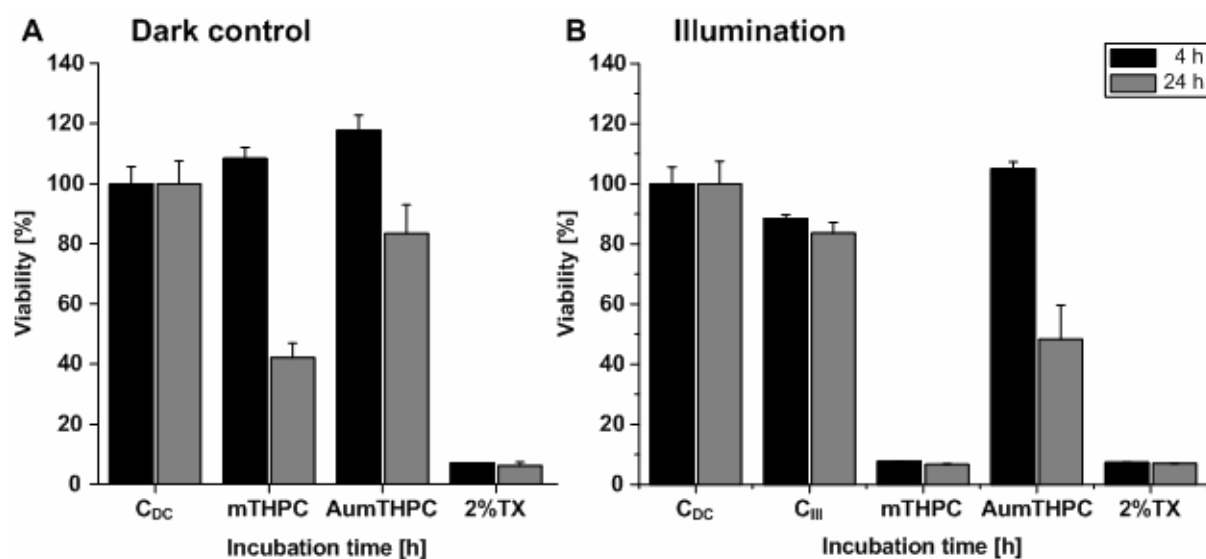


Figure 8: Determination of phototoxicity of free and bound mTHPC. HT29 cells were exposed to free mTHPC or mTHPC-loaded mAuNP (corresponding to a mTHPC concentration of 3 $\mu\text{g}/\text{mL}$ and an AuNP concentration of 100 $\mu\text{g mL}^{-1}$) for 4 h and 24 h followed by illumination (652 nm; 5 J cm^{-2} , 500 s). The cell viability was measured by WST-1 assay as described in the experimental section. Each result represents the mean viability \pm standard deviation (SD) of three experiments. Cell viability was calculated as percentage of viable cells compared to untreated control cells. Untreated cells were used as negative control (C_{DC}: dark control cells; C_{III}: illuminated control cells) and 2 % Triton X-100 (2 % TX) treated cells as positive control.

6.4 Conclusion

In conclusion, our results emphasize the usage of modified gold nanoparticles (mAuNP) as drug delivery system for the hydrophobic photosensitizer mTHPC. A modification of citrate-stabilized AuNP with an adapted layer-by-layer technique

resulted in stable non-toxic mAuNP. AuNP with PSS as outer layer were taken up by HT29 cells and the mTHPC was released delayed. It could be shown that the incorporation of the photosensitizer into the surrounding layers led to reduction of dark toxicity compared to free mTHPC. The phototoxicity of mTHPC-loaded mAuNP was demonstrated. Caused by the delayed release of mTHPC, the efficiency after 24 hours was 50 %, compared to free mTHPC with 90 % efficiency. The reduced dark toxicity in combination with the delayed release could be a huge advantage considering adverse effects due to free mTHPC in healthy tissue. A further modification of mTHPC-loaded mAuNP with cancer cell type specific ligands, such as antibodies, could enable a higher and more specific accumulation of such mAuNP in tumor cells compared to mAuNP without such antibodies.

6.5 Supporting information

Figure S1: Zeta potential: A) of modified AuNP; B) of modified AuNP with drug: number is equal to the layer number of unwashed modified AuNP in water* once washed modified AuNP in water, ** twice washed modified AuNP in water, M: modified AuNP dispersed in cell culture medium of HT29 cells.

Figure S2: Cellular uptake and intracellular distribution of free mTHPC. HT29 cells were cultured on glass slides and incubated with free mTHPC ($3 \mu\text{g mL}^{-1}$) for 24 h at 37°C . For visualization, the cell membrane was stained with concanavalin A Alexa Fluor 488 (green). (A, B) mTHPC accumulation in HT29 cells (red); (C) phase contrast picture of the cells.

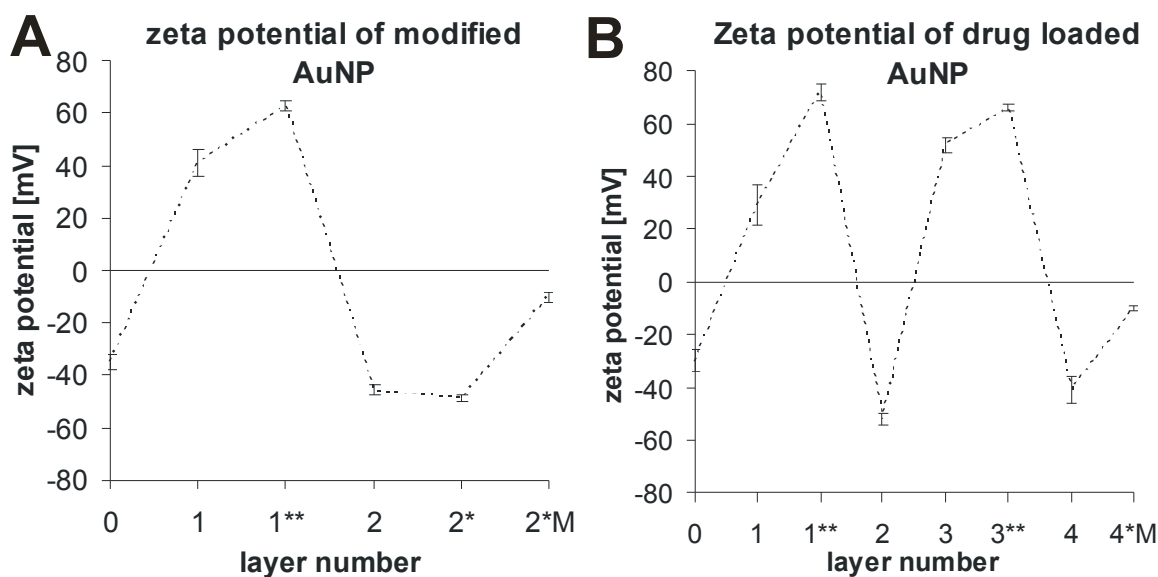


Figure S1: ζ -potential: A) of modified AuNP; B) of modified AuNP with drug: number is equal to the layer number of unwashed modified AuNP in water* once washed modified AuNP in water, ** twice washed modified AuNP in water, M: modified AuNP dispersed in cell culture medium of HT29 cells.

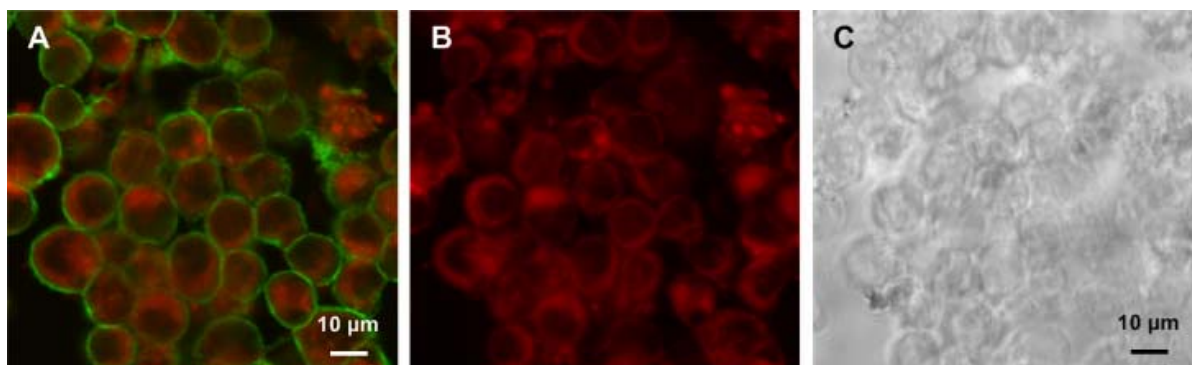


Figure S2: Cellular uptake and intracellular distribution of free mTHPC. HT29 cells were cultured on glass slides and incubated with free mTHPC ($3 \mu\text{g mL}^{-1}$) for 24 h at 37°C . For visualization, the cell membrane was stained with concanavalin A Alexa Fluor 488 (green). (A, B) mTHPC accumulation in HT29 cells (red); (C) phase contrast picture of the cells.

References:

- [1] T. J. Dougherty, C. J. Gomer, B. W. Henderson, G. Jori, D. Kessel, M. Korbelik, J. Moan, Q. Peng. Photodynamic therapy. *J Natl Cancer Inst.* **1998**; 90 (12), 889-905.
- [2] M. A. MacCormack. Photodynamic therapy. *Adv Dermatol.* **2006**; 22, 219-58.
- [3] P. J. Lou, H. R. Jager, L. Jones, T. Theodossy, S. G. Bown, C. Hopper. Interstitial photodynamic therapy as salvage treatment for recurrent head and neck cancer. *Br J Cancer.* **2004**; 91 (3), 441-6.
- [4] S. Marchal, A. Francois, D. Dumas, F. Guillemin, L. Bezdetsnaya. Relationship between subcellular localisation of Foscan and caspase activation in photosensitised MCF-7 cells. *Br J Cancer.* **2007**; 96 (6), 944-51.
- [5] M. Ochsner. Photophysical and photobiological processes in the photodynamic therapy of tumours. *J Photochem Photobiol B.* **1997**; 39 (1), 1-18.
- [6] P. Westerman, T. Glanzmann, S. Andrejevic, D. R. Braichotte, M. Forrer, G. A. Wagnieres, P. Monnier, H. van den Bergh, J. P. Mach, S. Folli. Long circulating half-life and high tumor selectivity of the photosensitizer meta-tetrahydroxyphenylchlorin conjugated to polyethylene glycol in nude mice grafted with a human colon carcinoma. *Int J Cancer.* **1998**; 76 (6), 842-50.
- [7] D. Bechet, P. Couleaud, C. Frochot, M. L. Viriot, F. Guillemin, M. Barberi-Heyob. Nanoparticles as vehicles for delivery of photodynamic therapy agents. *Trends Biotechnol.* **2008**; 26 (11), 612-21.
- [8] D. K. Chatterjee, L. S. Fong, Y. Zhang. Nanoparticles in photodynamic therapy: an emerging paradigm. *Adv Drug Deliv Rev.* **2008**; 60 (15), 1627-37.
- [9] K. Cho, X. Wang, S. Nie, Z. G. Chen, D. M. Shin. Therapeutic nanoparticles for drug delivery in cancer. *Clin Cancer Res.* **2008**; 14 (5), 1310-6.
- [10] R. Duncan. The dawning era of polymer therapeutics. *Nat Rev Drug Discov.* **2003**; 2 (5), 347-60.
- [11] H. B. Ris, H. J. Altermatt, R. Inderbitzi, R. Hess, B. Nachbur, J. C. Stewart, Q. Wang, C. K. Lim, R. Bonnett, M. C. Berenbaum, et al. Photodynamic therapy with chlorins for diffuse malignant mesothelioma: initial clinical results. *Br J Cancer.* **1991**; 64 (6), 1116-20.
- [12] J. Fang, H. Nakamura, H. Maeda. The EPR effect: Unique features of tumor blood vessels for drug delivery, factors involved, and limitations and augmentation of the effect. *Adv Drug Deliv Rev.* **2010**.
- [13] D. Fukumura, R. K. Jain. Tumor microvasculature and microenvironment: targets for anti-angiogenesis and normalization. *Microvasc Res.* **2007**; 74 (2-3), 72-84.

- [14] G. Decher, J. Hong, J. Schmitt. Buildup of ultrathin multilayer films by a self-assembly process: III. Consecutively alternating adsorption of anionic and cationic polyelectrolytes on charged surfaces. *Thin Solid Films*. **1992**; 210/211, 831-835.
- [15] R. Sardar, A. M. Funston, P. Mulvaney, R. W. Murray. Gold nanoparticles: past, present, and future. *Langmuir*. **2009**; 25 (24), 13840-51.
- [16] M. E. Wieder, D. C. Hone, M. J. Cook, M. M. Handsley, J. Gavrilovic, D. A. Russell. Intracellular photodynamic therapy with photosensitizer-nanoparticle conjugates: cancer therapy using a 'Trojan horse'. *Photochem Photobiol Sci*. **2006**; 5 (8), 727-34.
- [17] N. Reum, C. Lehr, A. Wiehe, U. Schaefer, M. Schneider, inventors; Solubility enhancement of water insoluble Substances using Freeze Drying and polymeric complexation. Germany patent DE10 2010025476.2. 2010.
- [18] C. A. Mirkin. Programming the assembly of two- and three-dimensional architectures with DNA and nanoscale inorganic building blocks. *Inorg Chem*. **2000**; 39 (11), 2258-72.
- [19] G. Schneider, G. Decher. From Functional Core/Shell Nanoparticles Prepared via Layer-by-Layer Deposition to Empty Nanospheres. *Nano Lett*. **2004**; 4 (10), 1833-1839.
- [20] M. Chanana, A. Gliozzi, A. Diaspro, I. Chodnevskaja, S. Huewel, V. Moskalenko, K. Ulrichs, H. J. Galla, S. Krol. Interaction of polyelectrolytes and their composites with living cells. *Nano Lett*. **2005**; 5 (12), 2605-12.
- [21] G. Schneider, G. Decher. Functional core/shell nanoparticles via layer-by-layer assembly. investigation of the experimental parameters for controlling particle aggregation and for enhancing dispersion stability. *Langmuir*. **2008**; 24 (5), 1778-89.
- [22] W. Haiss, N. T. Thanh, J. Aveyard, D. G. Fernig. Determination of size and concentration of gold nanoparticles from UV-vis spectra. *Anal Chem*. **2007**; 79 (11), 4215-21.
- [23] E. Boisselier, D. Astruc. Gold nanoparticles in nanomedicine: preparations, imaging, diagnostics, therapies and toxicity. *Chem Soc Rev*. **2009**; 38 (6), 1759-82.
- [24] S. De Paoli Lacerda, J. Park, C. Meuse, D. Pristinski, M. Becker, A. Karim, J. F. Douglas. Interaction of Gold Nanoparticles with Common Human Blood Proteins. *ACS Nano*. **2009**; 4 (1), 365-79.
- [25] C. Schulze, A. Kroll, C.-M. Lehr, U. F. Schäfer, K. Becker, J. Schnekenburger, C. Schulze Isfort, R. Landsiedel, W. Wohllebe. Not ready to use - Overcoming pitfalls when dispersing nanoparticles in physiological media. *Nanotoxicology*. **2008**; 2 (2), 51-61.

- [26] N. Reum, C. Fink-Straube, T. Klein, R. W. Hartmann, C. M. Lehr, M. Schneider. Multilayer coating of gold nanoparticles with drug-polymer coadsorbates. *Langmuir*. **2010**; 26 (22), 16901-8.
- [27] C. S. Weisbecker, M. V. Merritt, G. M. Whitesides. Molecular Self-Assembly of Aliphatic Thiols on Gold Colloids. *Langmuir*. **1996**; 12 (16), 3763-3772.
- [28] O. Bourdon, V. Mosqueira, P. Legrand, J. Blais. A comparative study of the cellular uptake, localization and phototoxicity of meta-tetra(hydroxyphenyl) chlorin encapsulated in surface-modified submicronic oil/water carriers in HT29 tumor cells. *J Photochem Photobiol B*. **2000**; 55 (2-3), 164-71.
- [29] W. N. Leung, X. Sun, N. K. Mak, C. M. Yow. Photodynamic effects of mTHPC on human colon adenocarcinoma cells: photocytotoxicity, subcellular localization and apoptosis. *Photochem Photobiol*. **2002**; 75 (4), 406-11.
- [30] C. M. Yow, J. Y. Chen, N. K. Mak, N. H. Cheung, A. W. Leung. Cellular uptake, subcellular localization and photodamaging effect of temoporfin (mTHPC) in nasopharyngeal carcinoma cells: comparison with hematoporphyrin derivative. *Cancer Lett*. **2000**; 157 (2), 123-31.
- [31] T. S. Hauck, A. A. Ghazani, W. C. Chan. Assessing the effect of surface chemistry on gold nanorod uptake, toxicity, and gene expression in mammalian cells. *Small*. **2008**; 4 (1), 153-9.
- [32] A. P. Leonov, J. Zheng, J. D. Clogston, S. T. Stern, A. K. Patri, A. Wei. Detoxification of gold nanorods by treatment with polystyrenesulfonate. *ACS Nano*. **2008**; 2 (12), 2481-8.
- [33] Y. Pan, S. Neuss, A. Leifert, M. Fischler, F. Wen, U. Simon, G. Schmid, W. Brandau, W. Jahnen-Dechent. Size-dependent cytotoxicity of gold nanoparticles. *Small*. **2007**; 3 (11), 1941-9.
- [34] R. A. Farrer, F. L. Butterfield, V. W. Chen, J. T. Fourkas. Highly efficient multiphoton-absorption-induced luminescence from gold nanoparticles. *Nano Lett*. **2005**; 5 (6), 1139-42.
- [35] M. Schneider, N. Reum, C. Lehr. Modular nanoscale systems for drug delivery and the investigation of cellular uptake mechanism-Characterisation of nanoparticles. *Nanotechnology for improving drug delivery across biological barriers*. **2008** 42, 31-35.
- [36] T. Kiesslich, J. Berlanda, K. Plaetzer, B. Krammer, F. Berr. Comparative characterization of the efficiency and cellular pharmacokinetics of Foscan- and Foslip-based photodynamic treatment in human biliary tract cancer cell lines. *Photochem Photobiol Sci*. **2007**; 6 (6), 619-27.

7 Overall Conclusion and Outlook

Photodynamic therapy (PDT) combines photosensitizer, visible light, and tissue oxygen for treatment of superficial tumors and non-cancerous diseases. The advantages of PDT are its high selectivity, minimal invasiveness, low side effects, and allowing for repetitive application. For non-dermatological applications, the photosensitizers are delivered systemically, which results in several problems caused by their typically high hydrophobicity. The selective therapeutic effect against tumor tissues can be provided by the structure of drugs and tumor physiology, especially the enhanced permeability and retention (EPR) effect. Improved targeting of photosensitizers would help to prevent the damage to the surrounding healthy tissue and lowering dose of drugs. Therefore, the use of nanotechnology in photosensitizer delivery is an attractive approach.

Recently published advances in the use of nanotechnology for PDT application include formulations of biodegradable and non-degradable nanoparticles as passive carriers for photosensitizing agents as well as active carriers which are characterized by attachment of specific ligands such as peptides, antibodies, aptamers, or small molecules to the nanoparticle surface.

In this study, non-degradable nanoparticles as passive carrier for the practically water insoluble photosensitizer (PS) 5,10,15,20-tetrakis(3-hydroxyphenyl)chlorin (mTHPC) or its model PS 5,10,15,20-tetrakis(3-hydroxyphenyl)porphyrin (mTHPP) were developed and investigated. The drug mTHPC is approved in head and neck cancer and has a promising potential to be applied in a lot of other diseases. As template for the development of surface modified nanoparticles with the so-called layer-by-layer (LbL) technology served gold nanoparticles (AuNP) with a diameter of around 15 nm.

For AuNP loading with the drug, a complex consisting of the negatively charged layer material poly(styrene sulfonate) sodium salt (PSS) and mTHPC was generated. The complex was characterized by its water solubility and therefore, the dramatically increased water solubility of mTHPC. The interactions between both molecules were identified and π - π interactions and H-bonds were the responsible mechanism for the complex formation. Furthermore, the complexation efficiency was determined with ~12 monomer units or 4-ethyl(styrene sulfonate) sodium salt units of PSS per mTHPC molecule independent of the PSS molecular weight. The photophysical

characterization of the complex resulted in a decreased singlet oxygen quantum yield of the complex compared to free mTHPC but in an increased phototoxicity tested with Jurkat cells. No toxicity of PSS could be observed in vitro indicating that the PSS/mTHPC complex has great prospects to become a potential drug delivery system for mTHPC, especially due to its simple and quick preparation.

For targeting of the complex and a potential reduced sensitivity to light the loading of nanoparticles was in the focus. Therefore, AuNP were surface modified by the attachment of the PSS/drug complex to the AuNP surface using the LbL technology. This approach would also allow a precise drug adjustment other than the pure number of particles. As positively charged layer material was used the extensively studied poly(allylamine hydrochloride) (PAH) and instead of the negatively charged polyelectrolyte PSS, the complex was utilized. By repeating these coating steps, the first drug-multilayered nanoparticulate formulation was prepared. By the way, the drug deposition efficiency was increased by the factor of 100 compared to standard LbL technique. Around 1000 drug molecules were attached to the surface of one AuNP with one complex layer. Additionally, it seems that the structure of the complex, which is adsorbed as complex with PAH on the AuNP surface, is in a random coiled structure. This insight could be gained estimating the amount of adsorbed polyelectrolyte in comparison with the determined amount of drug which has a fixed ratio to the carrier.

To clarify the potential of mTHPC loaded AuNP in medicine, detailed cellular investigations were carried out. The influence of the drug-free carrier system with PSS as outer layer on the HT29 cells, based on the BrdU-, WST-1-, and LDH-assay was investigated. No cytotoxic effects were observed by the unloaded drug delivery system, which was a very crucial result. Both, unloaded and mTHPC-loaded modified AuNP accumulated to the cells and some of both nanoparticles were found inside of the cells. The key result was the observation of the strong mTHPC release into the cytoplasm by the modified AuNP carriers. Following phototoxicity tests resulted in a delayed phototoxicity compared to the free drug. A great advantage of the mTHPC-loaded mAuNP was their strongly reduced dark toxicity in comparison to the free mTHPC. All in all, the modified AuNP can be considered as promising drug delivery system for water insoluble photosensitizers.

Nevertheless, further improvements of the drug delivery system could be necessary especially regarding its tumor specificity. To reach this aim, the attachment of cell

type specific ligands, such as antibodies to the drug carrier surface is an auspicious way. Furthermore, it is indispensable to learn more about the distribution, uptake or efficiency of the drug delivery system in the animal experiment if the administration of the carrier system is the aim.

8 List of Abbreviations

ABC	area between the curves
AUC	area under the curve
AuNP	gold nanoparticle/s
BrdU	5-bromo-2-deoxyuridine
BSE	backscattered electrons
C	carbon
CS	carrier system
DDS	drug delivery system
DNA	deoxyribonucleic acid
EPR	enhanced permeability and retention
ESS	4-ethyl(styrene sulfonate) sodium salt = monomer unit of PSS
EtOH	ethanol
FCS	fetal calf serum
H	hydrogen
HT29	human colon carcinoma cell line
ISC	intersystem crossing
LbL	layer-by-layer
LDH	lactate dehydrogenase
mAuNP	modified gold nanoparticle/s
mTHPC	5,10,15,20-tetrakis(3-hydroxyphenyl)chlorin
mTHPP	5,10,15,20-tetrakis(3-hydroxyphenyl)porphyrin
N	nitrogen
NCI	National Cancer Institute
NNI	National Nanotechnology Initiative
NP	nanoparticles
PAH	poly(allylamine hydrochloride)
PDT	photodynamic therapy
PE	polyelectrolyte
PS	photosensitizer
PSS	poly(styrene sulfonate) sodium salt
QY	singlet oxygen quantum yield
S	sulfur
SD	standard deviation
SE	secondary electrons
SEM	scanning electron microscopy
TEM	transmission electron microscopy
UV/vis	ultraviolet/visible
WST-1	water soluble tetrazolium (2-(2-methoxy-4-nitrophenyl)-3-(4-nitrophenyl)-5-(2,4-disulfophenyl)-2H-tetrazolium)

9 Curriculum Vitae

personal information

name	Nico Reum
date of birth	August 28 nd , 1977
place of birth	Suhl, Germany

doctoral thesis

2007-2011	Biopharmaceutics and Pharmaceutical Technology, Saarland University, Saarbruecken, Germany
-----------	---

work experience

2006	Boehringer Ingelheim Pharma GmbH und Co. KG, Ingelheim a. Rhein, Germany
------	---

undergraduate study

2000-2005	Pharmaceutical studies Johannes Gutenberg University, Mainz; Germany Pharmaceutical State Examination in October 2005 Certification as Pharmacist in December 2006
-----------	---

professional training

1997-2000	Laboratory assistant BASF-AG, Ludwigshafen a. Rhein, Germany
-----------	---

military service

1996-1997	Wildflecken, Germany
-----------	----------------------

professional experience and teaching

- 2008 and 2010 Lecturer and lab course supervisor, International Conference and Workshop on Biological Barriers and Nanomedicine: Advanced Drug Delivery and Predictive non vivo testing, Saarland University, Saarbruecken, Germany
- 2007-2010 Teaching assistant, seminars and supervision of the practical training in physical and chemical exercises, Biopharmaceutics and Pharmaceutical Technology, Saarland University, Saarbruecken, Germany
- 2003-2006 Training supervisor, "Schuelerlabor", Department of Chemistry, Johannes Gutenberg University, Mainz, Germany
- 2002-2005 Research assistant, Department Drug Delivery, Boehringer Ingelheim Pharma GmbH und Co. KG, Ingelheim a. Rhein, Germany

10 Publication List

A) Scientific Publications

M. Schneider, **N. Reum**, C.M. Lehr: “Modular nanoscale systems for drug delivery and the investigation of cellular uptake mechanism -Characterisation of nanoparticles“ In *42nd Académie des Alpilles: Nanotechnology for improving drug delivery across biological barriers*, vol. 42 (ed. C. M. Lehr), pp. 31-35. St. Remy: Gattefossé, **2008**.

N. Reum, C. Fink-Straube, T. Klein, R. W. Hartmann, C.-M. Lehr, M. Schneider: “Multilayer Coating of Gold Nanoparticle with Drug-Polymer Coadsorbates”, *Langmuir*; **2010**.

T. Schneider, A. Baldauf, L. A. Ba, V. Jamier, K. Yusuf, **N. Reum**, M. Schneider, A. Röseler, K. Becker, T. Burkholz, P. G. Winyard, M. Kelkel, M. Diederich and C. Jacob: “Selective antimicrobial activity associated with sulfur nanoparticles”, *Journal of Biomedical Nanotechnology*, accepted **2011**.

B) Patent Application

N. Reum, C.M. Lehr, U. Schäfer, A. Wiehe, M. Schneider: Application for a German patent: “Solubility enhancement of water insoluble Substances using Freeze Drying and polymeric complexation”, **2010**

C) Awards

Travel award sponsored by CRS local chapter Germany for poster and oral presentation at *37th Annual Meeting and Exposition of the Controlled Release Society*, Convention Center, Portland, Oregon, (USA), July 2010

Lecture award for invited oral presentation from the Controlled Release Society (International). *37th Annual Meeting and Exposition of the Controlled Release Society*, Convention Center, Portland, Oregon, (USA), July 2010

D) Contribution to Scientific Conferences

Podium:

N. Reum, A. Wiehe , C.M. Lehr, M. Schneider: “Nanocarrier based on Polyelectrolyte Multilayers for Photodynamic Therapy“ *Meeting and Exposition of the Controlled release Society Germany*, Halle (Germany), March 2009

N. Reum, C. Fink-Straube, K. Löw, H. von Briesen, C.M. Lehr, M. Schneider: “Multilayer Coating of Gold Nanoparticle with Drug-Polymer Coadsorbate “*37th Annual Meeting and Exposition of the Controlled Release Society*, Convention Center, Portland, Oregon, (USA), July 2010

Posters:

N. Reum, K. Löw, H. von Briesen, C.M. Lehr, M. Schneider: "From gold nanoparticles to drug delivery systems of modular architecture" *7th Conference and workshop on Biological barriers and Nanomedicine-Advanced Drug Delivery and Predictive non vivo Testing Technologies*, University of Saarland (Germany), February 2008

N. Reum, K. Löw, H. von Briesen, A. Wiehe , C.M. Lehr, M. Schneider: "Nanocarrier based on Polyelectrolyte Multilayers for Photodynamic Therapy" *35th Controlled Release Society Annual Meeting & Exposition*, Hilton New York (USA), July 2008

N. Reum, K. Löw, H. von Briesen, A. Wiehe , C.M. Lehr, M. Schneider: "Nanocarrier based on Polyelectrolyte Multilayers for Photodynamic Therapy" *7th Globalization of Pharmaceutics Education Network (GPEN)*, University of Leuven (Belgium), September 2008

K. Löw, **N. Reum**, S. Wagner, M. Schneider, H. v. Briesen: „Cytotoxicity and cellular accumulation of gold nanoparticles in human colon carcinoma cells" *GOLD 2009 the 5th international conference on gold science, technology and its applications*, Heidelberg (Germany), July 2009

N. Reum, A. Wiehe , C.M. Lehr, M. Schneider: "Nanocarrier based on Polyelectrolyte Multilayers for Photodynamic Therapy" *36th Annual Meeting and Exposition of the Controlled Release Society*, Bella Center Copenhagen (Denmark), July 2009

N. Reum, K. Löw, H. von Briesen, A. Wiehe , C.M. Lehr, M. Schneider: "Nanocarrier based on Polyelectrolyte Multilayers for Photodynamic Therapy" *8th Conference and workshop on Biological barriers and Nanomedicine-Advanced Drug Delivery and Predictive non vivo Testing Technologies*, University of Saarland (Germany), February 2010

N. Reum, C. Fink-Straube, K. Löw, H. von Briesen, C.M. Lehr, M. Schneider: "Multilayer Coating of Gold Nanoparticle with Drug-Polymer Coadsorbate " *37th Annual Meeting and Exposition of the Controlled Release Society*, Convention Center, Portland, Oregon, (USA), July 2010

J. Pohl, **N. Reum**, M. Schneider, B. Röder: "Investigation of novel water soluble polymer nanoparticles as carrier systems for photodynamic therapy" *Tetrapyrrole Discussion Group Meeting*, Humboldt University, Berlin, (Germany), September 2010

11 Danksagungen/Acknowledgements

Zunächst bedanke ich mich bei Herrn Prof. Dr. Claus Michael Lehr für die Optionen, an seinem Lehrstuhl wissenschaftlich zu arbeiten und die Gewährung vielfältiger Möglichkeiten meine Ergebnisse auf nationalen und internationalen Kongressen vorzustellen sowie seine stete Bereitschaft spontan auf Fragen einzugehen und Anregungen zu liefern.

Mein besonderer Dank geht an meinen Betreuer Herrn Jun. Prof. Dr. Marc Schneider, der mir jederzeit bei wissenschaftlichen Fragen mit hilfreichen Rat und Tat zur Seite stand. Auch für seine Art und Weise der Betreuung bin ich sehr dankbar, da sie mir die Möglichkeit gegeben hatte, meinen eigenen Weg zu finden.

Vielen Dank an Herrn Prof. Dr. Ulrich Schäfer für die vielen wertvollen Diskussionen und Ratschläge zu technischen sowie administrativen Problemen.

Bei den Gruppen von Prof. Beate Röder vom Institut für Physik/Photobiophysik der Humboldt Universität Berlin mit Judith Pohl, Kuan Chen und Annegret Preuß, und von Privatdozent Hagen von Briesen vom Fraunhofer Institut für Biomedizinische Forschung in St. Ingbert mit Karin Löw und Dr. Sylvia Wagner möchte ich mich sehr für die gute Zusammenarbeit im Rahmen des „Nano-Cancer“ Projektes bedanken.

Bei Herrn Jörg Schmauch bedanke ich mich ganz sehr für die Einführung und Unterstützung der transmissionselektronenmikroskopischen Messungen.

Dr. Claudia Fink-Straube danke ich für die elementaranalytischen und emissionsspektroskopischen Messungen und die damit verbundenen zahlreichen Diskussionen.

Bei Tobias Klein möchte ich mich für die Berechnungen und Bearbeitung der Molekülwechselwirkungen durch „Docking“ Software bedanken.

Dr. Silke Krol danke ich ganz herzlich für ihre wertvollen Hinweise und Diskussionen über die Anwendung der Layer-by-Layer Technik bei Nanopartikeln.

Dr. Nicole Daum möchte ich ganz herzlich für ihre hilfreichen Tipps und Diskussionen zum Thema Zellkulturen danken.

Keine Arbeit ist möglich ohne Finanzierung. Daher möchte ich mich herzlich beim BMBF (Bundesministerium für Bildung und Forschung) in Deutschland für die Förderung meiner Arbeit im Zusammenhang mit dem „Nano-Cancer“ Projekt (0312026A) bedanken.

Weiterhin möchte ich mich bei unseren Technikern, insbesondere bei Petra König, Leon Muijs, Peter Meiers und Heike Stumpf für ihre Unterstützung bedanken.

Ein großer Dank gilt selbstverständlich meinen ehemaligen Kollegen, besonders Marco, Noha, Katharina, Eva, Steffi, Claudia, Tsambika, Michael, Hagar, Xavier, Ke, Sandra, Anne, Ratnesh. Mit eurer Hilfe war so manches leichter zu bewältigen, egal ob es um rein wissenschaftliche Probleme ging oder um ganz alltägliche und scheinbar einfache menschliche Dinge. Die Zusammenarbeit mit euch hat mir sehr viel Spaß gemacht und mir wieder einmal gezeigt, wie wichtig Kommunikation und zwischenmenschliche Beziehungen auch am Arbeitsplatz sind.

Der bedeutendste Dank aber geht an die wichtigsten Personen in meinen jetzigen Leben. Das sind an erster Stelle meine Eltern, die stets an mich geglaubt haben und mich immer meinen eigenen Weg haben gehen lassen, auch wenn der mich immer weiter weg von meiner Heimat Thüringen geführt hat. Und meine Freundin, die nie an mir zweifelte, mir so viel Zeit gewährt hatte, wie ich für meine Arbeit brauchte, mir jederzeit zuhörte und unendlich interessante Gespräche mit mir führte, wann immer es möglich war. Vielen lieben Dank für alles!!!

Während meiner Promotion hatte ich die Möglichkeit viele interessante und außergewöhnliche Menschen kennenzulernen. Ich bitte alle Personen, die hier nicht erwähnt sind, um Verzeihung. Auch für diese Menschen empfinde ich große Achtung, Wertschätzung und Dankbarkeit.